ABSTRACT

Title of Dissertation: OBSERVED TELECONNECTIONS IN NORTHERN WINTER: SUBSEASONAL EVOLUTION AND TROPICAL LINKAGES

Stephen R. Baxter, Doctor of Philosophy, 2016

Dissertation directed by: Professor Sumant Nigam, Department of Atmospheric and Oceanic Science

Teleconnections refer to the climate variability links between non-contiguous geographic regions, and tend to be associated with variability in both space and time of the climate's semi-permanent circulation features. Teleconnections are well-developed in Northern winter, when they influence subseasonal-to-seasonal climate variability, notably, in surface temperature and precipitation. This work is comprised of four independent studies that improve understanding of tropical-extratropical teleconnections and their surface climate responses, subseasonal teleconnection evolution, and the utility of teleconnections in attribution of extreme climate events.

After an introduction to teleconnection analysis as well as the major teleconnection patterns and associated climatic footprints manifest during Northern winter, the lagged impact of the Madden-Julian Oscillation (MJO) on subseasonal climate variability is presented. It is found that monitoring of MJO-related velocity potential anomalies is sufficient to predict MJO impacts. These impacts include, for

example, the development of significant positive temperature anomalies over the eastern United States one to three weeks following an anomalous convective dipole with enhanced (suppressed) convection centered over the Indian Ocean (western Pacific).

Subseasonal teleconnection evolution is assessed with respect to the Pacific-North America (PNA) pattern and the North Atlantic Oscillation (NAO). This evolution is analyzed both in the presence and absence of MJO-related circulation anomalies. It is found that removal of the MJO results only in small shifts in the centers of action of the NAO and PNA, and that in either case there is a small but significant lag in which the NAO leads a PNA pattern of opposite phase. Barotropic vorticity analysis suggests that this relationship may result in part from excitation of Rossby waves by the NAO in the Asian waveguide.

An attempt is made to elegantly differentiate between the MJO extratropical response and patterns of variability more internal to the extratropics. Analysis of upper-level streamfunction anomalies is successful in this regard, and it is suggested that this is the preferred method for the real time monitoring of tropical-extratropical teleconnections.

The extreme 2013-2014 North American winter is reconstructed using teleconnection analysis, and it is found that the North Pacific Oscillation-West Pacific (NPO/WP) pattern was the leading contributor to climate anomalies over much of North America. Such attribution is cautionary given the propensity to implicate the tropics for all midlatitude climate anomalies based on the El Niño-Southern

Oscillation (ENSO) paradigm. A recent hypothesis of such tropical influence is presented and challenged.

OBSERVED TELECONNECTIONS IN NORTHERN WINTER: SUBSEASONAL EVOLUTION AND TROPICAL LINKAGES

by

Stephen R. Baxter

Dissertation submitted to the Faculty of the Graduate School of the
University of Maryland, College Park, in partial fulfillment
of the requirements for the degree of
Doctor of Philosophy
2016

Advisory Committee:
Dr. Sumant Nigam, Chair, Professor
Dr. Antonio Busalacchi, Professor
Dr. Sujay Kaushal, Associate Professor, Dean's Representative
Dr. Alfredo Ruiz-Barradas, Associate Research Professor
Dr. Scott Weaver, Adjunct Associate Professor

Dedication

For my loving and supportive family.

Acknowledgements

I would first like to acknowledge my advisor, Dr. Sumant Nigam, whose guidance over the past several years has been instrumental in my continued academic and professional growth. I was fortunate to have him as both a teacher and mentor, and I look forward to continuing our work together over the years to come. Additionally, Dr. Nigam was supportive of my full-time transition to the Climate Prediction Center after the completion of my Master's degree, and I thank him for his patience and understanding.

I also thank Dr. Scott Weaver, who I came to know as a student intern at the Climate Prediction Center. Scott was influential in my decision to attend the University of Maryland and introduced me to Dr. Nigam, who was his Ph.D. advisor. I am happy to have known Scott as a mentor, colleague, and friend. As a student, it was often stressed that a good professional mentor is essential to one's career development. I am lucky to have had the best.

I must thank the management of the Climate Prediction Center, especially Mike Halpert and Jon Gottschalck, for supporting the continuation of my Ph.D. program after I began working there full-time. I have so many great colleagues there who make me a better person and a better scientist. This dissertation is nothing like an ending, but the beginning of a long and fruitful career at CPC.

Saving the best for last, I am grateful to have the love and support of my family. My parents and siblings have been encouraging, especially during times of doubt and worry. Most importantly, I am blessed to have my wife Molly by my side.

She has been and continues to be my biggest supporter. Her love sustains me in my academic and professional endeavors. I also acknowledge in a special way my son, Justin, and our baby on the way. They constantly remind me of what's truly important in life.

Table of Contents

List of Figures

List of Acronyms

AO	Arctic Oscillation
CDB	Climate Diagnostics Bulletin
CFSR	Climate Forecast System Reanalysis
CPC	Climate Prediction Center
DJF	December, January, and February (Northern winter)
EA	East Atlantic
EEOF	Extended EOF analysis
ENSO	El Niño-Southern Oscillation
EOF	Empirical Orthogonal Function
EOT	Empirical Orthogonal Teleconnection
LV	Loading Vector
MJO	Madden-Julian Oscillation
NAO	North Atlantic Oscillation
NMME	National Multi-model Ensemble
NOAA	National Oceanic and Atmospheric Administration
NPM	North Pacific Mode
NPO	North Pacific Oscillation
OI	Optimal Interpolation
OLR	Outgoing Longwave Radiation
PC	Principal Component
PCA	Principal Component Analysis

PNA	Pacific-North America
REEOF	Rotated, extended EOF analysis
REOF	Rotated EOF analysis
RMM	Real-time Multivariate MJO Index
RPCA	Rotated Principal Component Analysis
RWS	Rossby Wave Source
SAT	Surface Air Temperature
SLP	Sea-level Pressure
SST	Sea Surface Temperature
TNH	Tropical-Northern Hemisphere
WH	Wheeler and Hendon
WP	West Pacific

Chapter 1: Introduction[1]

The term teleconnection is often used in atmospheric sciences to describe the climate links between geographically separated regions. The remote region need not exhibit fluctuations of the same sign in order to be "teleconnected". In fact, the interesting teleconnections often involve contemporaneous variations of opposite signs. These teleconnection patterns tend to be associated with the variability in space and time of the climate's semi-permanent features (e.g. Icelandic Low, Azores High). Teleconnection maps thus provide information about the structure of recurrent climate variability, especially its correlation-at-a-distance features. The maps are useful because climate variability is often manifest with such structure: For example, winter variations in temperature and rainfall over southern Europe and the Iberian Peninsula are frequently opposite to those over northwestern Europe and Scandinavia.

Teleconnections were first identified in the sea-level pressure field; prominent examples include Sir Gilbert Walker's identification of the North Atlantic Oscillation and the Southern Oscillation (Walker, 1924; Walker and Bliss, 1932). Such early analysis was guided by intuition and area of interest, while more recent analysis attempts a more objective identification of teleconnection patterns and hydroclimate impacts. So while teleconnections have now been studied for the better part of a century, advances are still being made in techniques of identification, with an especially keen interest in the ability to predict future climate variability as well as

[1] The introduction is based largely on the material contained in Nigam and Baxter (2014). That encyclopedia text has its origin in Nigam (2003). However, all analysis and figures presented in this chapter were conducted by the author during the course of dissertation research.

attribute observed climate events to some physical pattern of atmospheric variability. It is precisely the interest in being able to predict climate variability and conduct attribution analysis that in large part motivates this work.

Teleconnections, because they are climate phenomena, are identified on some climate time scale, for which day-to-day variations are neglected in favor of the of the lower-frequency, or "standing," variability. Time averaging periods ranging from pentads (five-day average) to months are used in this work. The connectivity of remote regions manifest in teleconnection analysis indicates the potential significance of remote forcing in the generation of regional climate anomalies. A teleconnection map based on contemporaneous correlations however cannot, by itself, discriminate between the forcing and response regions. The root physical underpinnings of teleconnection patterns is important in terms of predictability, and two teleconnection patterns whose physical mechanisms suggest prolonged predictability are the El Niño-Southern Oscillation (ENSO) midlatitude response and the extratropical response to the Madden-Julian Oscillation (MJO). Both of these patterns, however, tend to elude traditional teleconnection analysis.

The independent research studies that make up the subsequent chapters advance understanding of teleconnection patterns, especially in terms of their subseasonal evolution and tropical linkages, the latter known to be important for extended predictability of surface hydroclimate. In some cases, existing hypotheses will be challenged.

This chapter is structured as follows:

- The analysis methods generally used in teleconnection analysis are discussed.
- The various teleconnection patterns to be elucidated and analyzed in the subsequent chapters are introduced, along with, in some cases, their surface climate footprints.
- Motivating questions for the four independent research studies that constitute the next four chapters are presented.
- The structure of the remainder of the dissertation is laid out.

1.1 Methods of Teleconnection Analysis

There are several techniques that can be utilized to uncover teleconnection patterns, among them correlation analysis and principal component analysis. The latter is most relied upon throughout this work. Correlation analysis is the simpler of the two methods. Consider a meteorological field such as geopotential height which denotes the height of an isobaric surface in the atmosphere. Geopotential height, φ, is a function of longitude and latitude, and assume that it is defined at M grid points; φ_i represents height at the i-th longitude-latitude grid point. Geopotential height is also a function of time, and its monthly-mean value is assumed to be available for several winters (N winter months). Interest in the variability of climate leads to the consideration of departures of monthly-mean heights from their calendar month climatologies, with prime (') denoting the departures; $\varphi'_{i,k}$ represents the height departure at the i-th grid point in the k-th month. The correlation in height departures at two grid points, i and j, is denoted by H_{ij}, and defined as

$$H_{i,j} = \frac{\sum_{k=1}^{N} \varphi'_{i,k} \varphi'_{j,k}}{\left(\sum_{k=1}^{N} \varphi'^{2}_{i,k}\right)^{1/2} \left(\sum_{k=1}^{N} \varphi'^{2}_{j,k}\right)^{1/2}}$$

Knowledge of the correlation matrix, ***H***, can be used to construct a teleconnectivity map (***T***) which objectively identifies the base points associated with various teleconnection patterns. The map is constructed by associating the magnitude of the strongest negative correlation between a grid point and all others with that grid point, i.e., T_i = | Most negative member in the *i*-th row of the correlation matrix ***H*** |. The local maxima in this map (**T**) identify the potential base points. Linkage between the neighboring base points is assessed by examining the sites of their strongest negative correlations. A cluster of linked base points constitutes the core of the teleconnection pattern, and three prominent patterns are identifiable using this technique.

Climate teleconnections were first identified in the sea-level pressure field, a particularly ill-defined quantity over mountainous regions, and easily influenced by micro- and mesoscale meteorological processes. Therefore, upper-air data is preferred, especially geopotential height, whose horizontal and vertical gradients are proportional to wind and temperature, respectively, via geostrophic and hydrostatic balance.

Figure 1.1a shows the teleconnectivity in the 500-hPa geopotential height field during Northern winter. Winter is the preferred season for teleconnection analysis since that is when Rossby wave activity is maximized, and climate variability can be more succinctly decomposed into discrete teleconnection patterns (i.e. fewer patterns explain more variance). The map is constructed from correlation analysis of December, January, and February height anomalies from 0-90^{o}N for the

1979-2008 period; the data is from NOAA's Climate Forecast System Reanalysis (CFSR; Saha et al., 2010). This recent reanalysis takes advantage of the latest advances in data assimilation and incorporates important data from the satellite era, and thus only extends back to 1979. This figure is comparable to figure 7B in the pioneering study by Wallace and Gutzler. It identifies three major teleconnection patterns in the Northern Hemisphere: the NAO, the North Pacific Oscillation/West Pacific pattern (NPO/WP), and the Pacific-North America (PNA) pattern. The NAO and NPO/WP each consist of two base points over the Atlantic and Pacific basins, respectively. The PNA, as identified by Wallace and Gutzler, consists of four base points: the subtropical Pacific near the dateline, the Aleutians, interior northwestern North America, and the southeastern United States. Note, however, that the fourth base point over southeastern US is missing in Figure 1.1a.

This brings to light an issue regarding the stability of teleconnection patterns. Changing the domain and time period of the analysis can introduce some differences: Besides the missing PNA center, there are other differences between the seminal analysis of Wallace and Gutzler (1981) and Figure 1.1a. The NAO-related pattern exhibits a noticeable eastward shift, as does the third PNA center. Note that data set differences are unlikely to be the origin as the large-scale rotational flow is similarly represented in atmospheric data sets. While notable, the teleconnectivity differences are viewed as modest considering the non-overlapping periods of the two analyses. This assessment is supported by Figure 1.1b which shows the teleconnectivity map from a similar analysis of longer period data (1949-2009), one encompassing the previous non-overlapping periods. While the NAO centers and the third PNA center

here are more in accord with the Wallace and Gutzler analysis, the 4th PNA center remains indiscernible. Interestingly, the NPO/WP centers of action are also not identifiable in the longer period analysis. Even so, the overall structure of the teleconnectivity map is similar in Figure 1.1a.

Correlation analysis is a physically intuitive and objective method for identifying climate teleconnections but the obtained patterns may not be independent, especially, if spatial structures overlap. This, for instance, is the case in the Pacific, where three prominent patterns – PNA, NPO/WP, and the ENSO response (shown later) – overlap to varying extent in the extratropical sector. Not surprisingly, the correlation method proved unsuccessful in capturing the ENSO response in the extratropics as a teleconnection pattern. The 500-hPa level – a level of near-zero divergence – is, perhaps, not the level of choice for identifying tropical-extratropical interactions instigated by deep convective heating in the tropics. Horizontal divergence associated with deep convection, such as during El Nino winters, is usually strongest in the tropical upper troposphere (~200 hPa). The associated midlatitude response, on the other hand, is quasi-geostrophic in character, and hence approximately non-divergent. Tropical-extratropical interactions are thus best diagnosed at a pressure-level that captures the divergent outflow in the Tropics and that is near a non-divergent level in the extratropics. The 200-hPa level meets these criteria, to a large extent.

Repeating the correlation analysis of height fluctuations at 200 hPa did not yield any new information on teleconnectivity. In particular, no new base points were identified and the ENSO response in the extratropics remained unidentified as before.

Principal component analysis is an elegant and widely used method for determining the structure of recurrent variability. A common name for it is empirical orthogonal function (EOF) analysis. This method also analyzes the structure of the correlation matrix – the covariance matrix is preferred, though – but focuses on regions that account for a substantial portion of the temporal variance rather than just those which exhibit strong negative correlations with distant points in the domain. In contrast with the previous method, the technique yields both the spatial patterns of recurrent variability and the extent to which these are present, or projected, in the observed anomaly record. The projection, or amplitude, is called the principal component (PC) while the spatial pattern is referred to as the loading vector (LV) in the technical literature.

Recurrent variability patterns identified from principal component analysis are spatially and temporally independent, or orthogonal. Such relationship among patterns is often helpful in investigating the origin and governing mechanisms of variability but can be relaxed in one of the dimensions – space or time – if the orthogonality constraints prove restrictive. For example, it is conceivable for two temporally independent variability patterns to have overlapping spatial structure. Imposition of temporal and spatial orthogonality constraints in this case may not lead to a physically meaningful analysis.

The EOF analysis results in a series of spatial patterns, or loading vectors, each one explaining successively smaller portion of the total temporal variance. One can view these recurrent patterns as teleconnection patterns. The pattern amplitude is

given by the time dependent PC. The anomaly record can be reconstructed by summing the product of the spatial patterns (LVs) and their PCs.

Principal component analysis provides an efficient and unique characterization of recurrent variability in terms of a small number of uncorrelated spatial patterns. The patterns are chosen so that each one successively explains the maximal residual variance in the anomaly data set. For instance, the leading PC is obtained by requiring that it maximize the sum of the squared temporal correlation between itself and the anomaly time series at all spatial points in the domain. The resulting PCs are temporally orthogonal while the LVs are spatially orthogonal. Spatial orthogonality can however be restrictive and, in many cases, undesirable, as discussed earlier: Although the leading LV is not directly impacted, subsequent LVs are often constrained to have predictable geometric relationships vis-a-vis the leading pattern; domain geometry, thus, becomes an influencing factor, itself.

For these and other reasons, a variant of PCA analysis, called the rotated principal component analysis (RPCA), has become popular since it yields patterns that are no longer constrained to be spatially orthogonal. Therefore domain geometry is thus much less influential, though rotated PCs continue to be temporally orthogonal. The linear transformation (or solid rotation) of PCs that is widely used in meteorology is called the ‘varimax’ rotation. It is determined by the requirement that the variance of the squared correlations between each rotated PC and the original time series be maximized. Focusing on the variance, rather than sum (as in unrotated analysis), of the squared correlations increases spatial discrimination, and facilitates interpretation of the obtained patterns.

Only a subset of the leading PCs is typically rotated. Several criteria exist to guide the choice of this subset, especially the application of a scree test and the North et al. (1982) rule of thumb. However, testing the sensitivity of the resulting patterns to the number of rotated PCs also offers good practical guidance.

A more technical discussion of RPCA can be found in Barnston and Livezy (1987) where RPCA is advanced as a preeminent method for defining and monitoring of teleconnection patterns.

There are other analysis techniques that can be utilized in the study of teleconnection pattern, among them a method known as empirical orthogonal teleconnection (EOT). This technique is named such that is brings to mind EOFs, and is similar in that it yields temporally orthogonal time series. Developed by Van den Dool et al. (2000), EOT analysis is conducted by finding a base point in the domain that explains the most variance at all the other points combined, using linear regression. This leading spatial pattern is defined from the linear regression coefficients of this base point, while its time series is simply the raw time series at the base point. Subsequent patterns are obtained by repeating this procedure on a reduced data set, from which the first pattern has been linearly removed.

The analysis results in a series of spatial patterns, or EOTs, that are not constrained to be spatially orthogonal, but whose time series are independent. In this way, it is similar to RPCA. Other than the inherent simplicity, EOT analysis holds another advantage over RPCA: In RPCA, only a small subset of PCs is subject to rotation; no such truncation is required in EOT analysis. One downside to EOT analysis is that, similar to the traditional correlation analysis, it is based on the

variability explained by one grid point across the domain, while EOF LVs are fundamentally leading patterns of variability. Stated differently, for each EOT iteration the time series is constrained to be the raw time series at some grid point.

1.2 Leading Monthly Teleconnection Patterns in Northern Winter

The leading patterns of recurrent height variability are extracted from rotated principal component analysis and shown in Figure 1.2. The December, January, and February anomalies during 1979-2008 winters were analyzed in the 30°S-90°N domain. Analysis was conducted at the 200-hPa level in order to also capture the tropical-extratropical interactions (e.g., ENSO related) that are prominently manifest in the upper troposphere, for reasons stated earlier. Height anomalies were multiplied by the square-root of the cosine of latitude to achieve grid-area parity, which prevents polar regions with many more points on a regular latitude-longitude grid, from unduly influencing the analysis. The covariance, rather than correlation, matrix was analyzed so that regions with large variance can exert greater control on the analysis outcome. The eight leading PCs were rotated using the varimax criterion. The PCs are normalized and dimensionless and the spatial patterns (loading vectors) show nothing but the regression of the PCs onto the 200-hPa height field.

The leading pattern explains ~15% of the monthly variance in the domain, with two centers of action in the Atlantic sector. Note the spatial similarity to the Atlantic basin teleconnectivity structure in Figure 1.1. This leading pattern is clearly the NAO. Its structure is consistent with its historical characterization as a north-south dipole in sea-level pressure that represents out-of-phase fluctuations of the Icelandic Low and Azores High. For example, Hurrell's monthly NAO index is

constructed from the difference of normalized sea-level pressure anomalies at Ponta Delgada, Azores and Stykkisholmur, Iceland; the NAO pattern depicted in Figure 1.2 is thus in its positive phase, which strengthens the regional winter circulation features. The identification of NAO as the leading pattern in the 200-hPa analysis is important both for explanation of regional variance and for showing NAO variability to be temporally orthogonal to the other NH variability patterns. The NAO pattern is manifest on time-scales ranging from sub-seasonal to decadal, as seen in Figure 1.3. The NAO pattern is closely linked with meridional excursions of the Atlantic jet stream and associated storm tracks.

The second, third, and fourth leading patterns all have centers of action in the Pacific sector, attesting to RPCA's skill in separating overlapping spatial structures. The second leading pattern represents higher geopotential heights in all sectors of the northern subtropics, but especially over the central/eastern Pacific. Higher upper-level heights are typically associated with a warmer air-column underneath, since the atmospheric tends toward hydrostatic balance. The pattern of variability is thus associated with a warming of the tropics, such as during El Niño winters. The presence of a subtropical ridge to the southeast of the Hawaiian Islands is indicative of linkage with ENSO, for deep convection in this tropical Pacific sector and the related divergent outflow are linked with the development of an upper-level anti-cyclonic circulation in the subtropics. The subtropical ridge also reflects the southeastward extension of the Asian-Pacific jet in El Niño winters toward western North America. The ENSO pattern is also characterized by an east-west dipole near North America with a negative anomaly along and off the west coast and a positive

anomaly near the south shore of Hudson Bay. The PC associated with this spatial pattern exhibits mostly interannual variability and is correlated (r=0.6) with the Niño 3.4 index, which is the average sea-surface temperature anomaly in the central-eastern equatorial Pacific (5°S-5°N, 170°W-120°W) and operationally used to define the state of ENSO. While this pattern, which explains ~13% of the monthly winter variance, is characterized as the ENSO response, the related PC exhibits some long-term trend as well. It is remarkable that rotated principal component analysis of upper-tropospheric heights can identify the ENSO-related height pattern without any reference to the underlying SST variability. Note that traditional teleconnectivity (Figure 1.1) analysis of the 500-hPa height variability in the same period was unsuccessful in this regard, as is RPCA of the 500-hPa height field.

The third and fourth leading patterns of Northern winter height variability each explain ~11% of the monthly variance. The third leading pattern in Figure 1.2 consists of a north-south dipole in the North Pacific with a downstream height anomaly over eastern North America centered over Hudson Bay. This pattern is referred to as the NPO/WP pattern as the related sea-level pressure pattern (shown later) closely resembles the North Pacific Oscillation, a recurrent subseasonal variability pattern in sea-level pressure, first identified by Walker and Bliss in 1932. The 'West Pacific' part of the name is from Wallace and Gutzler's (1981) teleconnection analysis of 500-hPa heights. The NPO/WP pattern can be viewed as the NAO analog in the Pacific basin: both patterns describe subseasonal height fluctuations in the jet-exit regions of the climatological jets streams. The fluctuations have a meridional dipole structure with a stronger polar center in both cases, and

linked with meridional displacements of the jets and related storm tracks. A multivariate description of the NPO/WP pattern and its similarity with the NAO can be found in Linkin and Nigam (2008).

The fourth leading pattern is the PNA, defined by the coherent arcing pattern of height fluctuations of alternating signs, beginning with the center over Hawaii and followed by centers over the tip of the Aleutians, northwestern North America, and Southeast US. In the positive phase (depicted), the pattern consists of positive height anomalies over northwestern North America. In the Pacific sector, the height anomalies represent eastward displacement and meridonal focusing of the Asian-Pacific jet. It is interesting to note the position of the subtropical ridge in the PNA and ENSO-related patterns, as this is helpful in pattern identification: The ridge is over the Hawaiian Islands in the former but southeastward of Islands in the latter. The variability time scales of the patterns are also distinct: subseasonal and interannual, respectively (Fig. 1.3). The separation of the PNA and ENSO-related patterns is important as PNA was once viewed as the extratropical response of ENSO (e.g. Horel and Wallace, 1981). The PNA and NPO/WP patterns are also distinct, notwithstanding the broadly similar structure over the North Pacific–North American region; closer inspection reveals the two patterns to be in spatial quadrature in this sector; for example, the NPO/WP trough tracks the North American coastline, which is a nodal line in the PNA pattern.

1.3 Surface Temperature and Precipitation Impacts of the Leading Patterns

Teleconnection patterns are of considerable interest because of their impact on surface hydroclimate. Significant climate anomalies on subseasonal to interannual

time scales are often attributable to a dominant phase of one or more teleconnection patterns. Figure 1.4 shows the sea-level pressure, surface temperature, and precipitation footprints of the NAO. The temperature and precipitation data sets used in this analysis are from the Climate Research Unit of the University of East Anglia, namely the TS 3.1 climate database. (Note that in figures showing temperature and precipitation correlations, a contour interval of 0.15 is chosen. This value closely corresponds to the 85% confidence limit according to a student's t-test, while the second contour of 0.3 exceeds the 99% confidence limit.) The sea-level pressure pattern bears striking resemblance to the 200-hPa height pattern (Fig. 1.2a), indicating a generally equivalent-barotropic vertical structure. The strongest impacts of the NAO emerge over Europe and North Africa. The positive phase of the NAO results in nearly all of Europe experiencing above-normal temperatures, while cooler temperatures prevail from Saharan Africa east-northeastward to the eastern Mediterranean, Middle East, and the Arabian Peninsula. The temperature pattern at the surface results largely from advection of climatological temperature by the NAO circulation; for example, cooler temperatures over Africa arise from the cold advection by northeasterlies tracking the eastern flank of the high sea-level pressure cell. Correlation coefficients are shown in Figure 1.4 to indicate the significance of the impact, although they conceal the fact that temperature anomalies over Europe are larger than those over Africa. The precipitation pattern likewise shows a wet-dry dipole with northern Europe experiencing above-normal, and the Iberian Peninsula and southern Europe below-normal precipitation. This impact is not obvious from the geopotential and SLP patterns unless the impact of NAO on the jet stream, and thus

storm tracks, is considered. In the depicted positive phase, NAO results in enhanced zonal wind north of the Azores center and reduced zonal wind to the south. The northward displaced jet stream and storm track account, in part, for the observed precipitation dipole.

The NAO also influences the surface climate of North America as well, but to lesser extent than over Europe. A north-south dipole in temperature is again observed: cold in northeastern North America, warm to the south; both consistent with the regional sea-level pressure signal. The precipitation impacts are generally less coherent and significant than in Europe.

The surface signatures of the ENSO-related pattern are shown in Figure 1.5. The SLP signature is notably weak and focused in the Gulf of Alaska. Unlike NAO where regional thermal advection shaped surface temperature, the significant ENSO-related warming of the global northern Tropics (at both lower and upper levels) results from the propagation of atmospheric waves instigated by ENSO-related diabatic heating changes over the tropical Pacific. There is also a tendency for warmer winters across much of North America, centered on the US-Canadian border. Precipitation impacts are also notable in the deep Tropics, with drying in eastern South America and increased precipitation over eastern Africa. The ENSO-related pattern results in a southward shift of precipitation across North America with increased precipitation along the US West Coast and southern tier states. Noteworthy, too, are the positive precipitation anomalies over the northern Indian subcontinent, including the Himalayas. It is important to note that Figure 1.5 does not fully capture

the canonical ENSO impact on winter hydroclimate (e.g., as defined from correlations of the Nino3.4 SST index) but comes close in most regions.

The NPO/WP pattern results in significant modulation of the North American surface climate (Figure 1.6). The SLP pattern is robust and oriented much as the NAO's, reflecting similar variability mechanisms. The NPO/WP circulation in the lower troposphere leads to impressive temperature correlations (exceeding 0.6) over central-eastern North America from anomalous thermal advection and related meteorological feedbacks. Intrusion of the sub-Arctic air into the continental interior in the negative NPO/WP phase (weakened Aleutian Low) leads to below-normal temperatures, especially to the east of the Rockies, for example. The high correlations suggest that between one-quarter and one-half of the monthly temperature variance in the core influence region is explainable by NPO/WP variability. Importantly, this shows that the NPO/WP is a more influential pattern over North America than the NAO, whose strongest impacts are over Europe. The precipitation impact of the NPO/WP is weaker and the spatial pattern less coherent but potentially important in the Pacific Northwest and southern Great Plains. Like the NAO, the NPO results in meridional perturbation of the jet stream in its exit region; since this occurs over the wide Pacific Basin, the related storm track modification is not manifest in analysis of continental precipitation.

The PNA pattern's influence on North American surface hydroclimate (Figure 1.7) is, perhaps, most impressive. The sea-level pressure footprint in the Bering Sea and Gulf of Alaska is ~6 hPa, larger than of the other Pacific basin patterns, including ENSO. The temperature impact is characterized by a strong northwest-southeast

dipole across North America. Not surprisingly, the impact is focused on Northwest Canada and the Southeast US, the third and fourth centers of action of the pattern, respectively; again, with anomalous thermal advection defining the large-scale impact structure, if not its amplitude. The PNA response is defined by large correlations over interior eastern North America, centered on the Tennessee and Ohio Valleys and extending across the Great Lakes into northern Canada. A similarly signed signal is evident in the Pacific Northwest and Alaska as well. The positive-phase PNA precipitation response (Figure 1.7b) thus consists of only deficits across the US. The deficit over the eastern US results from the southward displacement of the Atlantic jet and storm track which are linked to the circulation anomalies associated with the third and fourth centers of the PNA height pattern.

1.4 Associated Sea Surface Temperature Anomalies

The above-described teleconnections represent standing modes of atmospheric circulation variability on subseasonal-to-interannual time scales. As such, it is of interest to inquire into the nature of related sea surface temperature (SST) anomalies, which in the Pacific basin can provide additional discrimination between the overlapping height variability patterns. Figure 1.8 shows the SST correlations of the four PCs. The NAO SST footprint reveals a characteristic tripole feature in the Atlantic basin, with cooler temperatures underneath strengthened westerlies in the north Atlantic. SST anomalies associated with the NAO also appear in the extratropical Pacific which are only slightly weaker than in the Atlantic. It is noteworthy that NAO variability is not correlated with tropical Pacific SSTs, at least contemporaneously during Northern winter months. Herein lies a great dilemma that

serves as the basis for a significant portion of contemporary sub-seasonal to interannual climate research: ENSO, which is slowly varying and more predictable on seasonal time scales, explains relatively little hydroclimate variance in the Northern extratropics. The NAO, by contrast, explains more surface climate variance but is substantially less predictable. Not surprisingly, the SST signature of the ENSO-related height pattern consists of large tropical correlations that resemble El Niño SSTs in the equatorial Pacific. Notable correlations are also present in the western Indian Ocean and the tropical and extratropical Atlantic. These include the well-documented ENSO links to warming of the adjacent basins, as well as capturing of more than just ENSO variability by this PC; including, possibly, the secular trend and multidecadal variability. The NPO/WP's SST correlations are not unlike NAO's Atlantic ones: a weak, tripolar, horseshoe-like structure in the extratropical basin; unlike NAO, however, it exhibits weak links with other basins.

The PNA SST correlations are broadly similar to the NPO's – a SST tongue extending from Japan into the midlatitude Pacific, surrounded by opposite-signed SSTs along the North American coast from the Aleutians to Baja Peninsula – but somewhat stronger, especially in the deep Tropics. A helpful distinction is the placement of the coastal anomalies: the off-coastal maximum in NPO/WP vis-à-vis the coastal maximum in PNA. The PNA SST correlations extend into the equatorial Pacific (Figure 1.8d), as noted above. This pattern was once thought to be the extratropical atmosphere's response to El Niño because of such correlations, despite the dominant intraseasonal time scales of its PC (or teleconnection index) and the modest correlation (0.3~0.4) of the latter with the Niño 3.4 SST index.

The contemporaneous SST correlations of the recurrent 200-hPa height variability patterns raise the interesting question of cause and effect: Are the height patterns forced by the underlying SST patterns, or vice-versa? The answer to this question is, unfortunately, complex as it is dependent on both the basin region and the variability pattern. Generally speaking, SST variations in the deep tropics (e.g., ENSO related) are influential on the atmosphere on monthly time scales whereas variations in the middle-high latitude basins are the response. Consider the NAO: In the displayed phase (positive), the SLP pattern (Figure 1.4c) strengthens both the Icelandic Low and Azores High along with a northward displacement of the jet stream and storm track. This will result in anomalous westerly wind stress on the ocean northward of the climatological jet position, leading to increased vertical mixing and latent-heat flux, and thus cooling of the surface layer. Similar arguments can be applied to the other associated SST centers in the central and southern North Atlantic.

1.5 Subseasonal Tropical Variability – Madden-Julian Oscillation

The ENSO-related pattern discussed above reveals one way in which the tropics can influence the extratropics: An interannual shift in the preferred area of tropical convection/precipitation leads to anomalous divergent motions, which generate a Rossby wave source that, in turn, alters midlatitude storm tracks and extratropical climate. Zonal variations in tropical convection occur on time scales other than interannual ones as well: The Madden-Julian Oscillation (MJO; Madden and Julian, 1971) – representing convection variability in the tropical Indian Ocean

and Western Pacific basins on 30-50 day time scales – can, like ENSO, influence the climate in the extratropics, albeit on subseasonal time scales.

When the MJO is active, convection is enhanced over the eastern Indian Ocean at the expense of the West Pacific. This generates an anomalous divergent circulation that leads to retraction of the East Asian jet. The jet retraction and related modulation of storm tracks influence the circulation and hydroclimate over the North Pacific and North American regions; for example, weaker Aleutian Low and higher than normal heights over eastern North America. These MJO influences can implicitly influence the NAO and PNA structure but only modestly as these teleconnection patterns are robustly manifest in the MJO-filtered data as well; this will be made clear in later chapters.

1.6 Annular Modes

Closely related to teleconnections are the annular modes, which have received considerable attention in recent years (e.g. Thompson and Wallace, 1998). While teleconnections are the climate links between geographically separated regions, the annular modes represent the seesaw (i.e., out-of-phase links) between the poles and the surrounding midlatitudes; annular modes can be viewed as the teleconnections of the polar region. The annular modes in the Northern and Southern Hemispheres are referred to as the Arctic and Antarctic Oscillation (AO and AAO), respectively. The annular pattern is obtained from EOF analysis of the monthly 1000 hPa geopotential height anomalies (700 hPa for SH) poleward of 20^{o} for the entire year (not shown). Key differences from the previous RPCA analysis are the lack of rotation of the PCs and the search for recurrent patterns among all calendar month (and not just winter)

anomalies. Note, unrotated analyses often generate more spatially extended patterns in order to maximize the explanation of variance. Also, 'annular pattern' rather than 'annular mode' is, perhaps, more reasonable terminology as only spatial (and not spatiotemporal) variability is analyzed for their extraction.

The annular modes bear close resemblance to the leading mode extracted from RPCA of 200-hPa heights in each hemisphere. The AO has a stronger, coherent center of action in the Aleutians in addition to the essential elements of the NAO pattern (Figure 1.2). Not surprisingly, AO's year-round temperature and precipitation impacts are very similar to the winter impacts of the NAO (cf. Figure 1.4**)**. The close similarity of AO and NAO has led many to question whether the NAO is merely a regional manifestation of the larger-scale annular mode (AO). For the remainder of this thesis, results will be discussed in terms of the NAO, since the methodology employed (RPCA) most frequently lends itself to more regionally-confined patterns, more consistent with analyses that target the NAO. In any case, the NAO and AO principal components are highly correlated, so the reader should not be overly troubled by the lack of explicit attention paid to the latter.

1.7 Motivating Topics

Thus far, some background on teleconnection patterns and their importance in studying climate variability has been presented. There are some keys areas in which the research results presented in subsequent chapters seek to improve understanding of teleconnection patterns and their physical underpinnings.

1. The MJO teleconnection pattern – The MJO is known to be important for influencing midlatitude climate variability, but this is often expressed in terms of its impact on well-studied patterns of climate variability such as the PNA and NAO (e.g. Johnson and Feldstein, 2010; Lin et al., 2009; Zhou and Miller, 2005). In many ways this is similar to the decades-old ENSO vs. PNA paradigm. Therefore, an effort is made to elucidate the MJO teleconnection pattern from a purely MJO-centric perspective (Chapter 2), followed by research that seeks that pattern among other temporally independent modes of variability.
2. Subseasonal teleconnection evolution -- Climate teleconnections, discussed above, were obtained from the analysis of monthly-averaged anomalies, using techniques keyed to an optimal accounting of the temporal variance. These attributes steered the analysis towards extraction of the mature-phase of the leading teleconnection patterns. Monthly-averaging filtered the large-scale synoptic waves in the troposphere and facilitated focus on the 'standing' component of low-frequency variability. A month is not too long a period in context of large-scale ocean-atmosphere interaction, but it is an extended averaging period in context of the dynamical and thermodynamical processes generating climate teleconnections. These processes may evolve rapidly – on pentad time scales – and their resolution is critical for the description of the nascent-to-mature and decay phases of the teleconnection patterns, and for advancing understanding of the excitation mechanisms. Insights into the

evolution of teleconnection patterns can advance the subseasonal prediction of the climate system.

3. Tropical linkages – Whether the observed evolution of teleconnection patterns is influenced by tropical convection is an important question that has strong implications for subseasonal prediction. The extratropical response to the MJO, which is fundamentally a mode of subseasonal tropical convective variability, is a clear example. However, there are many studies that link PNA development to anomalous tropical convection on subseasonal time scales (e.g. Franzke et al., 2011). More recently, there is some research that links anomalous convection and SSTs in the tropical West Pacific to extratropical atmospheric climate variability, albeit on monthly time scales (Seager et al., 2014; Hartmann, 2015). Chapters 4 and 5 will seek to further understanding of this problem using robust observational techniques.
4. Attribution of extreme events – Teleconnection analysis might be used to reconstruct observed climate anomalies. The utility of this process is tested in Chapter 5 with respect to a recent extreme winter. This process has the potential to bolster real-time attribution of climate anomalies and improve the operations to research (O2R) process in operational prediction centers.

1.8 Dissertation Structure

The following chapters consist of largely independent research studies that each address one or more of the motivating topics above. Most of the work has been published in *Journal of Climate* during the course of dissertation research, with another manuscript currently being prepared based on Chapter 4.

Chapter 2 presents the work published in Baxter et al. (2014), which assesses the subseasonal evolution of wintertime MJO impacts on the contiguous U.S. Additionally, this work establishes a preferred monitoring index for the MJO that best relates to extratropical impacts and itself may be more predictable. Chapter 3 is based on Baxter and Nigam (2013) which assesses the subseasonal evolution of teleconnection patterns, especially the PNA. Chapter 4 seeks to uncover the MJO teleconnection alongside the prominent patterns of variability presented thus far. In this way, it seeks a separation of the MJO from other patterns analogous to the PNA-ENSO separation shown above. The tropical linkages of the various patterns are analyzed. Chapter 5 is based largely on Baxter and Nigam (2015), which examines the key role of the NPO/WP pattern in generating the extreme 2013-14 winter over North America. The Hartmann (2015) hypothesis regarding the role of Pacific SSTs and tropical convection is presented and called into question. Chapter 6 summarizes and discusses key results, presents concluding remarks, and details prospects for future work.

Chapter 1 Figures

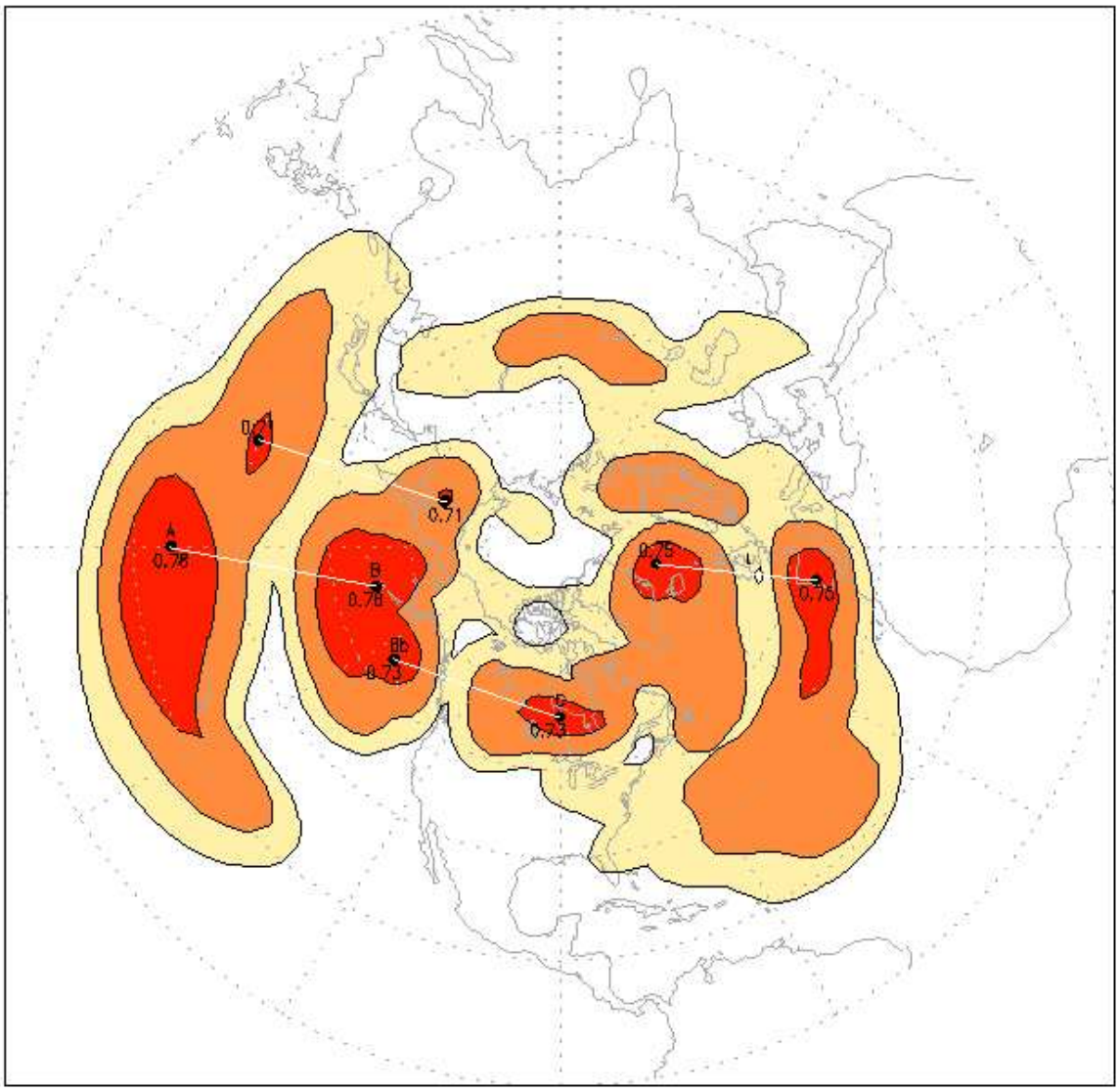

Figure 1.1a: 500-hPa geopotential height teleconnectivity map for Northern Hemisphere winter (DJF), comparable to seminal figure 7B in Wallace and Gutzler (1981). Contour/shading starts at a correlation of 0.5 and increases at 0.1 intervals. Points A, B, Bb, and C, refer to the centers of actions of the Pacific-North America (PNA) pattern. Points B and Bb are generally associated with the Aleutian Low center of action.

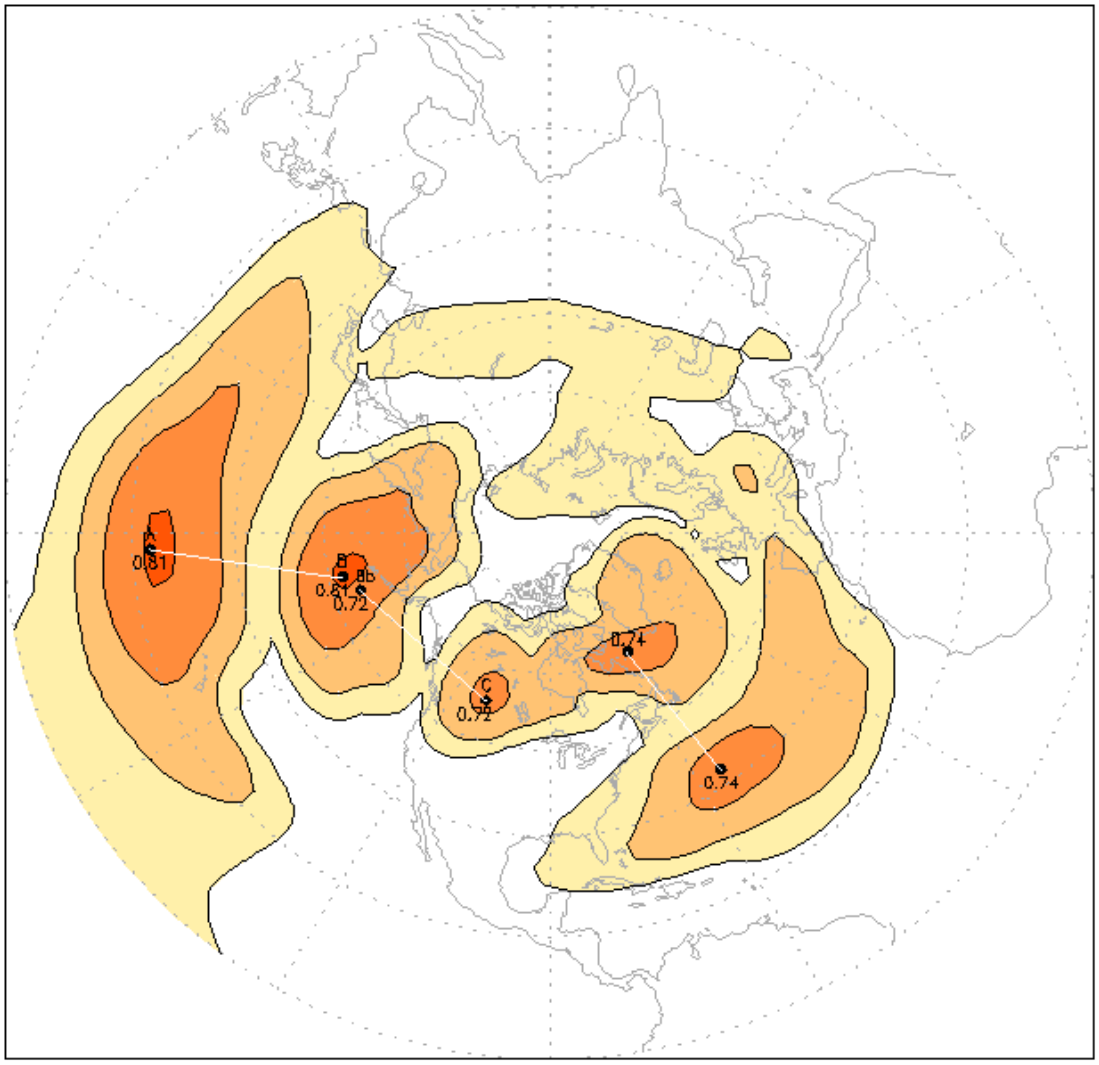

Figure 1.1b: 500-hPa geopotential height teleconnectivity map for Northern Hemisphere winter (DJF), comparable to seminal figure 7B in Wallace and Gutzler (1981) and Figure 1, except for a prolonged analysis period from 1949-2009. Contour/shading starts at a correlation of 0.5 and increases at 0.1 intervals. Points A, B, Bb, and C, refer to the centers of actions of the Pacific-North America (PNA) pattern. Points B and Bb are generally associated with the Aleutian Low center of action.

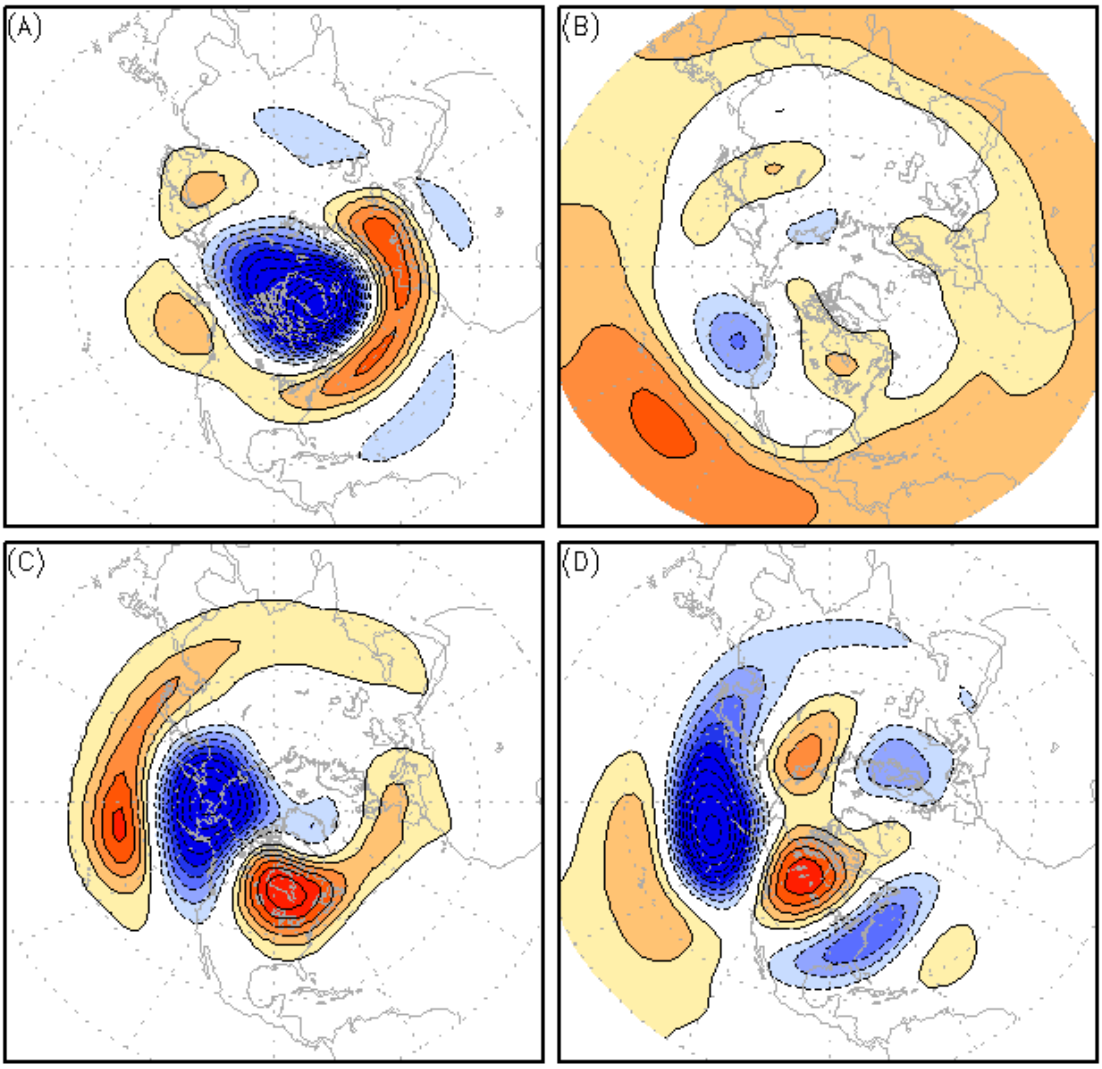

Figure 1.2: The four leading teleconnection patterns from a rotated EOF analysis conducted on monthly 200-hPa wintertime height anomalies: A) NAO, B) ENSO-related, C) NPO/WP, and D) PNA. The domain of the analysis is 30S-90N. Contour/shading interval is 10m; the zero contour is suppressed. Percentage of explained variance: A) 14.6, B) 12.5, C) 11.4, D) 11.1.

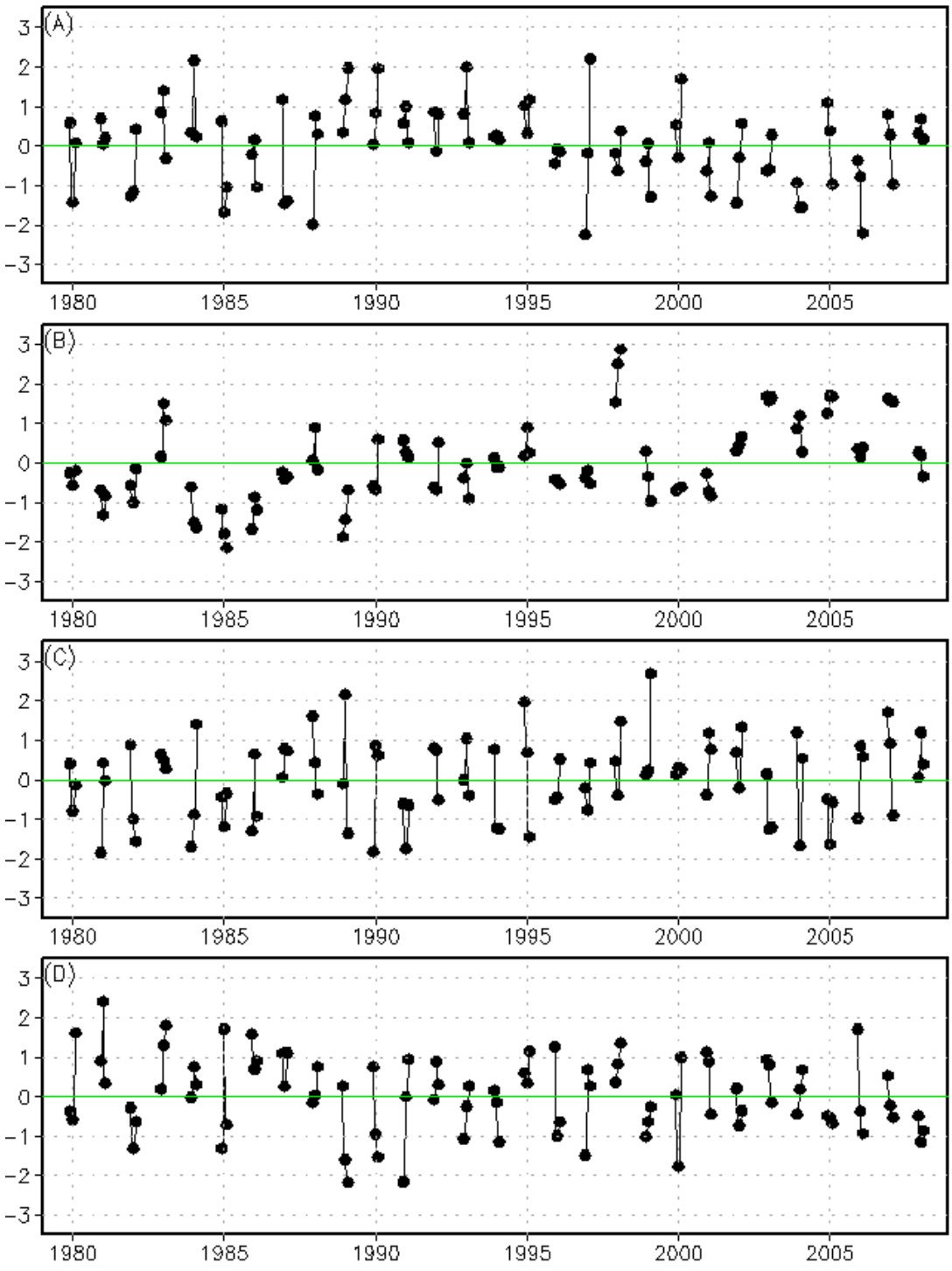

Figure 1.3: The principal component time series for each pattern is shown. A) NAO, B) ENSO-related, C) NPO/WP, D) PNA. Note that there are only values for the DJF season.

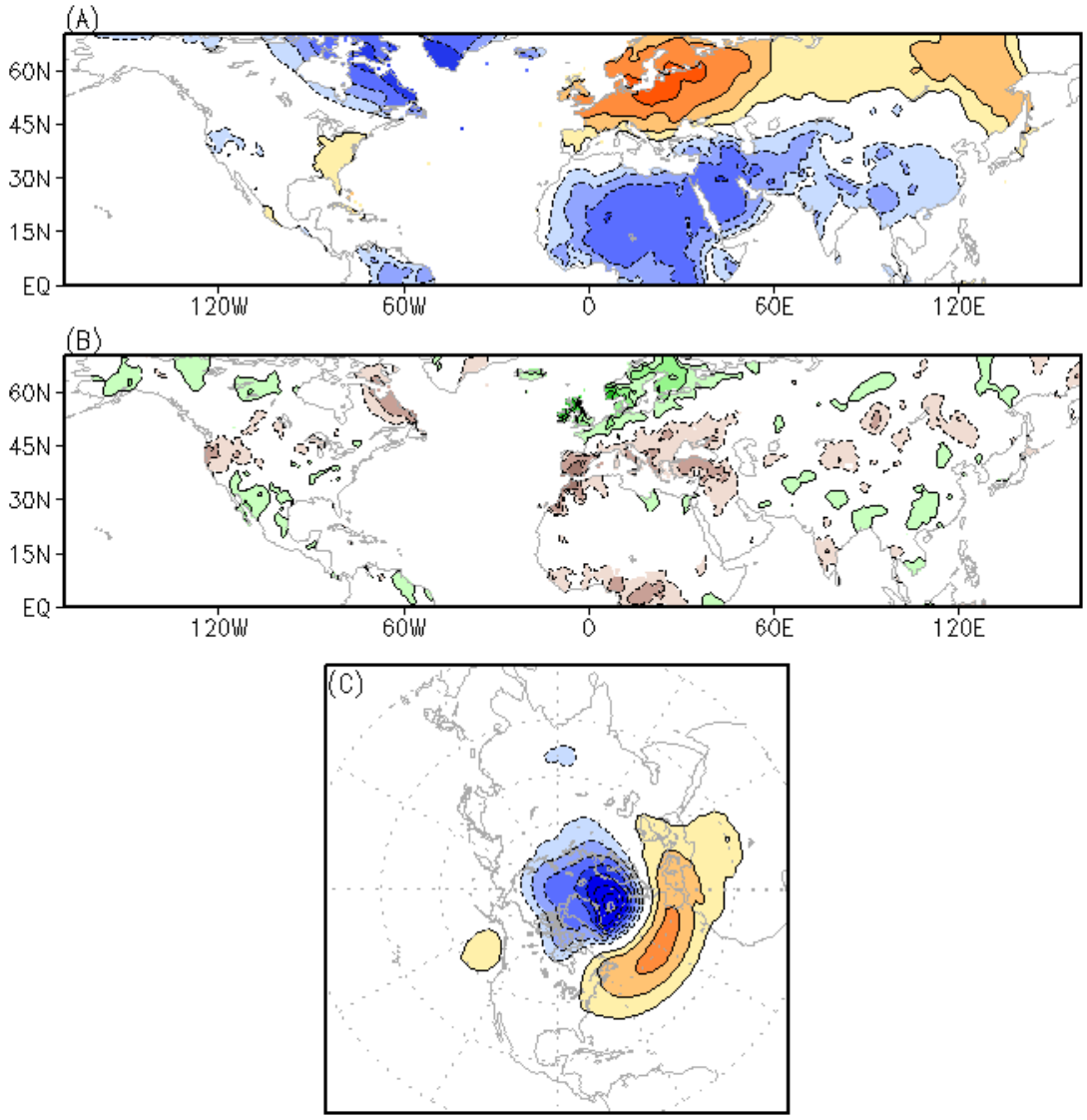

Figure 1.4: Temperature (A), precipitation (B), and sea-level pressure (C) footprints of the wintertime NAO pattern seen in figure 2. Correlation between NAO principal component and CRU temperature and precipitation is contoured at 0.15 intervals; the zero contour is suppressed. For sea-level pressure the regression coefficient between the principal component and the SLP field from the CFSR is contoured at 1-hPa intervals, and the zero contour is suppressed.

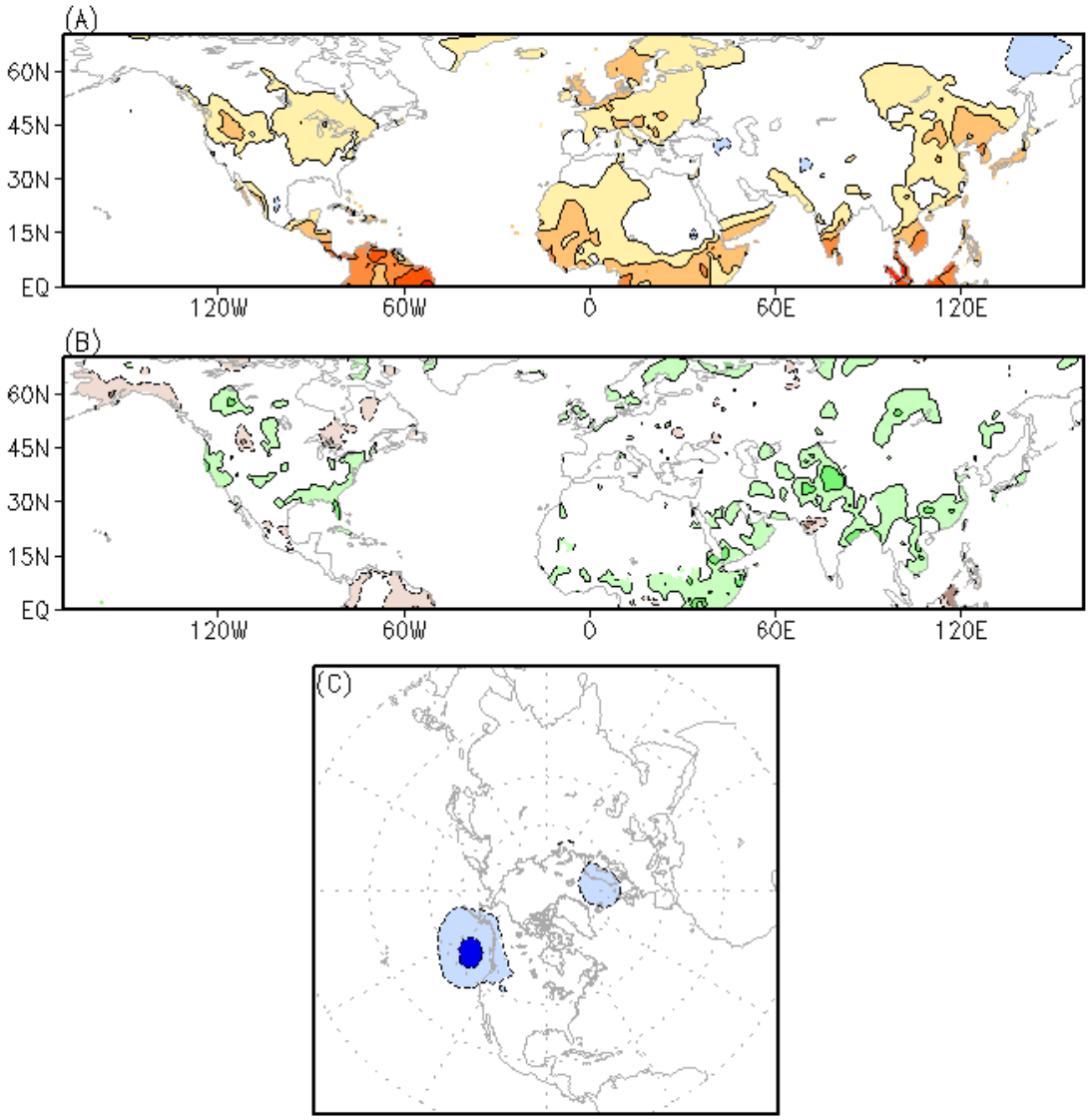

Figure 1.5: Same as in figure 3 expect for ENSO pattern.

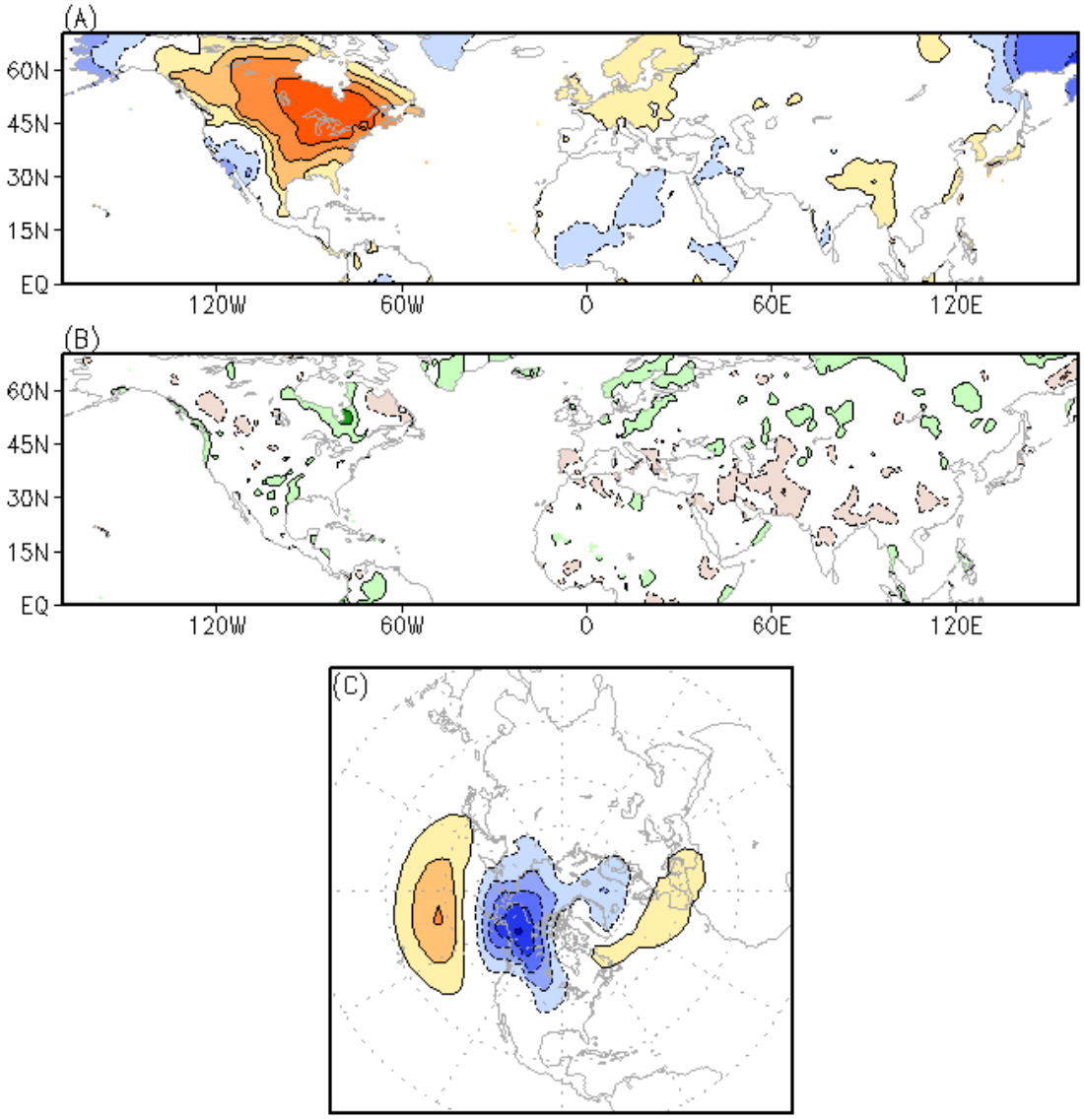

Figure 1.6: Same as in figure 3 except for the NPO/WP pattern.

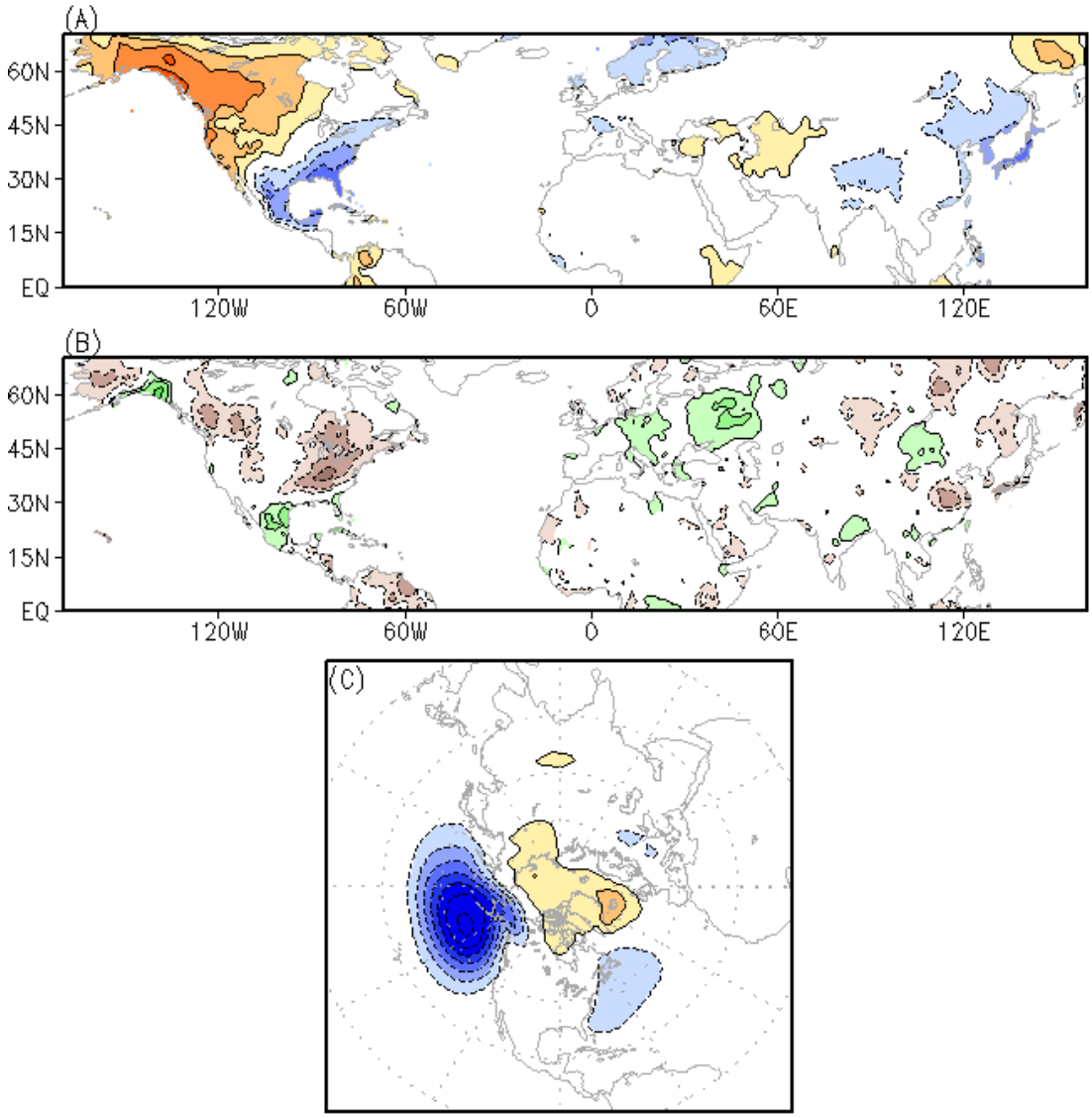

Figure 1.7: Same as in figure 3, except for the PNA pattern.

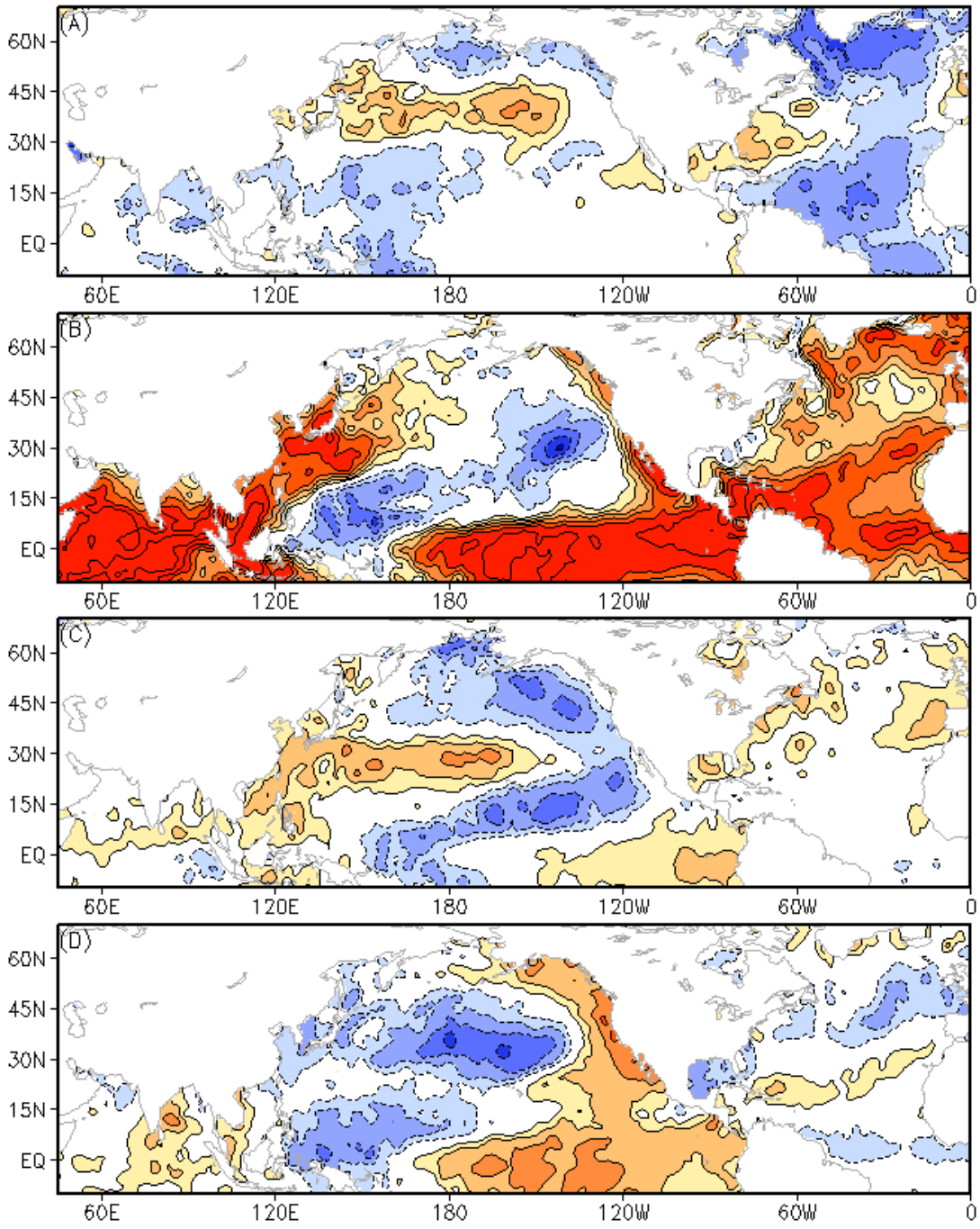

Figure 1.8: Correlation between the leading wintertime teleconnection patterns: A) NAO, B) ENSO-related, C) NPO/WP, D) PNA, and sea surface temperature anomalies. Contour/shading interval is 0.1 while the zero contour is suppressed.

Chapter 2: The MJO Extratropical Response and U.S. Climate Impacts

2.1 Background

The introductory chapter gave a broad background into teleconnection analysis and the various patterns that can be extracted via different types of analysis. It is found that a prominent pattern of atmospheric variability on monthly and seasonal time scales is related to ENSO, which influences the extratropics via the redistribution of convective heating and associated divergence in the tropics. The MJO is the dominant mode of subseasonal climate variability in the tropics, consisting of propagating patterns of convection coupled with upper- and lower-level winds (Madden and Julian 1971, 1972, 1994). One might expect, given the preceding discussion on ENSO, that the MJO could similarly impact the extratropics, albeit on subseasonal time scales. Indeed, numerous studies indicate that the MJO has a strong impact on climate variability in the extratropics through the propagation of a Rossby wave train associated with the anomalous tropical convection (Kiladis and Weickmann, 1992; Mo and Higgins, 1998; Matthews et al., 2004). The extratropical impacts of the MJO are often discussed in terms of the relationship between the MJO and major modes of extratropical climate variability, such as the Arctic Oscillation (AO) (Zhou and Miller, 2005; L'Heureux and Higgins, 2007) and North Atlantic Oscillation (NAO) (Lin et al., 2009). Riddle et al. (2012) details the lagged impacts of the MJO (as assessed by the Wheeler and Hendon (2004) MJO phases) on clusters of wintertime circulation anomalies over North America. These studies generally conclude that a positive (negative) NAO- (PNA-) type pattern follows a dipole of anomalous convection associated with the MJO where the convective phase is

centered over the Indian Ocean. The time scale for the tropical-extratropical teleconnection was found to range from about 10 to 20 days, with the impacts across the Pacific preceding those in the North Atlantic. Zhou et al. (2011) show the contemporaneous composites of temperature and precipitation by Wheeler and Hendon (2004) MJO phase, while Lin and Brunet (2008) show that the MJO has significant lagged impacts on Canadian wintertime surface air temperature (SAT). These studies underscore the development of positive temperature anomalies across parts of eastern North America following the aforementioned convective dipole associated with the MJO. Understanding the effects of MJO-related convection on the extratropics provides a useful tool in improving short term climate forecasts (~2-3 weeks).

Our purpose here is to investigate wintertime hydroclimate impacts of the MJO on the United States using lagged pentad composites. The use of lagged composites extends the limits of predictability when combined with skillful model forecasts of MJO evolution (Wang et al. 2013). Additionally lagged composites emphasize the physical nature of the subseasonal forcing, wherein there is necessarily some time lag between the initiation of anomalous convection and its mature extratropical response. The use of composites also allows for analysis of MJO impacts in terms of their manifestation in observations, not in terms of the effect on extracted patterns of circulation variability via data reduction techniques. The canonical patterns obtained from such techniques, such as the NAO and PNA, often constitute modes of variability intrinsic to the extratropical circulation. Chapter 3 will show that the linear removal of Wheeler and Hendon MJO footprints has little

bearing on the subseasonal evolution of the major global teleconnections in the 200-hPa height field, so it is important to assess the observed impact in order to appreciate the direct role of MJO forcing. We analyze composites that employ both the commonly used MJO index developed by Wheeler and Hendon (2004) and a velocity potential index used for real-time monitoring at NOAA's Climate Prediction Center (CPC). Comparing and contrasting the impacts captured by using both indices enables an assessment of the advantages and disadvantages of each index in the operational monitoring and forecasting context.

The data and methods used in the study, including a description of the two MJO indices in more detail, follow in the next section. Discussion of results and conclusions from this analysis follow in subsequent sections, respectively.

2.2 Data and Methods

a. Data

This study spans a period of 30 years (1979-2008). US surface air temperature (SAT) is derived from gridded COOP data at a 1o by 1o resolution (Janowiak et al., 1999). The CPC-unified precipitation data is used with a resolution of 0.25o by 0.25o (Xie et al., 2010). A square-root transformation is performed to normalize the precipitation data only for the purpose of significance testing. For atmospheric circulation, we use the latest data available from the Climate Forecast System Reanalysis (CFSR). This global data (200-hPa zonal wind and geopotential height) is gridded at a 2.5o by 2.5o resolution (Saha et al. 2010). At the same resolution, we employ outgoing longwave radiation (OLR) data from NOAA's polar-orbiting satellites (Liebmann and Smith, 1996) as a proxy for tropical convection.

In order to isolate subseasonal climate variability, the data is averaged over 5 days to construct the pentad data. For this wintertime study, winter is defined by the months December, January, and February and consists of 19 pentads beginning November 27. Pentad anomalies are then constructed by removing the raw, unfiltered pentad climatology. Finally, the seasonal mean anomaly is removed to eliminate interannual variability, thus isolating the subseasonal component of variability.

b. MJO Indices

As previously mentioned, two MJO indices are used in this study. The Wheeler and Hendon (2004) MJO index which is commonly referred to as the Real-time Multivariate MJO index (hereafter RMM) is a combination of the two leading principal components of a multivariate (outgoing longwave radiation (OLR), 850- and 200-hPa zonal wind) EOF analysis. These two PCs compose the two-dimensional phase diagram, divided into eight phases that correspond to the location of the enhanced convective phase of the MJO.

The CPC MJO index is constructed by calculating the extended EOF (EEOF) of 200-hPa velocity potential for 15 ENSO-neutral and weak ENSO winters during 1979-2000. The status of ENSO is determined using the official classification used operationally at CPC (http://www.cpc.ncep.noaa.gov/research_papers/ncep_cpc_atlas/8/ensoyrs.txt). Based on this classification, there are 15 winters (November-April) utilized in the analysis. Extended EOF analysis differs from traditional EOF analysis in that a time series of spatial patterns is substituted at each time step, allowing for a clean spatio-temporal analysis of the data. In this application, a ten pentad window is utilized. The first

EEOF consists of ten, time-lagged patterns that describe eastward propagation with a time scale of about 50 days. Ten MJO indices are constructed by projecting unfiltered pentad 200-hPa velocity potential onto each of the ten patterns that collectively constitute the first EEOF mode. This method of using some filtering in deriving the MJO loading patterns, but not filtering in real time, is similar to the method employed by Schreck et al. (2013). Negative indices correspond to the convectively active phase at the various longitudes (Figure 2.1).

c. Compositing and analysis procedures

Pentad composites are constructed by RMM phase and amplitude. Pentads are selected when the pentad amplitude of the RMM index is greater than or equal to one standard deviation. Likewise, composites based on the CPC MJO indices are constructed by selecting pentads where the index is greater than or equal to one standard deviation. We do not attempt to constrain the composites by assessing propagation of the convective anomaly. Such constraints would be difficult to implement in real time and would require subjective limits requiring data-limiting sensitivity analysis. Furthermore, the impacts of tropical convection on the extratropical circulation are not so much dependent on their eastward propagation as much as their not having too fast a phase speed.

Composites are made of OLR to assess where both the RMM index and the CPC index agree on the location of MJO related tropical convection. RMM phases 3 and 7 coincide with the active phases of CPC MJO indices 1 and 6, respectively. Figure 2.2 shows the dipole of tropical enhanced convection / suppressed convection between the Indian Ocean and the western Pacific that occurs during RMM phase 3

and CPC index 1 (spatial correlation of approximately 0.95). This dipole reverses during RMM phase 7 and CPC index 6 (not shown). Additionally, RMM phases 3 and 7 are the most frequently occurring phases during DJF.

In this study, we focus on the time-lagged, wintertime response of U.S. temperature and precipitation, as well as global 200-hPa circulation, to CPC indices 1 and 6 (RMM phases 3 and 7). Furthermore, composites are constructed for pentads in which CPC index 1 is greater than 1.0, but the RMM index has amplitude less than 1.0 or is not in phase 3. This method allows for a comprehensive analysis regarding the manner in which the two different indices capture MJO-related convection and its U.S. impacts. For example, if the characteristic convective dipole is present between the Indian and West Pacific Oceans and projects onto the CPC index 1 loading pattern but not onto the RMM index in phase 3, the resulting composites will be revealing in terms of determining the operational suitability of each index for use in extended range forecast applications. Statistical significance is calculated using a Student's t-test on standardized anomaly composites.

2.3 Results

a. United States SAT anomalies

In order to analyze MJO impacts on wintertime U.S. SAT, lagged composites are constructed for each RMM phase. This analysis reveals two primary findings: a) the development of a substantial positive SAT anomaly in the eastern U.S. following RMM phase 3, and b) the development of a negative SAT anomaly across much of the U.S. following phase 7 (not shown). The corresponding CPC MJO indices (1 and 6, respectively) reveal nearly identical SAT anomalies (Figure 2.3). However, the

CPC index composites contain significantly more pentads than the Wheeler and Hendon (WH, RMM) composites (WH3, n=58; WH7, n=52; CPC1, n=96; CPC6, n=79). This difference in sample size has three primary causes: 1) The RMM index calculation includes explicit removal of interannual variability, while the CPC index retains interannual variability, 2) The RMM index is more easily influenced by other tropical modes (i.e. atmospheric Kelvin waves and equatorial Rossby waves), and 3) The CPC index is not as easily broken down into distinct phases, so there are times when the convective maximum is shifted slightly east or west and the system projects on CPC index 1. Figure 2.3 shows the lagged SAT composite with respect to CPC index 1. The SAT anomaly reaches a maximum at a three pentad lag, centered over the Ohio Valley and Great Lakes with a magnitude in excess of 2oC. Likewise, the negative SAT anomaly that develops following a convective anomaly captured by CPC index 6 (not shown) maximizes at lags three and four.

This distinct evolution of a SAT anomaly following the development of an Indian Ocean/West Pacific convective anomaly dipole suggests that the convection captured by RMM phases 3 and 7 (CPC indices 1 and 6) are mainly responsible for MJO-related impacts in the U.S. This is supported by Lin et al. (2007) who suggested that extratropical response to tropical forcing fully develops in approximately two weeks. These composites appear to be consistent with the results of Lin and Brunet (2009), whose analysis was confined exclusively to Canada. These results also confirm in large part what Riddle et al. (2012) found in terms of lagged response to MJO forcing over the North America. That study, however, used cluster analysis to identify leading patterns of variability over North America, and found that three of

them are strongly influenced by MJO convective forcing. The composite patterns revealed here suggest that the MJO response is shifted slightly to the north when compared to Riddle et al. (2012). Additionally, the results are similar to what Zhou et al. (2011) found in terms of contemporaneous MJO composites, specifically a similar response during phases 4, 5, and 6 in that analysis, which is clearly seen here as a lagged response to forcing in phase 3. This is important because it suggests that the lagged response to phase 3 in RMM and CPC1 is robust and may be used to advance the lead time of skillful climate forecasts over certain regions of the U.S.

b. United States precipitation anomalies

In addition to the substantial SAT anomalies that develop in response to MJO forcing, significant precipitation anomalies occur. Several studies (Mo and Higgins, 1998; Higgins et al., 2000) have established connections between MJO-related tropical convection and U.S. West Coast precipitation. Our contemporaneous composites (not shown) of precipitation agree with this well-known relationship, namely, a positive West Coast precipitation anomaly during RMM phase 3.

Of greater importance to this study are the precipitation impacts that occur one to four pentads following a tropical convective anomaly. Figure 2.4 shows a side-by-side comparison of lagged (lag 1-3 pentads) precipitation composites with respect to RMM MJO phase 3 and CPC index 1. At a three pentad lead, both composites agree on enhanced precipitation from the southern Plains to the Great Lakes, and decreased precipitation in the Southeast, mainly Florida. Lin et al. (2010) used a simple modeling analysis to show that anomalous convection in the Indian Ocean and subsidence in the West Pacific forces a similar precipitation response in the eastern

half of the U.S. A physical explanation for this precipitation response will be explored in the next subsection by analyzing the 200-hPa circulation response to MJO forcing. These results are consistent with what Becker et al. (2011) and Zhou et al. (2011) showed using contemporaneous composites based on the RMM index.

Another interesting result of our analysis is the difference in West Coast precipitation, especially at lags of two and three pentads. The RMM composite places a significant negative anomaly over northern California at a two pentad lag, while the larger CPC index 1 composite is statistically insignificant at that lag. The origin of this discrepancy is not readily apparent and will be explored in a subsequent section.

c. *Circulation anomalies*

In order to physically explain the MJO's U.S. winter hydroclimate impacts, composites of 200-hPa geopotential height (Figure 2.5) and zonal wind are constructed. A contemporaneous positive height anomaly exists over India and in the North Pacific (a modulation of the Aleutian Low) in both the RMM phase 3 composite and CPC index 1 composite. This height anomaly teleconnects to one developing over eastern North America. This teleconnection is supported by Lin and Brunet (2008) who indicated a Rossby wave train results in circulation anomalies over North America in response to MJO-related convection. Furthermore, results from Bader and Latif (2005) suggest that a positive height anomaly over India is teleconnected to a positive height anomaly over eastern North America. While the positive height anomaly builds over eastern North America, negative height anomalies shift eastward across the high-latitude portions of the continent. This is

interesting given that Baxter and Nigam (2013) showed that the canonical PNA and NAO patterns obtained via rotated EOF analysis tend to exhibit some retrogression at high latitudes, suggesting that the MJO response seen here cannot simply be dismissed as a manifestation of the PNA or NAO. The composite pattern culminates with a westward-shifted NAO-type dipole across the North Atlantic and eastern North America.

These large-scale circulation impacts can also be seen in the 200-hPa zonal wind composites. Anomalous convection in the eastern Indian Ocean and subsidence in the West Pacific is associated with a retraction of the East Asian jet. Figure 2.6 shows the lagged (lags 1-4) composites of 200-hPa zonal wind anomalies overlaid with the climatological zonal wind at 200 hPa. Coinciding with the developing height anomalies over North America, a tripole of zonal wind anomalies develops at lags of two to four pentads across eastern North America and the North Atlantic.

Combining the 200-hPa geopotential height and zonal wind anomalies infers a northward moving and weakening eastern North American jet stream two to four pentads after a substantial positive convective anomaly in the eastern Indian Ocean. Synoptically, this moves the right entrance region associated with enhanced upward motion north of its climatological position resulting in the observed precipitation anomalies (discussed in section 4b) at the same lag. Subsidence in the Indian Ocean and convection in the Western Pacific (RMM phase 3; CPC index 6) produces a similar, but opposite extratropical response (not shown). The response is not perfectly linear, but this is not surprising given that there is a substantial nonlinear

component to the extratropical response to tropical forcing (Lin and Derome, 2004; Hoerling et al., 1997).

d. Differences in impacts between RMM and CPC indices

So far we have shown that using composites based on the RMM MJO index and those based on CPC indices are very similar when they both capture the same tropical convective anomaly. In order to assess which index is a better operational tool, composites were made of temperature, precipitation, and circulation fields when CPC index 1 indicated an upper-level divergence anomaly over the eastern Indian Ocean, but the RMM index was either out of phase 3 or had amplitude less than 1.0. There are 56 such pentads over the 30-year period, most of which are characterized by the RMM index indicating a different phase. Interestingly, the composite of OLR is nearly identical to composites of OLR based on RMM phase 3 and CPC index 1 individually.

At a lag of two to four pentads, very similar SAT and hydroclimate impacts are observed across the eastern two-thirds of the US (Figure 2.7 compared to Figures 2.3 and 2.4). A major difference in precipitation occurs in northern California at a two pentad lag, where the RMM phase 3 composite (Figure 2.4) shows a dry anomaly but the composite based on CPC index 1 when the RMM index is not in phase 3 shows a substantial positive precipitation anomaly. Figure 2.8 confirms that the evolution of 200-hPa geopotential height anomalies is nearly identical in this composite to those composites based on the total sample of MJO events captured by either index.

Composites of surface air temperature and 200-hPa geopotential height when the Wheeler and Hendon index is in phase 3, but the amplitude of CPC MJO index 1 is less than one standard deviation, reveal an incoherent wave pattern with a less significant surface temperature footprint (not shown). While the sample size in this situation is fairly small, it does suggest that projection onto the velocity potential index serves as a necessary condition for U.S. impacts. Indeed, a plausible physical hypothesis of extratropical MJO teleconnections hinges on the development of subtropical vorticity anomalies that are forced by anomalous meridional divergence in the tropics. It therefore seems reasonable that in the absence of a substantial upper-level velocity potential anomaly there is not likely to be a robust wave response in the extratropics.

When taken together, the above results suggest that a significant convective anomaly dipole (greater than one standard deviation) between the eastern Indian Ocean and the West Pacific forces a substantial climate response in the U.S. The CPC MJO index provides a simpler and more physically sound means through which to observe the patterns of convection that force U.S. climate variability, since the RMM index, which includes only zonal wind components and OLR data, may not accurately capture the meridional divergent circulation. Additionally, since OLR is not utilized, the extended range predictability of large-scale tropical velocity potential anomalies may be promising in the current suite of extended range climate models.

2.4 Discussion and Implications

The composite analysis reveals the observed impact of MJO convective forcing on the U.S. during northern winter for select areas of anomalous convection (i.e. RMM phase 3/7). The greatest lagged impacts occur following convection captured by CPC indices 1 and 6 (RMM phase 3 and 7). These lagged temperature and precipitation footprints also show up as contemporaneous impacts during RMM phase 5 (active CPC index 3/4). Because the lagged composites are similar to the contemporaneous composites (not shown), they must be preferred in an operational setting since they extend lead time and are also more physically consistent with the occurring phenomenon. While Rossby waves can break into the Tropics and be important for organizing or preconditioning MJO events (Lin et al., 2009), we are primarily concerned with lagged effect of tropical forcing on the extratropics at the subseasonal time scale. The extent to which contemporaneous composites are significant can only be due to the lagged impact from previously occurring anomalous convection that propagated in a canonical fashion, or from the feedback of ongoing extratropical circulation anomalies onto the tropical variability.

The composite analysis also reveals that while the extratropical circulation pattern forced by the MJO may project onto the NAO or PNA loading patterns, it is clearly neither in a canonical sense. This leads to a hypothesis which suggests that the observed impacts from each MJO event are some combination of the composite pattern revealed in the analysis and the evolving extratropical state. The MJO response can be modified by the modes of variability intrinsic to the extratropical circulation (NAO, PNA, etc.). However, the tendency toward preferred states of

various extratropical patterns is real and due to aliasing of the tropical-extratropical teleconnection onto those loading patterns. Those loading patterns are traditionally calculated in ways that minimize the tropical response on subseasonal time scales by utilizing variables that emphasize variability nearer the pole and are overwhelmingly due to extratropical dynamics.

In light of the above discussion regarding the potential differentiation between the MJO response and internal extratropical variability, it may be instructive to think about the amount of pentad-to-pentad variance explained by the MJO extratropical response. Furthermore, this can be put in the context of similar analysis conducted with extratropical modes of variability. Utilizing correlation analysis between the CPC MJO index and the temperature, precipitation, and circulation fields (not shown), it is found that MJO-like convective forcing explains about 5-9% of the temperature and precipitation variance across the main impact regions east of the Rocky Mountains (composites shown in Figures 2.3 and 2.4). In the circulation field, 8-10% of the variance in 200-hPa height (and zonal wind) is explained across the Pacific-North America region. These figures are on par with variance explained by the pentad index of the Arctic Oscillation (AO, Thompson and Wallace, 1998), a major mode of variability monitored especially during northern winter. The AO index explains 6-10% of the surface temperature variance over regions similar to those impacted strongest by the MJO. This discussion is included to provide the reader some context as to the relative importance of the MJO extratropical response.

The result of the composite analysis utilizing the CPC MJO index suggests that a simple velocity potential index may be preferable in an operational setting

when designing an objective prediction tool based on MJO activity. There are two possible weaknesses in the RMM index that give the CPC index an advantage in this regard: 1) the velocity potential field is not as easily influenced by weaker, transient convective modes as low-level winds and OLR, and 2) by removing the 120-day mean to isolate interannual variability, the RMM index may be losing valuable information about the base state that does not necessarily correspond to ENSO. Perhaps more fundamentally, a velocity potential index more succinctly captures the physical source of the extratropical teleconnections, namely, the generation of subtropical and midlatitude circulation anomalies via the presence of a tropical vorticity source (upper-level divergence/convergence). There have been some recent attempts to address these issues in the RMM framework. Ventrice et al. (2013), for example, developed an index similar to the RMM except that velocity potential is substituted for OLR. While that study did not explicitly look at the extratropical ramifications, it seems plausible that such analysis would be useful in the context of issues discussed here. Developing and evaluating an objective prediction tool utilizing the CPC MJO index (or another velocity potential index) is an important next step in extending the skill of climate predictions to weeks 3 and 4, and such efforts are currently ongoing.

The following chapter will extend the analysis presented in the introductory chapter to the subseasonal domain. In that context, an important question is whether the MJO circulation response identified here emerges as a leading pattern of variability in a principal component analysis.

Chapter 2 Figures

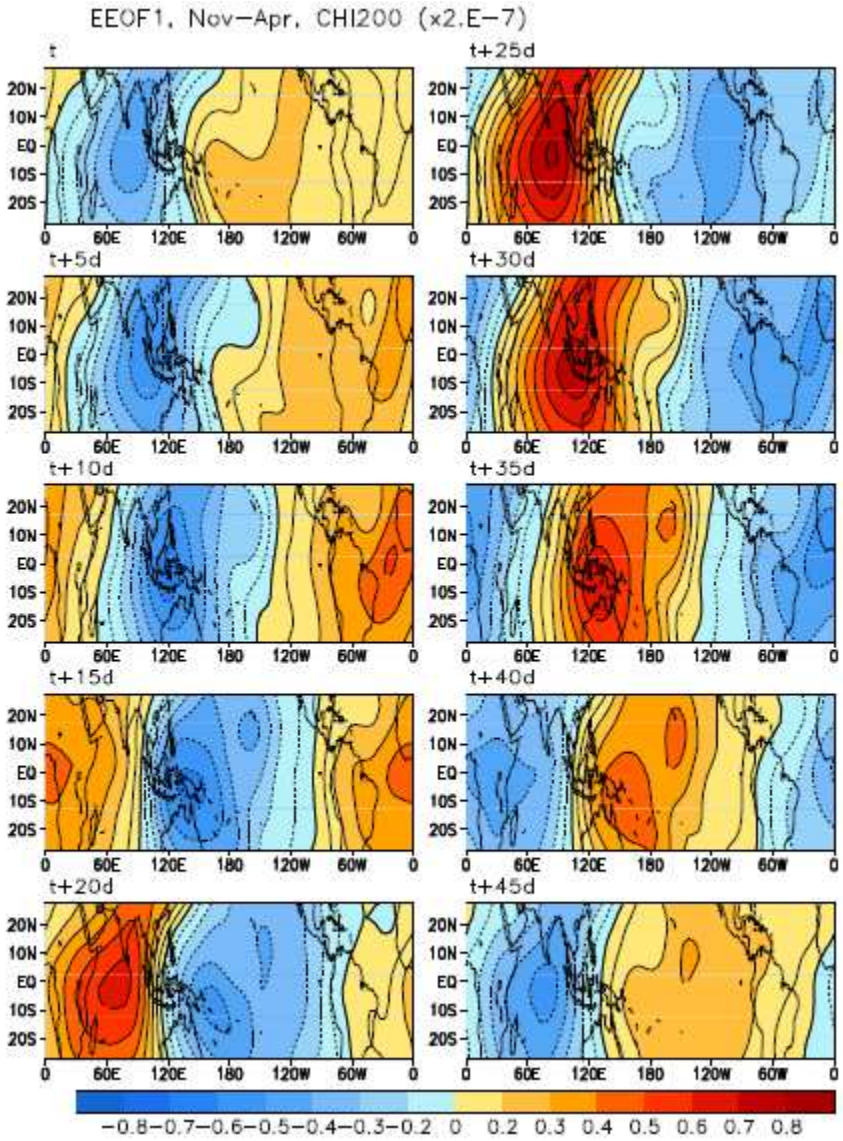

Figure 2.1: The first EEOF of the pentad velocity potential at 200-hPa for ENSO-neutral and weak ENSO winters (November-April) during 1979-2000. Together the time-lagged patterns comprise the canonical MJO evolution.

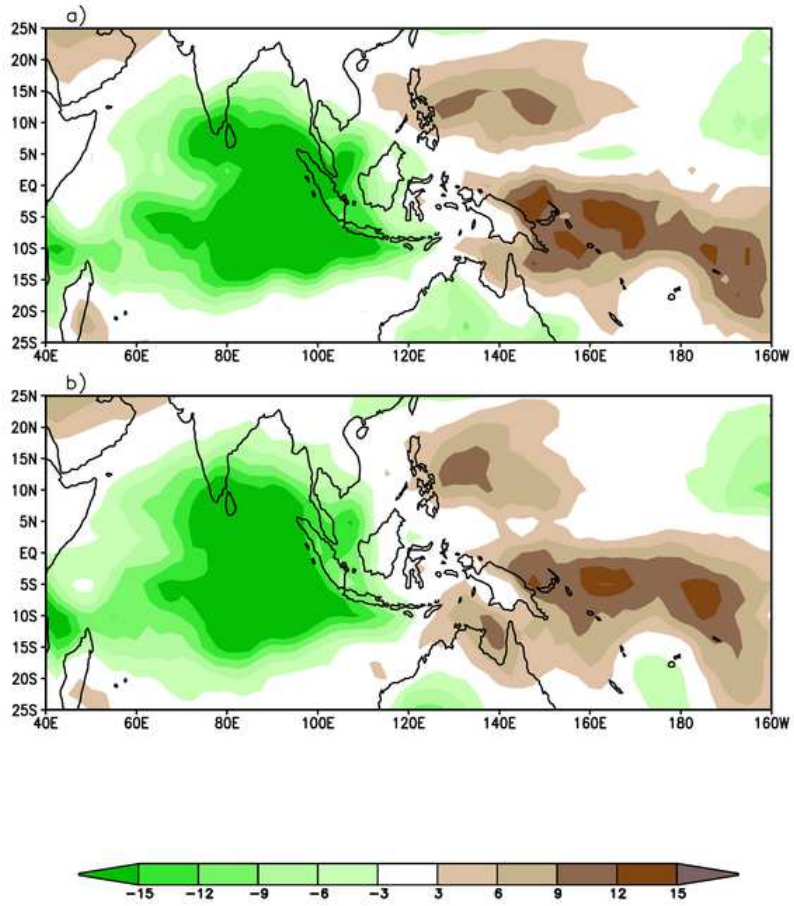

Figure 2.2: a) DJF pentad OLR composite during RMM phase 3 (n=58). b) DJF pentad OLR composite when CPC MJO index 1 is less than one standard deviation (n=96).

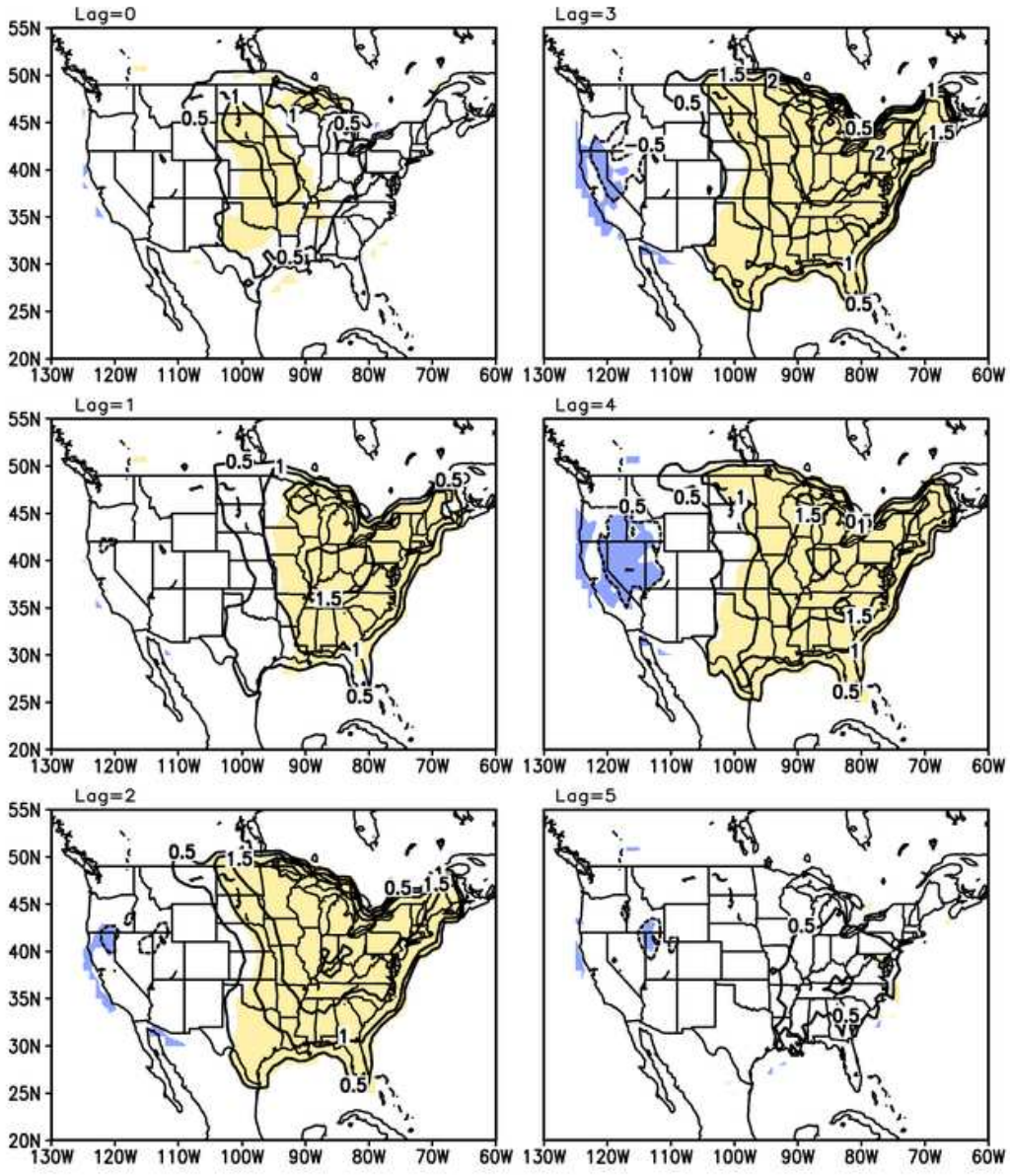

Figure 2.3: Contoured DJF SAT lagged (lag 0-5) pentad composite when CPC MJO index 1 is less than one standard deviation (contour interval=0.5^{o} C). Shaded area represents significance at the 95% confidence limit.

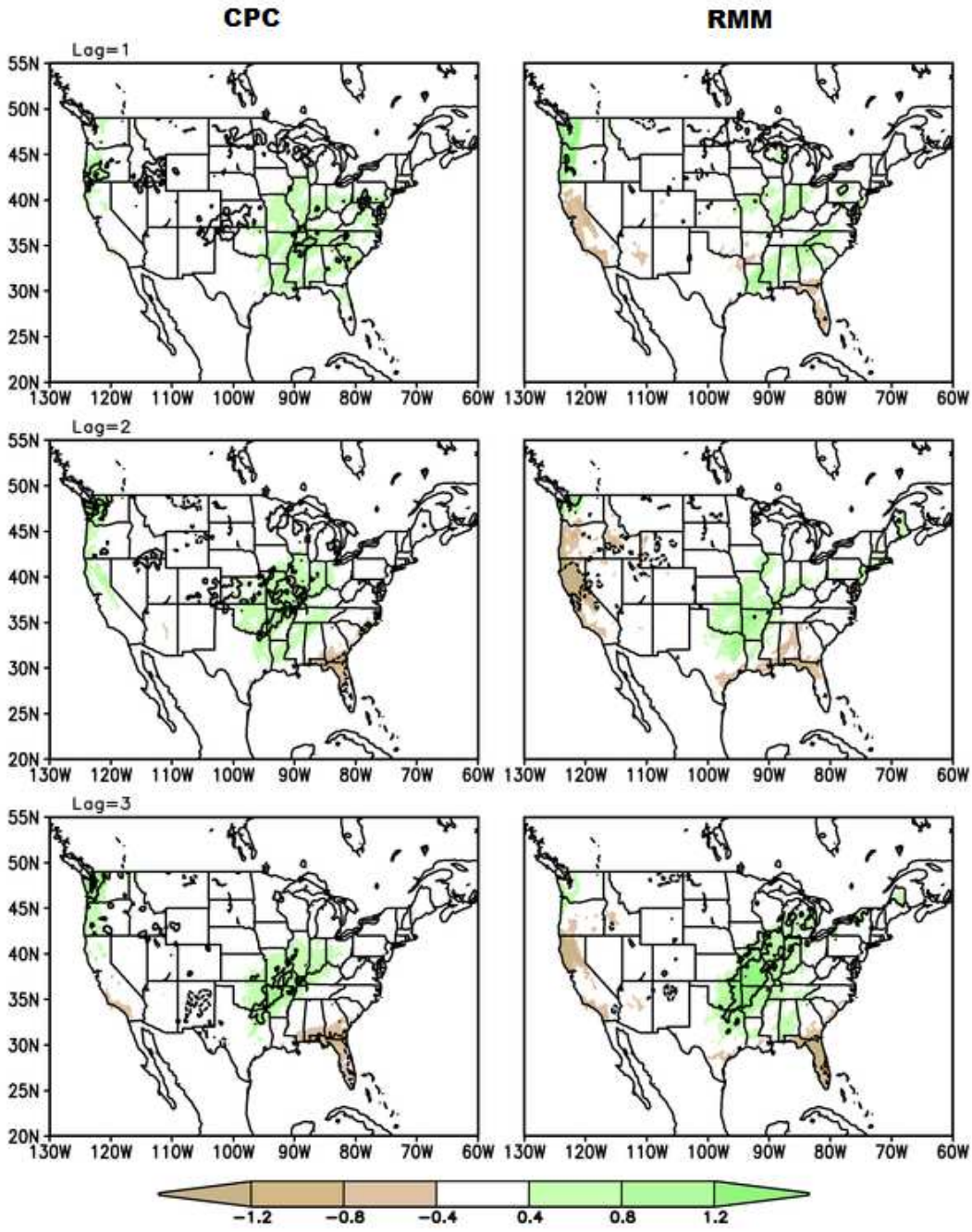

Figure 2.4: Left: Lagged pentad (lag 1-3) CPC MJO index 1 precipitation composite (mm/day). Right: Lagged pentad (lag 1-3) RMM phase 3 precipitation composite. Contour represents significance at the 95% level.

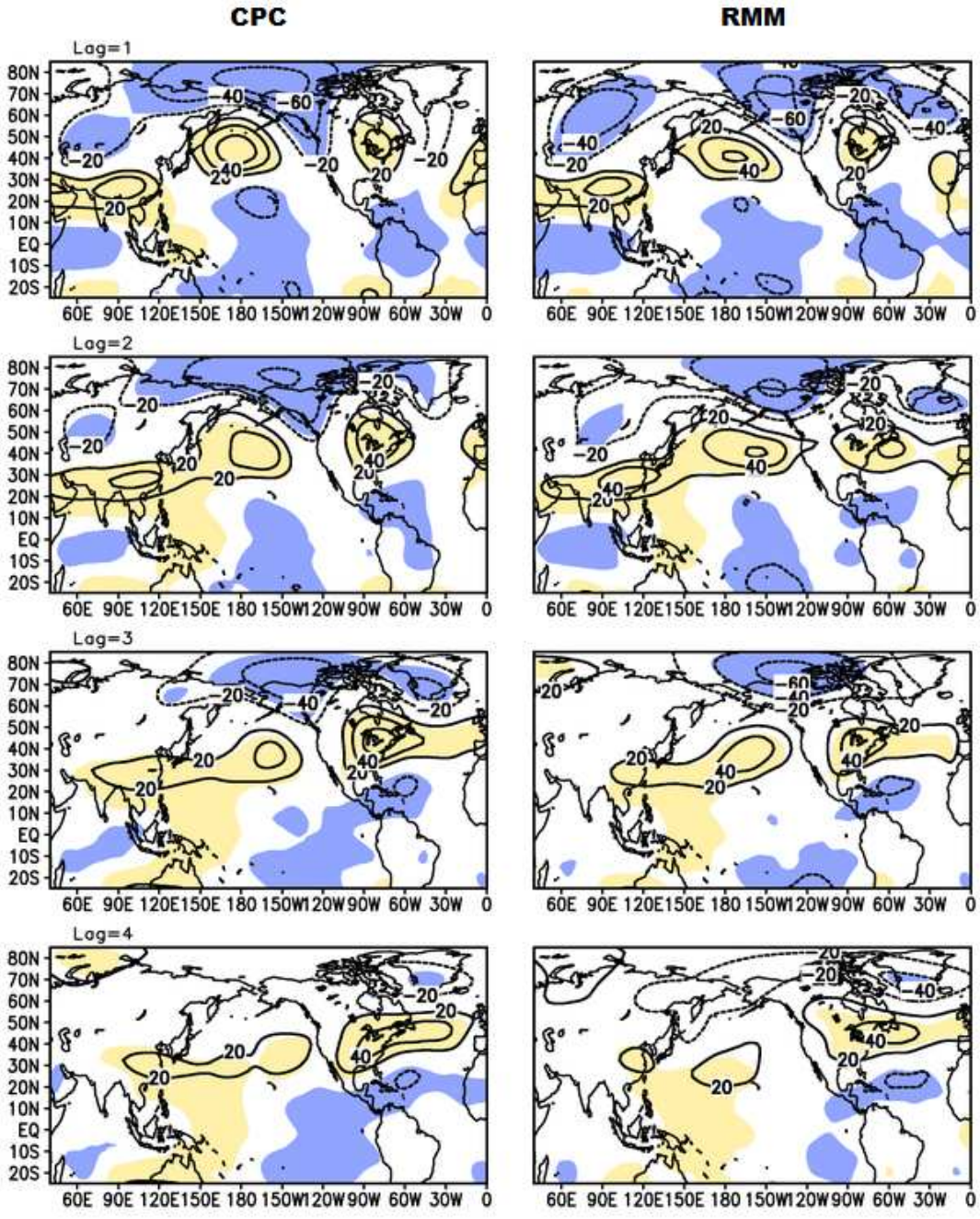

Figure 2.5: Left: Contoured CPC MJO index 1 lagged (lag 1-4) composite of 200-hPa geopotential height (m). Right: Same as left but for RMM phase 3. Shading represents significance at the 95% confidence limit.

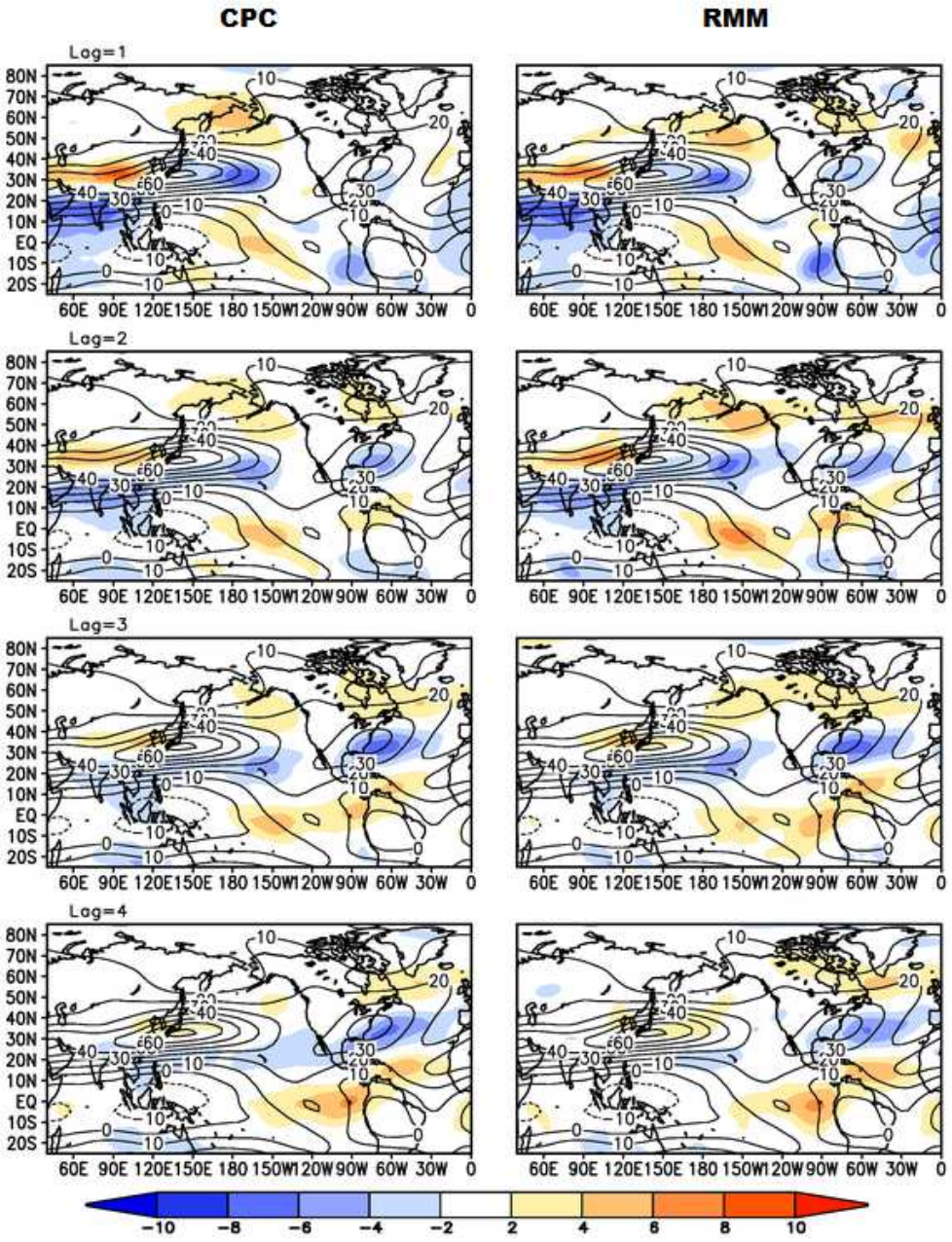

Figure 2.6: Left: Shaded lagged pentad composite of 200-hPa zonal wind (m/s) for CPC MJO index 1. Right: Same as left but for RMM phase 3. DJF climatology is contoured.

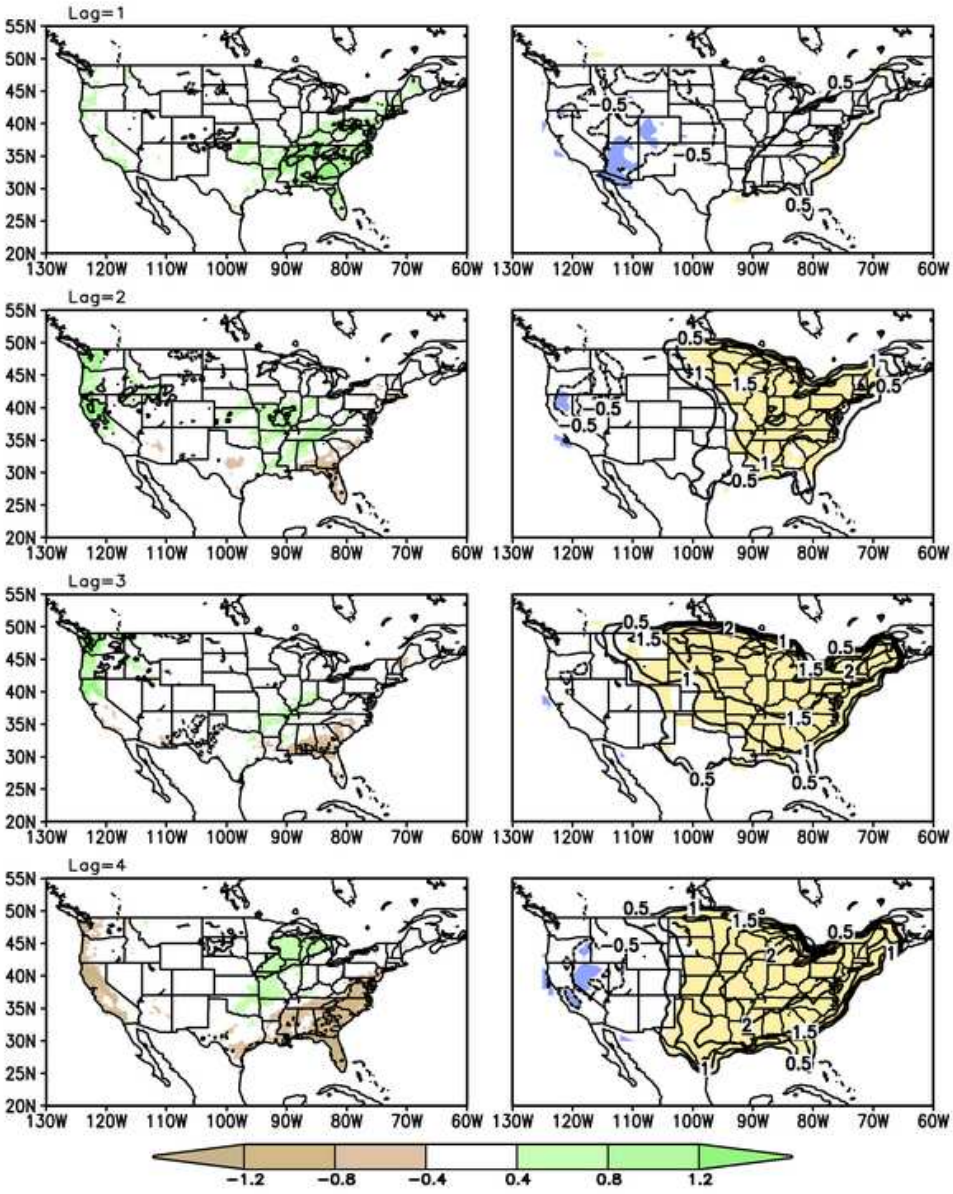

Figure 2.7: Left: Lagged (lag 1-4) pentad composite of precipitation (mm/day) when CPC MJO index 1 threshold is met, but the RMM index is not in phase 3. Significance at the 95% limit is contoured. Right: Lagged pentad composite of SAT is contoured at 0.5ºC interval when CPC MJO index 1 threshold is met, but the RMM is not in phase 3. Significance at the 95% limit is shaded. (n=56)

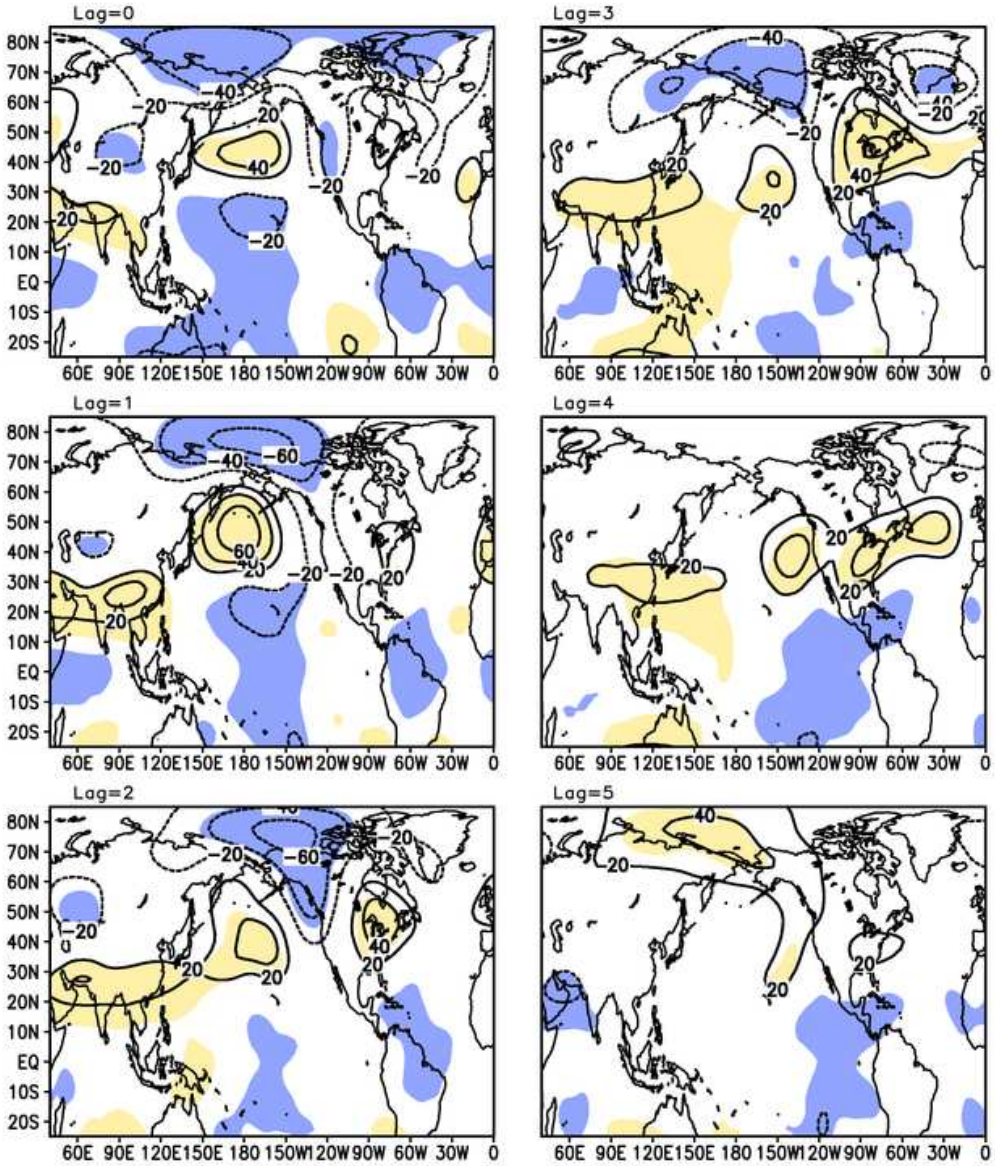

Figure 2.8: Contoured lagged (lag 0-5) pentad composite of 200-hPa geopotential height (m) when CPC MJO index 1 threshold is met, but RMM index is not in phase 3 (n=56). Shading represents significance at the 95% limit.

Chapter 3: Subseasonal Teleconnection Analysis: PNA Development and Its Relationship to the NAO

3.1 Background

The Pacific–North American (PNA) teleconnection pattern is a major mode of Northern Hemispheric midlatitude climate variability (e.g. Wallace and Gutzler 1981). The well-known pattern consists of four centers of action with alternating signs: the subtropical northeastern Pacific, the Gulf of Alaska, northwestern North America, and the southeastern United States (Figure 1.2). The pattern has important implications for sensible hydroclimate variability, particularly during winter over North America (Figure 1.7). Better understanding of the development of PNA patterns can have a positive impact on intraseasonal climate prediction where current prediction is relatively weak. Currently, we are afforded reasonable forecast skill out to two weeks or so from traditionally numerical weather prediction. Longer-lead climate forecasts are made possible because of slowly varying boundary conditions (e.g., ENSO). However, the subseasonal time frame that exists between the two (weeks 3–5) remains a difficult problem. Being able to identify any nascent phase is potentially helpful in terms of being able to diagnose the climate state and therefore increase the ability to predict its evolution.

A recent study by Franzke et al. (2011) used composite analysis among other techniques to show that both phases of the PNA can be weakly excited by tropical convection before achieving its mature amplitude 8–12 days later. It is suggested there that tropical convection plays an essential role in the excitation of PNA events. Additionally, intraseasonal tropical convection related to the Madden–Julian

oscillation (MJO; Madden and Julian 1971, 1972) has been shown to contribute to both PNA development (Higgins and Mo 1997) and the North Atlantic Oscillation (NAO; Lin et al. 2009). The aforementioned studies would suggest that weakened convection in the eastern Indian Ocean and enhanced convection in the western tropical Pacific [a high real-time multivariate MJO (RMM) 2 index] would lead to a positive PNA followed by a negative NAO. As we will show, the intraseasonal analysis bears out something quite different, with the NAO leading a PNA of opposite sign.

This study uses empirical orthogonal function (EOF) analysis to identify teleconnection patterns, with particular emphasis on the PNA, and assesses how that might be sensitive to the MJO. The data and methods used are detailed in the next section. Additionally, we assess the lagged relationship between the PNA and NAO and seek some physical explanation for the observed results. These are detailed in section 3. A brief discussion of results follows in the last subsection.

3.2 Data and Methods

We employ the state-of-the-art Climate Forecast System Reanalysis (CFSR; Saha et al. 2010) for rotated extended empirical orthogonal function (REEOF) analysis on Northern Hemispheric extended wintertime (November–March, 1979–2008) 200-hPa height anomalies at pentad resolution that have been latitudinally weighted. The extended EOF analysis, in contrast with traditional EOF analysis, produces loading vectors that consist of a five-pentad series of spatial patterns associated with a single principal component time series. This allows us to potentially elucidate nascent teleconnection phases as they actually appear in the data, rather than

their statistical representation in lead–lag regressions. While many teleconnection analyses are conducted at the 500-hPa level, we use the 200-hPa level since we are interested in the potential interaction between the tropics and the midlatitudes. Indeed, Chapter 1 highlights the benefits of analysis at 200-hPa, wherein the tropics may have a more direct impact on the analysis. The equivalent barotropic nature of the teleconnections that emerges when any method of removing daily fluctuations is used allows us to utilize 200 hPa without loss of the essential centers of action. The analysis is conducted using the covariance matrix and the seven leading modes are rotated using the varimax criterion (Barnston and Livezy 1987) to allow for more spatial discrimination.

The analysis is repeated, this time using data from which the MJO is linearly removed by subtracting the contemporaneous regressions of the Wheeler and Hendon RMM 1 and RMM 2. These indices were created from the CFSR using the method established by Wheeler and Hendon (2004) to capture the propagating nature of MJO-related convection. The RMM 1 regression onto outgoing longwave radiation (OLR) reveals a convective heating source over the Maritime Continent; RMM 2 captures a dipole between the Indian Ocean and west Pacific.

Rotated, but nonextended, EOF analysis (REOF) is also conducted to compare with the REEOF analysis with the goal of being able to assess the value that extended EOF analysis adds to the study. A series of lead–lag regressions are then performed.

To understand the physical connection between the NAO and PNA, we look at simple terms in the barotropic vorticity equation, namely, the beta term that accounts for advection of planetary vorticity and the orographic forcing term. Each is

assessed using the NAO's principal component (from the REEOF) regression onto the different wind fields used in each term.

3.3 Results of Subseasonal Analysis

The REEOF analysis pulls out the most frequently occurring five-pentad series of 200-hPa height anomaly patterns. In this framework, the NAO emerges as the leading mode (Fig. 3.1), explaining 6.7% of the total variance. The PNA pattern emerges as the fourth-leading mode (Fig. 3.1), explaining 4.6% of the variance. The modes are displayed as the regression of the normalized principal components (PCs) onto the height field. The seemingly small percentage of explained variance is due to the nature of the extended analysis, since in the place of each spatial pattern in the covariance matrix, a five-pentad series of patterns is used, increasing the total variance. Note that the figures shown here constitute the negative phase of the traditional teleconnection definitions. This polarity difference is unimportant. The second- and third-leading modes (not shown) may be associated with separate development and decaying phases of a mode similar to the North Pacific Oscillation, something that warrants further analysis.

Figure 3.1 yields two interesting results: 1) the maximum amplitude of the PNA mode appears closer to T − 1 (T is used for the time sequence of spatial patterns, while t will be used to refer to the time series itself), so the mode is focusing slightly more on the decaying phase of the PNA, and 2) there is an NAO-type anomaly of opposite sign preceding the PNA that exhibits noticeable westward propagation through the sequence. A similarly interesting result from Fig. 3.1 shows that the NAO pattern seems to peak nearer to T + 1. Therefore, both loading vectors are asymmetric

about T = 0. In this way, the purely statistical analysis could be revealing something very physical about the underlying system, namely, that the development and decay of the PNA and NAO may be related on subseasonal time scales. Because matrix algebra constrains the principal components to be temporally independent, shifting the series of spatial patterns within the loading vector must compensate for any robust physical connection between the two modes.

From the nonextended REOF analysis, the NAO and PNA emerge as modes 1 and 2, explaining 10.4% and 7.8% of the variance, respectively (Fig. 3.2). There is a sizable difference between the patterns that emerge from the REEOF analysis and the lead–lag regressions associated with the nonextended analysis. This is consistent with analysis of Nigam (2003), which used weekly lead–lag regressions from a nonextended analysis to assess evolution of the PNA pattern. This difference highlights the importance and relative novelty of using REEOF analysis in subseasonal teleconnection studies.

Sensitivity to the number of modes rotated in the analysis was tested using the nonextended REOF. The PNA pattern emerges as a leading pattern, explaining roughly the same percentage of variance whether 4, 10, or the chosen 7 modes are rotated (not shown). This is expected given that the two leading patterns (NAO and PNA) are not as likely to be as sensitive to the number of rotated modes as would be subsequent modes in the analysis.

Next, we assess how linear removal of two orthogonal MJO principal components affects both the REOF analysis and the REEOF analysis. The PNA and NAO emerge as leading modes at fourth and first, respectively, in the REEOF

analysis; this is the same as in the original analysis. In the nonextended analysis, however, MJO filtering results in the PNA falling from the second- to the third-leading mode of variability. Figure 3.3 shows the PNA and NAO in their respective mature phases in the REEOF analysis when the MJO has been removed. These figures are nearly identical to those that fall out of the original analysis. There is no noticeable shift in space or time of the essential centers of action. The only visually identifiable change in the PNA pattern occurs over south-central and Southeast Asia, which makes sense since that is where the MJO has a very strong footprint in the geopotential height field (Figure 2.4).

Closer inspection, however, reveals that the MJO removal results in a very modest shift (an order of magnitude weaker) in the centers of action of both the PNA and the NAO. Figure 3.4 shows the difference between the original and MJO-filtered analysis from the nonextended analysis. The differences are plotted in the context of the original mature patterns. The mid- and high-latitude PNA centers are generally shifted east, while the NAO centers of action are shifted northwest. In the PNA case, the differences appear visually as a wave train emanating from the MJO source region.

As previously mentioned, the evolution of the PNA pattern reveals an NAO-type pattern of opposite sign that precedes the mature PNA. The lag correlation between the PNA mode and the NAO mode is shown in Fig. 3.5; results from the original and MJO-filtered REEOF analyses are both plotted, as are results from the REOF and station-based analyses. The lag correlation is greatest in the REEOF analysis, with a positive PNA lagging a negative NAO by two or three pentads and

vice versa. The magnitude of the lag may be exaggerated in the REEOF analysis since the NAO mode peaks near T + 1 and the PNA appears to peak prior to T = 0. Additionally, the REEOF PCs vary more slowly, lending themselves to higher lag correlations and thus reducing degrees of freedom. That being said, the REOF analysis reveals the same qualitative result (Fig. 3.5), and the peak amplitudes are statistically significant beyond a 99% confidence limit. A similar analysis using station-based NAO and PNA indices (Fig. 3.5) reveals the same lag at one to two pentads, also lending further support to our methodology.

A more aesthetically satisfying portrayal of this lag between the NAO and a PNA of opposite phase is also seen in Fig. 3.5. That scatterplot reveals an anticipated negative slope between the NAO at time *t* and the PNA at time *t* + 3. The clear clustering in the negative quadrants shows that this relationship is not an artificial product of outliers. Furthermore, the presence of some apparent outliers in the first quadrant suggests the relationship may be more robust than the correlation coefficients themselves reveal.

While this intraseasonal relationship between the NAO and the PNA is both novel and robust by itself, we must be interested in positing some physical explanation for the observed interaction. With that goal in mind, simple terms in the barotropic vorticity equation are evaluated with respect to the NAO:

$$\frac{\partial \zeta}{\partial t} = -\beta v_{200\,\mathrm{mb}}^{\mathrm{NAO}} - \frac{f}{H}(\mathbf{V}_{850\,\mathrm{mb}}^{\mathrm{NAO}} \cdot \nabla h) - (\mathbf{V}_{200\,\mathrm{mb}}^{\mathrm{NAO}} \cdot \nabla \zeta \mathrm{clim}),$$

where ζ is the relative vorticity at 200 hPa and β is the meridional derivative of the Coriolis parameter f. The meridional wind is given by v, and $\mathbf{V}$ is the vector wind. The topography h is used, as is H, which is the height of the troposphere, assumed here to be a constant 10 km. Superscript NAO means this is the regression coefficient

of the REEOF PC that constitutes the NAO onto the wind at a level given by the subscript. The term on the left-hand side is the local tendency term. The right-hand side consists of the beta term, the divergence term, and the relative vorticity advection term. The outstanding question is whether the NAO can force the PNA via retrogression of mid- and high-latitude anomalies, rapid downstream energy propagation, or both. The terms analyzed are the beta term, which consists of beta multiplied by the NAO regression onto the meridional wind at 200 hPa; the orographic forcing term (divergence term), which is calculated as the dot product between the NAO regression onto the 850-hPa wind field and the gradient of topography; and the advection of climatological relative vorticity by the NAO regression onto the 200-hPa wind. We can neglect any advection of anomalous NAO relative vorticity because of the concentric, symmetric nature of the teleconnection footprints. Figure 3.6 shows the total advection and orographic terms as well as their sum. This sum constitutes the opposite of local relative vorticity tendency ($-\partial\zeta/\partial t$), which is proportional to geopotential height tendency. The analysis is particularly revealing because the use of beta allows for a more tropical signature while the meridional wind allows for a better sense of wave propagation. The regression of the teleconnections onto the zonal wind is certainly of much larger magnitude than the regression onto the meridional wind, but it is in fact the meridional wind that may be more important because of its inclusion in the beta term.

Figure 6 reveals that the NAO indeed forces a wave pattern that starts in the northern tropics near the zonal jet maximum that is climatologically present near the Arabian Peninsula. This pattern seems to terminate at the end of the East Asian jet

stream, which coincides with the semipermanent Aleutian low, a main center of action of the PNA. At the same time, the beta term supports a retrogression of NAO anomalies westward across northern North America. Additionally, the orographic term strongly supports the beta forcing in two key areas: south-central Asia (Himalayas) and the Alaskan panhandle.

3.4 Discussion

The PNA emerges as a leading pattern of variability from REEOF analysis of 29 extended winter seasons at pentad resolution with an interesting lagged connection to the NAO, with the NAO leading a PNA pattern of the opposite sign. The REEOF PNA pattern shows a peak closer to time T − 1, while the NAO pattern from the same analysis peaks closer to T + 1. Given that the two modes in this analysis are statistically constrained to be temporally independent, this may highlight an intrinsic and physical connection between the two on intraseasonal time scales. The manifestation of this connection on subseasonal time scales is particularly interesting given that historically little attention is paid to the identification of teleconnections at this temporal resolution. It is our belief that further understanding the physical basis of this relationship will aid in efforts to predict climate variability in this time frame, which is of growing importance.

When the analysis is repeated on the data from which the MJO has been linearly removed, there is little visually noticeable difference. In fact, the only small differences appear as subtle shifts in the modes' centers of action. The fact that MJO removal has little or no impact reveals two points, both of which are likely valid: 1) nonlinear and lagged impacts of the MJO cannot be removed and thus the MJO is still

contributing in a small way and 2) while MJO or related intraseasonal tropical convection trigger PNA events, the PNA is likely a mode of variability intrinsic to the midlatitude atmosphere, occurring even in the absence of canonical MJO-related tropical convection. It has been noted by other studies (e.g., Lin and Brunet 2009; Lin et al. 2010) that the MJO impacts North America via a Rossby wave train that is instigated by an MJO-induced convective dipole between the eastern Indian Ocean and the western Pacific Ocean. These MJO impacts therefore necessarily exist at some lag. It is therefore likely that even linear impacts of the MJO on the PNA and especially the NAO are not being removed because they exist at some lag (~3 pentads in the case of the NAO, less for PNA). This would not be a problem by itself since, in a perfectly propagating MJO, lagged impacts from RMM 2 manifest themselves as contemporaneous impacts from RMM 1. However, not all MJO events are ideal, and thus, it is likely that the MJO removal is far from perfect. Additionally, contribution from other subseasonal tropical convective signals (e.g., atmospheric Kelvin waves and equatorial Rossby waves) cannot be precluded. Again, the key finding here is that MJO is not essential for the existence of the PNA.

As mentioned previously, it is important to advance a hypothesis on the physical basis for the connection between the NAO and the PNA. The brief analysis of the simple barotropic vorticity equation indeed gives some indication of how the NAO may be forcing the PNA. The total advection term shows the vorticity forcing from the NAO results in both westward propagation of the longwave pattern across North America and in energy propagation to the Arabian Peninsula and through southern and eastern Asia, culminating in the Pacific. This is remarkably consistent

with the results of Hoskins and Ambrizzi (1993), which found preferred propagation from Europe to the Arabian Peninsula. Additionally, they showed how the East Asian jet stream serves as a Rossby waveguide. It is in this light that we suggest the NAO excites a wave train in the vicinity of the Arabian Sea that ultimately forces a PNA pattern of opposite sign. This in combination with westward propagation of high-latitude NAO anomalies that accounts for the observed connection between the NAO and the PNA.

The next chapter consists of a follow-up study that seeks the MJO teleconnection alongside patterns of variability that might be inherent to the extratropics. The present study demonstrates that the PNA and NAO patterns are subtly affected by the inclusion of MJO-associated circulation anomalies, but still emerge intact in MJO-reduced data. If possible, an ideal analysis would separate the MJO response pattern from the PNA and NAO in time, such that attribution of climate anomalies might be closer linked to discrete physical mechanisms.

Chapter 3 Figures

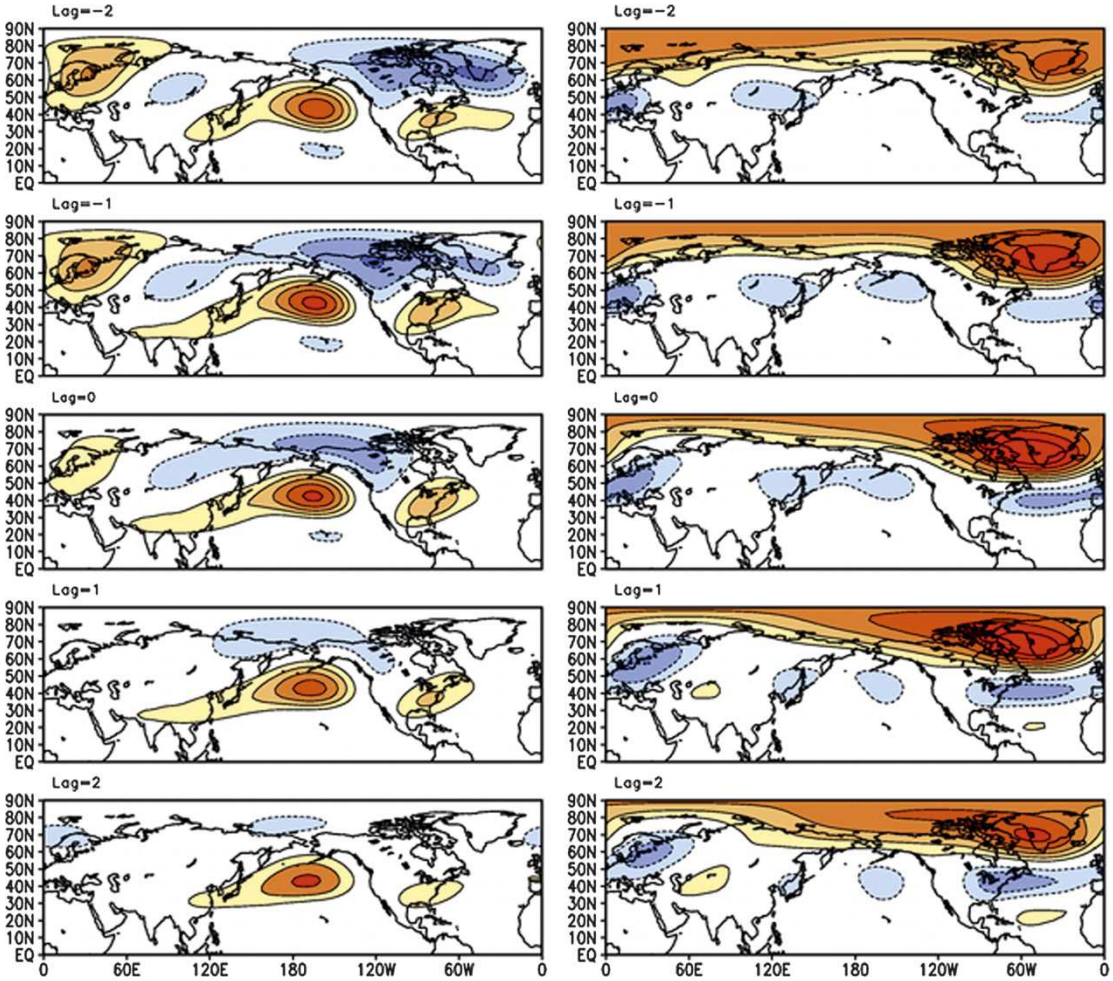

Figure 3.1: (left) REEOF mode 4, constituting the PNA pattern. The pattern seems to reach maximum amplitude at lags 0 and −1. Contour interval is 20 m. (right) REEOF mode 1, constituting the NAO pattern. This pattern peaks at lags 0 and 1. Contour interval is 20 m.

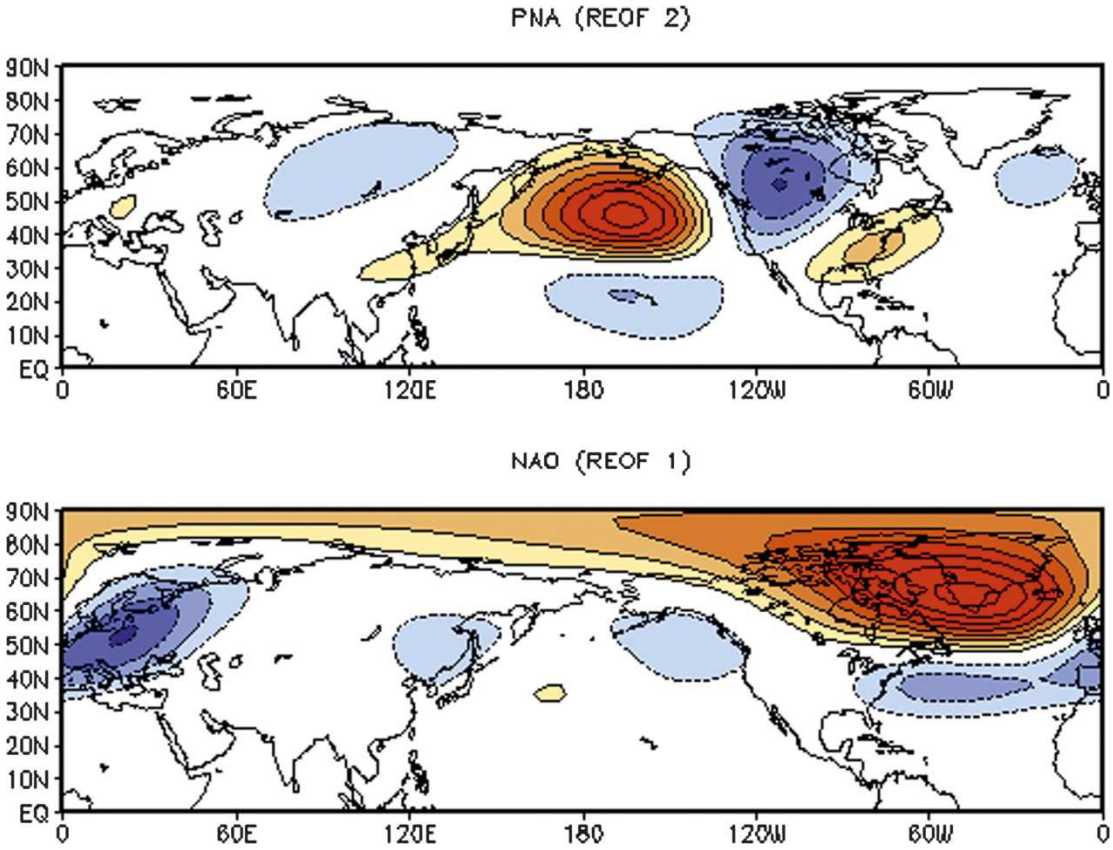

Figure 3.2: The two leading modes that emerge from the REOF analysis constitute the (top) PNA and (bottom) NAO. Contour interval is 20 m.

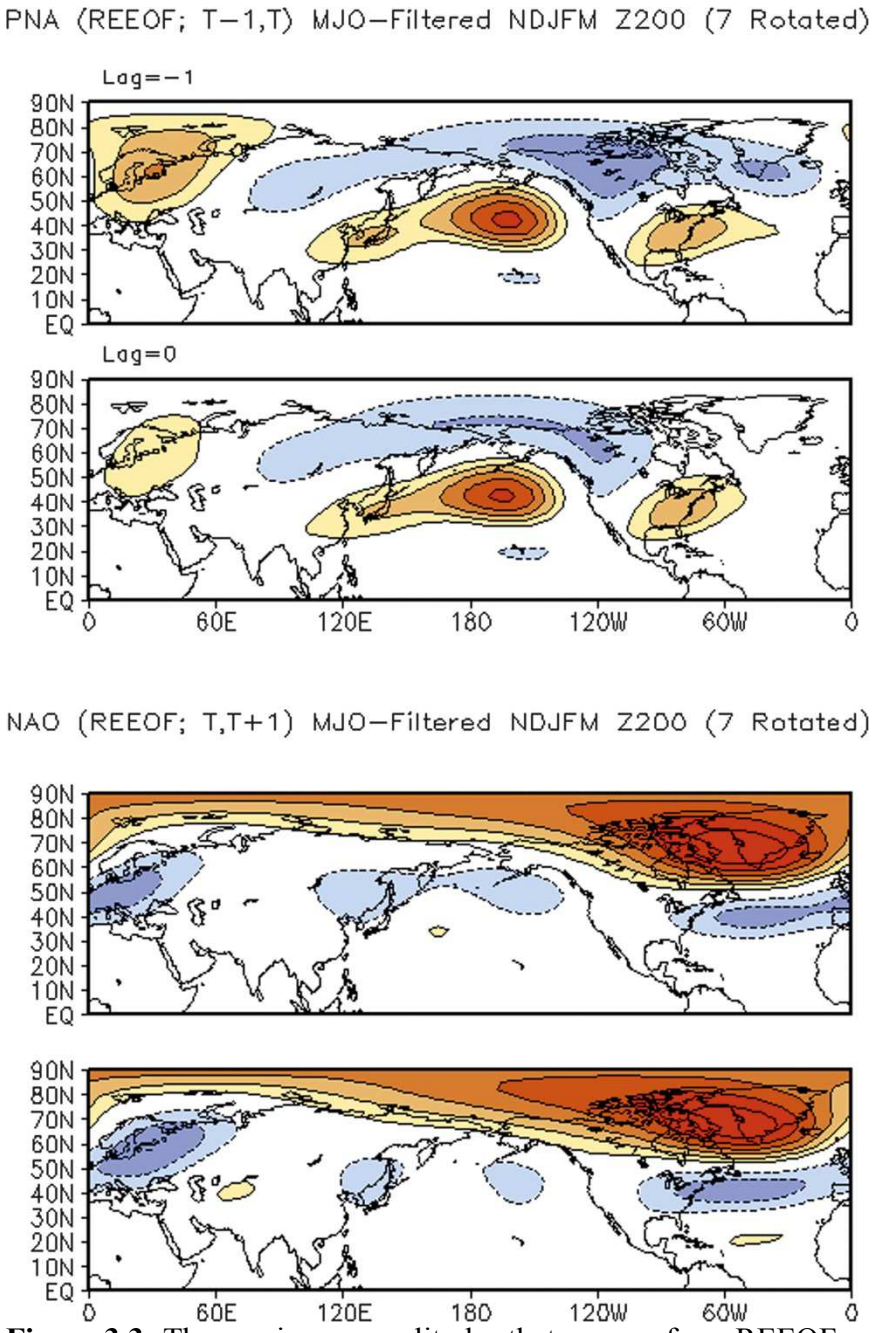

Figure 3.3: The maximum amplitudes that emerge from REEOF analysis with MJO-filtered data for the (top) PNA and (bottom) NAO patterns. Contour interval is 20 m.

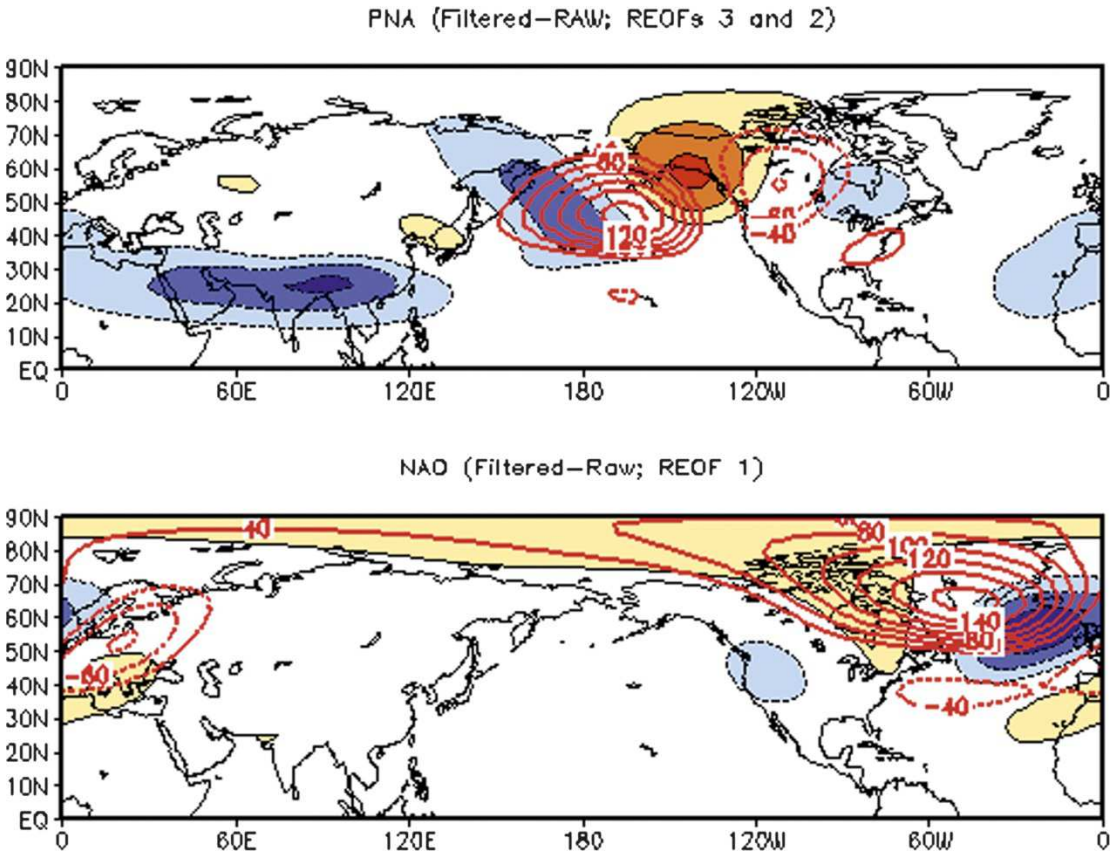

Figure 3.4: Red contours show mature (top) PNA and (bottom) NAO from REOF analysis; shading is the difference between MJO-filtered and nonfiltered analysis. Contour interval is 3 m.

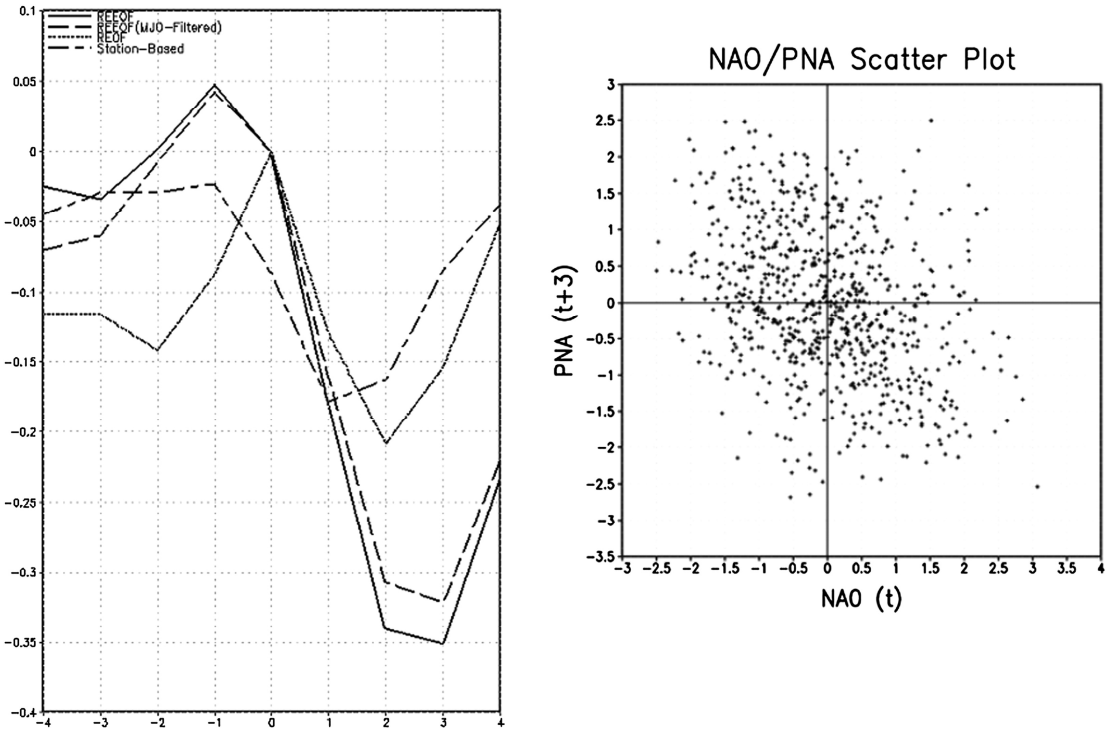

Figure 3.5: (left) Correlation between the NAO and PNA indices as defined by REEOF analysis, REEOF analysis from which the MJO was linearly removed, REOF analysis, and a station-based analysis at 500 hPa. Correlation coefficients are a function of lagged pentads. Positive lag corresponds to PNA lagging the NAO. (right) Scatterplot of principal component is shown for PNA at time t + 3 and NAO at time t emerging from REEOF analysis. There is noticeable clustering in the negative quadrants.

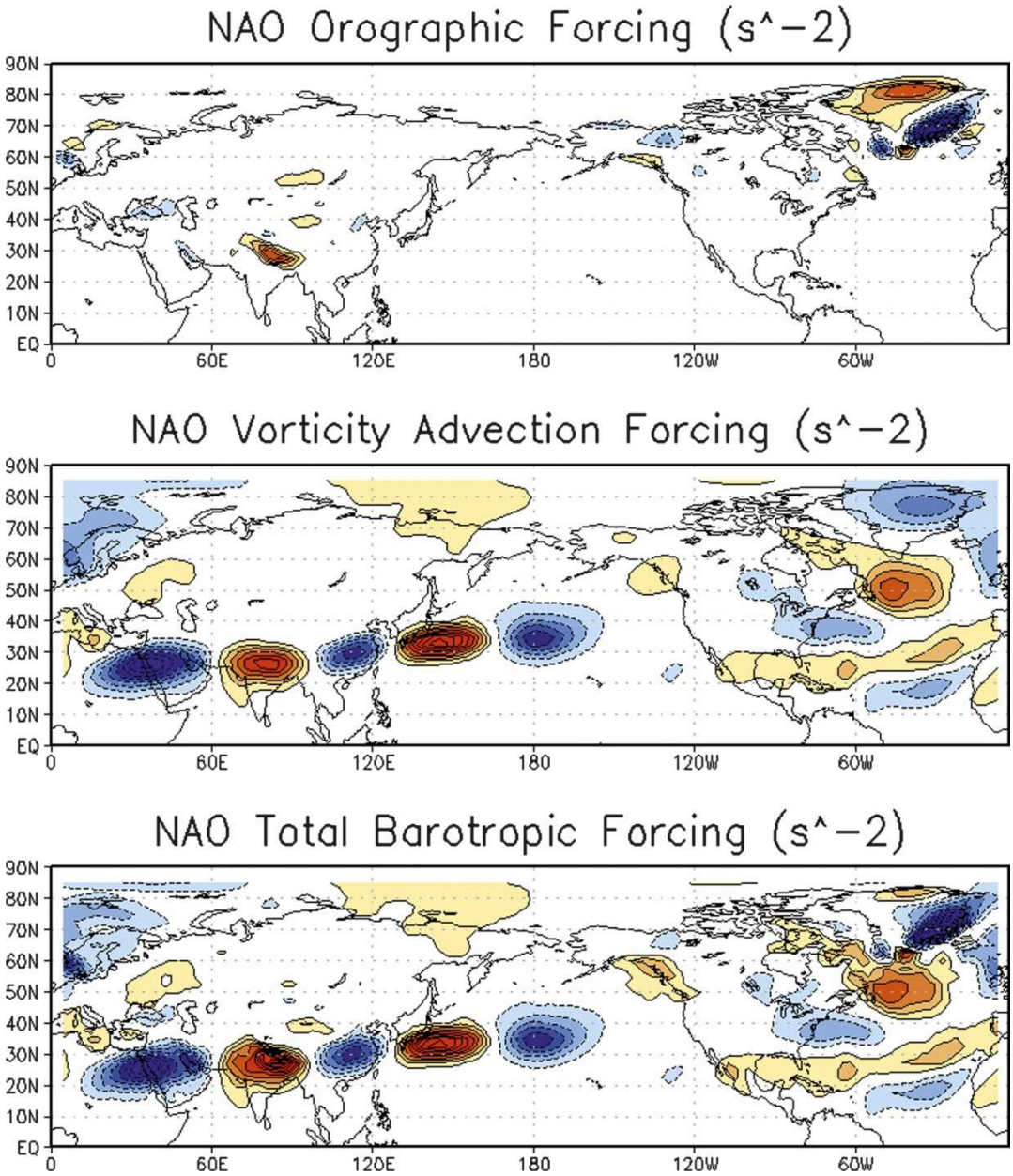

Figure 3.6: Three terms in the barotropic vorticity equation are evaluated with respect to the NAO regression on the respective circulation fields: (top) orographic forcing, (middle) the sum of the beta term and advection of the climatological relative vorticity, and (bottom) the sum of all three. The contour interval is 10^{-11} s^{-2}. Each panel shows the contribution of that term to negative vorticity tendency ($-\partial\zeta/\partial t$), so the warm colors are proportional to positive height tendency.

Chapter 4: Streamfunction as a Preferred Variable for Subseasonal Teleconnection Analysis

4.1 Background

Previous chapters discuss the importance of teleconnection analysis as a basis for understanding low-frequency (i.e. super-synoptic to seasonal) atmospheric variability. Such teleconnection patterns serve as building blocks with which one can reconstruct observed atmospheric climate anomalies, as explored in the next chapter. While teleconnection analysis has traditionally been conducted to explore recurrent patterns of variability confined to the extratropics (e.g. Wallace and Gutzler, 1981; Barnston and Livezy, 1987), there are two clear examples of teleconnection patterns rooted in the subtropics, namely, the atmospheric responses (ranging from the subtropics to the extratropics) to the Madden-Julian Oscillation (MJO) and the El Niño-Southern Oscillation (ENSO). The former is more dominant on subseasonal time scales, while the latter is perhaps the most well-known mode of interannual variability.

In Chapter 2, the MJO extratropical response was identified using composite analysis utilizing two different metrics of MJO activity: the popular Wheeler and Hendon (2004) index and a simple velocity potential index derived and monitored by the Climate Prediction Center (CPC). The results of that chapter show that the MJO can be a useful predictor of subseasonal hydroclimate variability over the contiguous United States, a powerful result given the growing interest in climate prediction that spans the gap between Week-2 forecasts and monthly/seasonal forecasts. That

analysis reveals a pattern consistent with various studies highlighting a relationship between the MJO and the Pacific-North America (PNA) pattern as well as the North Atlantic Oscillation (NAO). However, the correlation between the PNA and the MJO (as assessed by either the RMM or CPC index) is modest, on the order of 0.3 or less, as is the correlation between the NAO and MJO. Additionally, a visual inspection of the MJO response pattern revealed in Chapter 2 and the loading patterns of either the PNA or NAO reveals that there are important differences, and thus the PNA and NAO cannot simply be thought of as an MJO response.

This dilemma is similar to that faced when comparing the PNA and the extratropical response to ENSO. While traditional teleconnection analysis often links PNA and ENSO, an alternative, more physically appropriate analysis reveals that they are quite different. Using 200-hPa geopotential height in a rotated empirical orthogonal function (EOF) analysis yields a PNA pattern as separate from the canonical ENSO response, as shown in the introductory chapter. This separation does not readily occur when using 500-hPa geopotential height, as that variable exhibits less tropical and subtropical variance. In that framework then, extratropical variability that is associated with the ENSO response is aliased into the other extratropical patterns of variability, including the PNA. The analysis presented in the previous chapter did indeed use 200-hPa geopotential height, but a pattern resembling the MJO response detailed in Chapter 2 did not emerge. This is likely because the 200-hPa geopotential height variability on subseasonal time scales is much larger at higher latitudes, which are therefore emphasized in an EOF analysis which utilizes the covariance matrix.

The remedy pursued here is to utilize 200-hPa streamfunction, which places the subtropics and the middle and high latitudes on a more equal footing. This is preferred to using the correlation matrix in the EOF analysis since it allows for longitudes that exhibit more variability to be emphasized. *The goal of this analysis is to more elegantly separate the MJO-related extratropical response from internal extratropical patterns.* Additionally, this analysis is targeted toward looking at any tropical footprints of the other known teleconnection patterns. This will involve inspection of various fields in addition to streamfunction, such as velocity potential, outgoing longwave radiation (OLR), and sea-surface temperature (SST). To assess whether a given pattern might have its underpinnings in the tropics, the Rossby wave source term (RWS, Sardeshmukh and Hoskins, 1988) will be evaluated, especially with respect to the terms that are known to be closely related to tropical forcing.

What follows is a detailed description of the data and methods used in this analysis, a discussion of the results, and finally, the conclusions drawn from this work and their implications for the field and future research.

4.2 Data and Methods

For this analysis, 200-hPa streamfunction is utilized for the reasons just discussed. In many ways, the analysis is similar to that conducted in Chapter 3; namely, extended EOF analysis is utilized to capture the spatio-temporal variability of the 200-hPa streamfunction field at pentad resolution. The analysis period is 35 winter seasons from 1979-2014, and the spatial domain consists of the entire Northern Hemisphere. This analysis focuses on December, January, and February (DJF), the three months that together make up meteorological winter. Winter is

therefore taken to be the 19 pentads that span those three months. The data are extended using a five pentad window, and two pentads on each side of the 19-pentad season are allowed into the analysis so that the principal components (PCs) are defined for each of the 19 pentads. The leading eight modes are subject to varimax rotation to allow for more spatial discrimination. The number of rotated modes was selected using a scree test and by using the North et al. (1982) criteria. In this framework, a substantial break in the eigenvalues between modes eight and nine occur, beyond which all patterns are likely within the sampling error range. However, to be sure, variants of the analysis are performed rotating as many as ten and as few as six modes. The main results of this analysis are independent of the number of rotated modes, and so the optimal eight modes are retained for this analysis.

The 200-hPa streamfunction, 200-hPa velocity potential, and OLR fields, are all from the latest Climate Forecast System Reanalysis (CFSR, Saha et al., 2010). In the RWS analysis, absolute vorticity is also obtained from the CFSR database. SST data is obtained from a weekly Optimal Interpolation V2 (Reynolds et al. 2002) dataset that has been interpolated to pentad resolution. The seasonal cycle is removed from all data where appropriate.

The leading eight patterns from the rotated, extended EOF analysis are shown as linear regressions of the PCs onto the 200-hPa geopotential height field to allow for easy comparison with the other figures shown throughout this dissertation and in the literature. The footprints of the PCs onto velocity potential, OLR, SST, and RWS, are shown as the linear correlation of the PC with the variable of interest.

A small portion of the analysis will refer to the CPC MJO index, which is defined and used in Chapter 2. Specifically, the index that targets the dipole of anomalous convection between the eastern Indian Ocean and the West Pacific is used, which is similar to RMM2 in the Wheeler and Hendon framework.

The RWS, *S*, is calculated as defined in Sardeshmukh and Hoskins (1988). In flux form:

$$S = -\nabla \cdot (\boldsymbol{V}_\chi \eta)$$

Where $\boldsymbol{V}_\chi$ is the divergent component of the horizontal wind, and η is the absolute vorticity. Thus the units take the form of vorticity tendency. Expanding the term yields more physical components, namely, the stretching term and the advection of the absolute vorticity by the divergent wind:

$$S = -\boldsymbol{V}_\chi \cdot \nabla\eta - \eta(\nabla \cdot \boldsymbol{V}_\chi)$$

This term shows how tropical convection serves as a Rossby wave source by exciting vorticity perturbations in the subtropics via divergent outflow. A more mature analysis involves breaking the RWS into a climatological component and an anomalous component:

$$S = S_c + S_a$$

Carrying this operation down through the individual terms in the RWS yields a climatological term and both linear and non-linear terms. The terms of interest here are the linear terms as defined in Qin and Robinson (1993) that constitute the tropical component. Specifically, the advection of the climatological absolute vorticity by the meridional divergent wind is targeted:

$$S = -v'_\chi \cdot \nabla\eta_c$$

The rotated, extended EOF analysis is then repeated on the 200-hPa streamfunction data from which the trailing 24 pentad (120 day) mean anomaly has been removed to isolate subseasonal variability. This procedure accomplishes the goal of removing variability on interannual or longer time scales, while at the same time being suitable for real time monitoring of the climate system. The results of this parallel analysis are useful, though they will not be explored in depth here, since the main benefits of the streamfunction analysis are achieved using the unfiltered data, in which the interannual variability may be important for attribution of subseasonal climate anomalies, such as in the case of ongoing ENSO events.

4.3 Results of Streamfunction Analysis

The results of the rotated, extended EOF analysis of streamfunction reveal the spatio-temporal evolution of several key patterns of subseasonal climate variability. The patterns that are readily identified are the MJO extratropical response, the ENSO response, the North Pacific Oscillation/West Pacific pattern (NPO/WP), the NAO, and the PNA. Figure 4.1 shows the autocorrelation curves for each of the eight PCs that fall out of the analysis. The PCs are shown in descending order, and labeled according to the teleconnection pattern, based on result from the first three chapters, best described by that PC. The + (-) denotes the development (decay) phase of that particular pattern. Immediately evident is the low-frequency nature of the so-called ENSO pattern, whose identification is based in part on this longer time horizon. Another interesting feature is the more slowly varying nature of the PC that constitutes the NAO, consistent with the prevailing understanding of the NAO as varying on multiple time scales, from subseasonal to decadal. The other patterns

generally exhibit e-folding times of three pentads or less. The ensuing discussion of results is organized by teleconnection pattern. Following a discussion of each pattern, results of the RWS analysis are discussed.

a. The MJO Response

The leading two principal components together comprise the MJO response, and together explain 19.9% of the total variance. Figures 4.2 and 4.4 show the time evolution from -2 to +2 pentads of the 200-hPa geopotential height regressions alongside the velocity potential footprints of each pattern. PC2 is best characterized as the development of the response pattern, while PC1 targets the decay. Not surprisingly, these patterns are highly correlated (r=0.9) at a lag of three pentads, which PC2 leading PC1.

These patterns are notable for their robust velocity potential footprints in the tropics, closely matching the patterns obtained in Figure 2.1. The development of the MJO extratropical response is associated with, and preceded, by anomalous upper-level convergence (divergence) over the Pacific (Indian Ocean). The development of positive (negative) 200-hPa height anomalies over South Asia (central, subtropical Pacific) is consistent with the anomalous upper-level divergence (convergence) to the south. This is consistent with tropical forcing via the advection of absolute vorticity by the anomalous meridional divergent wind, a topic that will be explored in more depth in a later section.

Figures 4.3 and 4.5 show the time evolution of the OLR and SST correlations associated with this pattern. We focus on Figure 4.5 to highlight the development of the MJO extratropical response. The 200-hPa geopotential height response is

preceded by the development of a convective dipole from the Indian Ocean to the western Pacific, confirming what is suspected upon inspection of Figure 4.4. The modest but persistent SST signature across the equatorial Pacific suggests that some low-frequency variability may be influencing the pattern. Interannual variability of the MJO is not well-studied, but a recent paper by Lin et al. (2015) highlights the impact of interannual MJO activity on NAO variability. We will revisit this issue in the subsection concerning the NAO. Even in the absence of interannual variability, there is a relationship between the MJO response and equatorial Pacific SSTs, albeit weaker (not shown). In both cases such a response is consistent with the acceleration of the trade winds to the east of the enhanced convection. More consistent is the cooling of the Indian Ocean associated with the passage of anomalous MJO-related convection.

The low-frequency SST variability associated with this MJO mode may also be related to ENSO. While a subsequent pattern more clearly captures standing ENSO variability, this weaker, but persistent signature nearer the dateline may be related to the so-called El Niño Modoki (Ashok et al., 2007) or non-canonical ENSO (Guan and Nigam, 2007). In Figure 4.5, the SST footprint is weak in the East Pacific, and strongest in the central Pacific, consistent with the aforementioned 'flavors' of ENSO. While further discussion of the interannual implications of this analysis is beyond the scope of this thesis, it is worth noting that a new hypothesis is generated. That hypothesis states that the anomalous warming (or cooling) of the central Pacific may lead to a preferred state of subseasonal tropical activity closely related to the MJO.

Given the above discussion of the leading two PCs, it is not surprising that there exists a strong relationship between those PCs and those that intentionally target MJO activity. The correlation between either of the leading PCs and the CPC MJO index peaks at r=0.62, with PC2 leading CPC MJO index 1(refer to Chapter 2) by one pentad. The final evidence in favor of solidifying the argument that PCs 1 and 2 comprise the MJO extratropical response is a direct, quantitative comparison between the regression pattern obtained in Figure 4.4 and the regression of CPC MJO index 1 onto the same 200-hPa geopotential height field. Figure 4.6 shows the regression of CPC MJO index 1 onto the 200-hPa height field from lag=0 to lag=4 pentads. This is plotted alongside the regression of PC2 onto the same height field at lag=1 to lag=5 pentads. The offset is made to put the two indices on par given the one-pentad lag between them. This analysis reveals a striking similarity between the patterns, with spatial correlations from top to bottom of 0.82, 0.82, 0.84, 0.88, and 0.92, respectively. Additionally, the amplitudes of the regressions based on PC2 are higher than in the case of the CPC MJO index (this comparison can be made since both indices are normalized). This is a welcome result, and shows that the MJO extratropical response can be effectively deduced from the data without even direct knowledge of the divergent circulation.

This result also highlights the importance of using extend EOF analysis to diagnose the evolution of the MJO response on subseasonal time scales. An alternative approach might involve using non-extended, traditional EOF analysis of 200-hPa streamfunction, followed by lead/lag regression of the principal components. However, in that framework, the MJO response as observed in this work is not readily

observed (not shown). Only by using an extended data matrix in which the time evolution of the streamfunction field is explicitly included is this result achieved.

b. The ENSO Response

The third principle component closely resembles ENSO, with the polarity shown in Figure 4.7 being consistent with El Niño. The 200-hPa geopotential height footprint is recognizable based on the positive height center located southeast of Hawaii and a negative anomaly centered over the northeastern Pacific. Such a height pattern is therefore associated with an extension of the subtropical jet stream eastward across the Pacific toward western North America. This is consistent with the overview of this teleconnection pattern on seasonal time scales given in Chapter 1.

The particularly important aspect of this analysis, however, is that it is shown to explain some variance on subseasonal time scales. This is particularly relevant to subseasonal prediction efforts that include Weeks 3 and 4. Johnson et al. (2014) showed inclusion of ENSO as a predictor in a simple composite framework can enhance the skill of an otherwise MJO-based statistical forecast. The result shown here suggests that such a statistical prediction could be improved by inclusion of an objective metric of the subseasonal climate variability attributed to ENSO.

Due to the interannual nature of the ENSO phenomenon, the series of spatial patterns reveals a relative stationarity, especially with respect to the aforementioned two centers of action over the eastern Pacific. However, there are some nuanced differences throughout the five-pentad window that are worth mentioning. The geopotential height center near Hudson Bay grows substantially throughout the period, while the center over southeastern Asia subtly weakens with time. In the case

of the former, it is likely that the analysis emphasizes the time lag between convective forcing and the remote response. That is, given a stationary forcing mechanism, the steady-state teleconnection pattern is achieved at some lag.

Figure 4.8 conclusively links PC3 with ENSO based on the strong and coherent patterns seen in the OLR and SST correlations. In both cases, the patterns are stationary and reveal the classic ENSO response. There is a dipole of anomalous OLR between the central Pacific and the Maritime Continent, while SST correlations peak in excess of 0.7 in the benchmark Niño 3.4 region. Flanking the equatorial SST anomalies to both the north and south are anomalies of opposite, consistent with the known ENSO response.

c. The NPO/WP

The NPO/WP is a leading pattern of climate variability (e.g. Linkin and Nigam, 2008) that strongly influences surface temperature, and to lesser extent, precipitation variability over North America. This pattern was introduced in Chapter 1, and will be extensively highlighted in the next chapter, and emerges as the 4th PC in this analysis. Figure 4.9 reveals the characteristic dipole over the North Pacific, with the polarity displayed here typically referred to as the negative phase, keeping the same nomenclature as that for its North Atlantic counterpart. As seen in Chapter 1, this pattern is associated with a strong temperature footprint over much of North America.

Figure 4.9 also shows that this pattern is not associated with any strong pattern of 200-hPa velocity potential. The strongest divergent anomaly is observed at lag=-1

north of Hawaii, consistent with the anomalous secondary circulation induced by the center of action just east of the Date Line. The tendency for 200-hPa convergence over the equatorial Pacific grows with time, meaning it cannot be a forcing mechanism for the observed circulation pattern, but could be a weak response. The only plausible tropical forcing mechanism remaining is the divergent anomaly center over the far eastern Maritime Continent and western Pacific, though it too is weak compared to anomalous divergent circulation associated with the MJO extratropical response. This will be revisited in a discussion about the results of the RWS analysis to follow.

The correlations between the NPO/WP and both OLR and SST are shown in Figure 4.10. The OLR pattern is very stationary though weak, and suggests some lower-frequency variability may be present. The OLR correlations are dominated by higher latitude signals where OLR is more a proxy for temperature, highlighting the strong influence the NPO/WP pattern has on surface temperature over North America. The SST correlations in Figure 4.10 show an evolution more typical of midlatitude climate variability; the strongest SST footprint lags the anomalous atmospheric circulation. The acceleration of surface westerly winds near and just south of 30^{o} N leads to the growth of negative SST anomalies. In a horseshoe-shaped region around this feature, the growth of positive SST anomalies is observed. Ultimately, this pattern resembles a pattern known as the North Pacific Mode (NPM), a pattern of SST variability that will be discussed in the next chapter. This pattern of evolution is even clearer when low-frequency variability is explicitly removed via the subtraction of the 24-pentad mean anomaly from the streamfunction data prior to

analysis. While not shown here, that pattern is nearly identical to that seen in Figure 4.10, but with correlations starting near zero across the extratropical Pacific.

The gradual increase in the weak SST correlation over the western near-equatorial Pacific is consistent with the so-called seasonal footprinting mechanism, through with an NPO-like pattern induces positive SST anomalies over the West Pacific such that the system may evolve toward an El Niño event (Vimont, 2001, 2003).

At this point, we include a brief discussion of PC8, which is the pattern least associated with a canonical pattern of variability thus far identified in this work. This discussion is included here because there is some similarity between the NPO/WP and the PC8 200-hPa height regression, with PC8 associated with the evolution from a negative to a positive NPO/WP. The 4th PC (NPO/WP) lags PC8 with a correlation of -0.33 and lag=2, but it also leads with a correlation of 0.29 at lag=-2. In this way, the pattern shown in Figure 4.17 might be thought of as an NPO/WP transition pattern, albeit rather weakly.

The OLR and SST regressions revealed in Figure 4.18 show an ENSO-like pattern, with the maximum OLR correlation centered near or just west of the Date Line and nearly collocated with the peak SST correlation early in the five-pentad evolution. Taken in the context of the above discussion on the evolution of the circulation pattern, it suggests a weak tendency for negative to positive NPO/WP transitions to occur during cold ENSO years, and the opposite for warm ENSO years. However, this pattern is retained even in the so-called filtered analysis, but with even weaker SST, OLR, and velocity potential footprints. Thus, much remains unknown with respect to this pattern, and its relative importance.

d. The NAO

The NAO is perhaps the most well-known teleconnection pattern, associated with sea-level pressure variations between the semi-permanent Icelandic Low and Azores High. Its hydroclimate footprint is strongest in Europe, but extends westward to include eastern North America; Chapter 1 gives a more thorough introduction of this prominent teleconnection. In this analysis it emerges as the 5th leading pattern, with its 200-hPa geopotential height evolution depicted in Figure 4.11. Here it takes on a more annular structure, while still being centered over the North Atlantic, and its polarity commonly associated with the negative phase. Figure 4.11 also reveals that the NAO has a stronger relationship with 200-hPa velocity potential anomalies over the tropics than does the NPO/WP. Comparison with Figure 4.2 suggests that the NAO as deduced in this analysis may lag MJO forcing (with sign opposite to that shown in Figures 4.2-4.3), a result consistent with studies linking the MJO to NAO and annular mode variability (e.g. Lin et al., 2009; Zhou and Miller, 2005). Extending the lead regressions back to t=-6 pentads (not shown) reveals a weak pattern, though one consistent with eastward propagating MJO activity. Also noteworthy in Figure 4.11 is that a weak, but coherent velocity potential pattern propagates eastward with enhanced upper-level divergence (convergence) over the Maritime Continent (East Pacific) by lag=1. This is also consistent with Lin et al. (2009) that suggested a negative NAO might excite an enhanced phase of the MJO over the Indian Ocean. However, this pattern does not result in a notable transition away from this pattern as might be expected given the current body of literature. Given the NAO's relatively low frequency (Figure 4.1) in this analysis, it is not surprising that extending the

lead/lag periods on either side of Figure 4.11 do not result in a large change in the 200-hPa geopotential height pattern. Therefore, it is suggested that the NAO is primarily a pattern of variability internal to the extratropics, but may be excited by MJO-related convection. That is, the pattern observed in Figure 4.2 may sometimes persist on low-frequency time scales.

Figure 4.12 shows the correlations of PC5 with OLR and SST. There is nothing particularly noteworthy about these patterns in light of the above discussion. Not surprisingly, the strongest SST correlations are in the extratropics and lag the anomalous atmospheric circulation in a predictable fashion. The OLR correlations are consistent with the discussion of the evolution of the 200-hPa velocity potential field, with weak negative (positive) correlations developing over the eastern Indian Ocean and Maritime Continent (western and central Pacific).

e. The PNA

The PNA pattern is a well-known teleconnection pattern that has been discussed throughout this work. It is highlighted by an arcing pattern of four centers of action spanning from the subtropics west of the Hawaii to the North Pacific, northwestern North America, and, finally, the southeastern United States. Many previous studies have linked the PNA to MJO-related convection (e.g. Mori and Watanabe, 2008) and even ENSO-related convection (Horel and Wallace, 1981). In the case of the former, it is suggested that a negative (positive) PNA is preferred when the enhanced (suppressed) phase of the MJO spans from the Bay of Bengal to the West Pacific (Bao and Hartmann, 2014). In the latter, El Niño is thought to incite a positive PNA via anomalous diabatic heating and associated upper-level divergence

over the central equatorial Pacific. As shown in Chapter 1, an analysis that allows for more tropical influence (e.g. using geopotential height at 200-hPa instead of 500-hPa) can distinguish between a PNA pattern and the ENSO response. In short, principal component analysis using a variable emphasizing the extratropics and/or explicitly excluding the tropics from the analysis domain is more likely to have variance explained by ENSO aliased into the extratropical teleconnections.

In this analysis, the PNA emerges as the 6th and 7th PCs, with PC6 (PC7) associated with PNA development (decay). The two-pentad lag correlation between these time series is 0.75, with PC6 leading PC7. Figure 4.13 shows the 200-hPa height regressions associated with PNA development. As in Chapter 3, the PNA is preceded by an NAO-like dipole in the North Atlantic and anomalous heights over northeastern Europe. The evolution of the associated velocity potential patterns reveals the strongest divergent anomalies centered over the midlatitudes, from Asia to the eastern Pacific, shifting eastward as the pattern matures. A divergent anomaly develops south of Hawaii, consistent with the development of the low-latitude center of action west of Hawaii.

Figure 4.14 is revealing in the context of the prevailing understanding of the PNA, namely, that tropical convection plays a prominent role in its excitation. Mori and Watanabe (2008) estimated that 30% of PNA events are attributable to MJO-related convection, but Figure 4.14 reveals a very weak association between tropical convection and the PNA. In fact, the pattern shows positive PNA development very weakly preceded by enhanced convection in the Indian Ocean, and contemporaneous, remote links in Figure 4.16 are strongest over the Maritime Continent. In any case,

the strongest OLR signature develops in a west-east dipole near 15oN from northeast of the Philippines to south of Hawaii. To first order, this is consistent with the expected secondary circulation and thus not considered a forcing mechanism but rather a hydroclimate response associated with the PNA itself. This issue will be revisited in the discussion of the RWS analysis to follow.

Figure 4.15 is associated with the decay phase of the PNA pattern, though it displays some differences in the mature pattern with Figure 4.13. Generally, there is a somewhat different connection to the North Atlantic, with the decay phase having a contemporaneous link to the North Atlantic. There, the 200-hPa geopotential height center is nearly orthogonal to the NAO-like dipole that precedes PC6 in Figure 4.13; elsewhere, features are generally similar to Figure 4.13.

The SST footprint of the PNA pattern revealed in Figure 4.15 reveals some important insights, based on the both the history of the PNA-ENSO paradigm and the analysis given in the introductory chapter. Remarkably absent is any correlation with SSTs in the equatorial Pacific, suggesting a clean separation between a PNA pattern of extratropical origin, and both the MJO and ENSO extratropical responses. In Chapter 1, the PNA pattern extracted on monthly time scales still retains some SST signature in the equatorial Pacific. The results presented from this analysis suggest that this could be partly due to lower-frequency MJO tendencies being manifest in part as PNA variability. This could also be related to non-canonical ENSO variability as discussed in a preceding subsection, which discusses the possibility of interannual central Pacific SST variability leading to a preferred pattern of subseasonal MJO-related convective variability. In the extratropical Pacific, the PNA pattern is

observed as leading the development of an SST pattern featuring the extension of cold SST anomalies eastward from Japan, with warm SST anomalies extending from near Hawaii to the West Coast of North America.

f. Insights from the RWS analysis

The RWS term defined in Sardeshmukh and Hoskins (1988) is designed to allow for a physical link between equatorial heating/divergence and the generation of a remote vorticity source away from the equator. Here we emphasize the vorticity tendency generated by the advection of climatological absolute vorticity by the anomalous meridional divergent wind:

$$S = -v_\chi' \cdot \nabla \eta_c \qquad (1)$$

Analysis of this sort can be difficult to interpret due to a tendency toward Sverdrup balance, wherein the tendency term is negligible as the stretching term balances the total advection term. However, the analysis can still be quite useful in contributing to a diagnosis of whether a particular pattern is consistent with tropical forcing. In order to make such a determination, we look for a tropically based velocity potential anomaly that corresponds to a height response in line with the RWS term (1). Analysis is conducted by correlating (1) with the PCs discussed in preceding subsections.

Figure 4.19 shows the evolution of this RWS term with respect to both the 2nd PC comprising the development of the MJO response and PC3, closely associated with ENSO. The sign is such that the positive (negative) values are proportional to positive (negative) height tendency in the Northern Hemisphere. In the case of the MJO response, negative values are observed in the tropical and subtropical west-central

Pacific basin, a region with growing negative height anomalies in Figure 4.3. Likewise, over southern Asia, RWS anomalies are such that positive height tendency is inferred, and that is precisely what is observed in Figure 4.3. Therefore we can confidently implicate the tropics as a casual mechanism for the observed pattern in Figure 4.3 based on 1) a robust equatorial velocity potential footprint, and 2) the development of height anomalies consistent with the resulting tropical RWS term.

A similar argument can be made for the ENSO pattern. Here, however, the situation is likely in Sverdrup balance, since this is a low-frequency pattern that can be thought of as a steady-state response to anomalous convection over the central equatorial Pacific. The RWS term would correspond to positive height anomalies oriented in a northwest to southeast fashion extending from west of Hawaii to near the equator. Figure 4.7 is fairly consistent with this portrayal. Also, the RWS term suggests negative height anomalies over southeastern Asia, which is also consistent with Figure 4.7.

Figure 4.20 shows two patterns where a causal tropical mechanism cannot be readily inferred: the NPO/WP (PC4) and the PNA (PC6). In the case of the NPO/WP, the RWS term suggests a positive height tendency just east of China, but positive height anomalies are not observed here in Figure 4.9. Likewise over Hawaii, negative height anomalies are inferred. While this region is nearly orthogonal to the center of action near 30^{o}N, the tendency over time is to move nearer climatology. This strong RWS footprint is likely resulting from the secondary circulation associated with the midlatitude center of action over the central Pacific, and little connection to the tropics can be made.

The PNA pattern, too, is associated with strong RWS footprint, manifest here as four centers of action, each in a quadrant around the robust geopotential height center of action associated with Aleutian Low variability, suggesting the divergent circulations are extratropical in origin. This is consistent with Figure 4.13, which shows that the velocity potential signature is strong in the midlatitudes and weak in the tropics. Particularly revealing is the dichotomy between the positive height tendency inferred by the RWS term centered near 25^{o}N, 120^{o}E, and the observed 200-hPa height regressions for the same area. This is near the development of weak negative height anomalies through the period. The positive subtropical center of action west of Hawaii in Figure 4.13 is also coincident with weak negative RWS correlations. Therefore, like the NPO/WP, the PNA cannot be readily attributed to tropical forcing in this context.

4.4 Summary and Discussion

This analysis highlights the importance of using streamfunction in conjunction with time-extended EOF analysis to extract teleconnection patterns that can be attributed to tropical or extratropical forcing. This analysis eliminates the need to assess the impact of the MJO or ENSO on the PNA, per se, as the various PCs constitute the patterns in ways that are more consistent with the underlying forcing mechanisms. Specifically of interest here is whether these teleconnections can trace their origins to anomalous tropical convection, and this analysis largely succeeds on that front. While such an elegant separation of the NAO and the MJO is not achieved, it does reinforce the body of literature that links the two. The contribution from this work is to suggest that low-frequency NAO variability may be excited by higher-

frequency MJO variability. Some key points and implications from this Chapter follow:

- The extratropical MJO response can be explicitly identified using subseasonal analysis of 200-hPa streamfunction, without any direct knowledge of the divergent circulation.
- The link between anomalous tropical convection and the PNA is severed in this context, wherein the MJO teleconnection is explicitly captured. Likewise, the connection between the PNA and equatorial Pacific SSTs is also refuted.
- A causal link between tropical convection and the NPO/WP cannot be readily established.
- This analysis could be useful in subseasonal attribution analysis, an exercise of interest to operational centers and academic institutions alike.
- An important future endeavor is to evaluate the state-of-the-art subseasonal-to-seasonal (S2S) model suite using a similar analysis.

Chapter 4 Figures

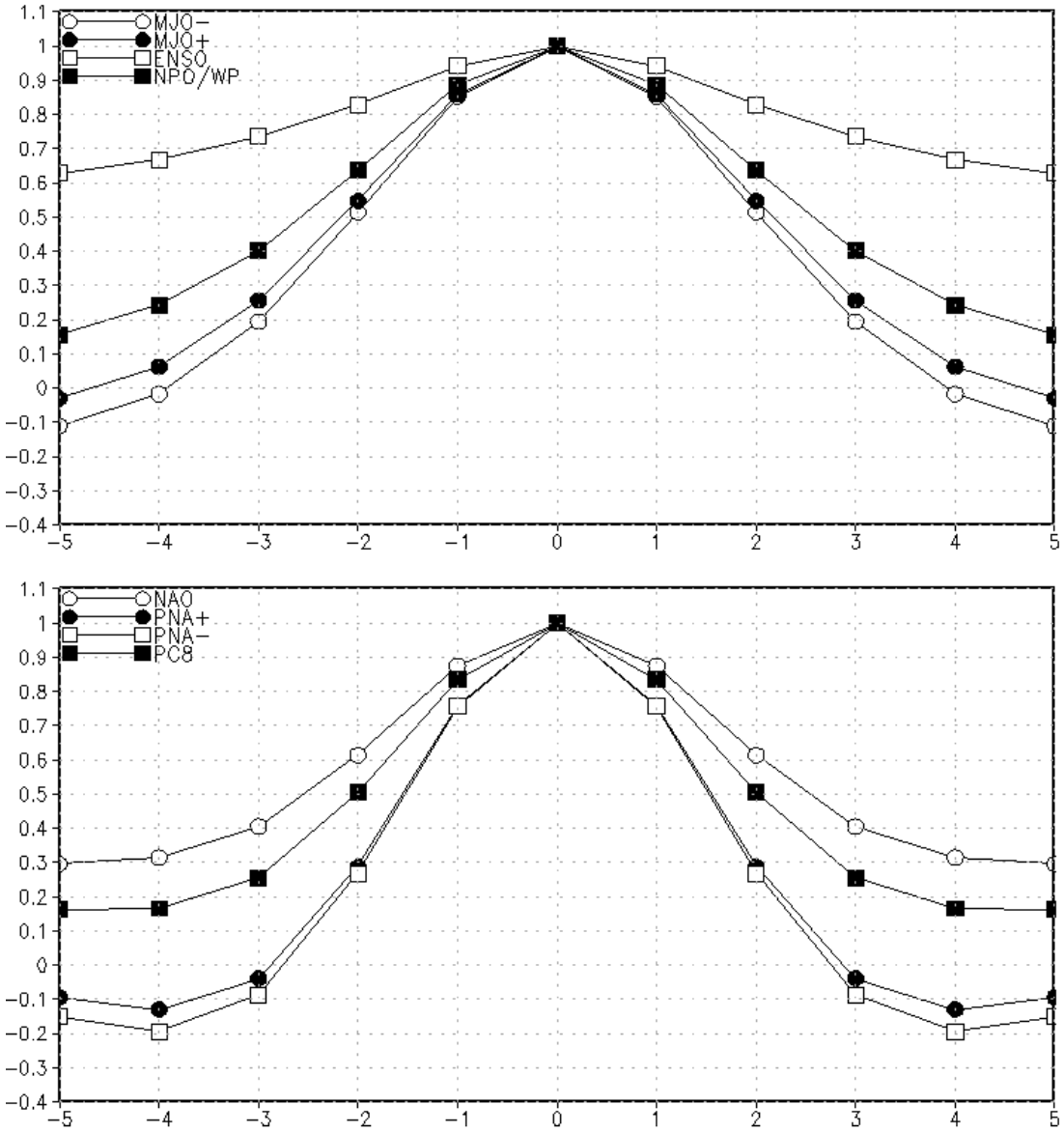

Figure 4.1: Autocorrelation curves for each of the eight principal components. The legends list the pattern names in descending order based on percentage of variance explained.

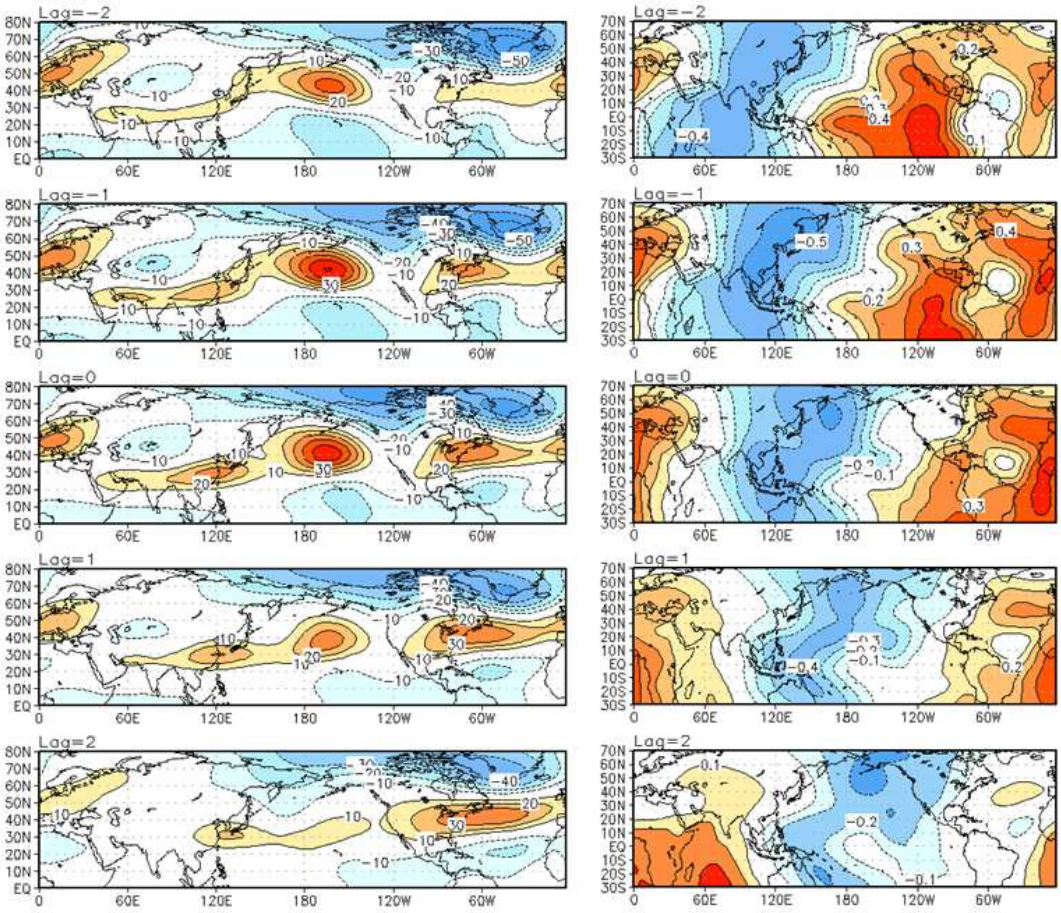

Figure 4.2: Left: lead/lag regression (-2 to +2 pentads) of the 1st principal component (10.1% of explained variance) onto the 200-hPa height field. The height field is used rather than streamfunction to facilitate more direct comparison with teleconnection patterns obtained via other analyses. This pattern closely resembles the extratropical MJO response. The contour/shading interval is 10m, with the zero contours suppressed. Right: Correlation of the first principal component with 200-hPa velocity potential. A key feature here is the strong connection to the deep tropics. An eastward propagating pattern is observed, consistent with MJO evolution. The contour/shading interval is 0.1, with the zero contours suppressed.

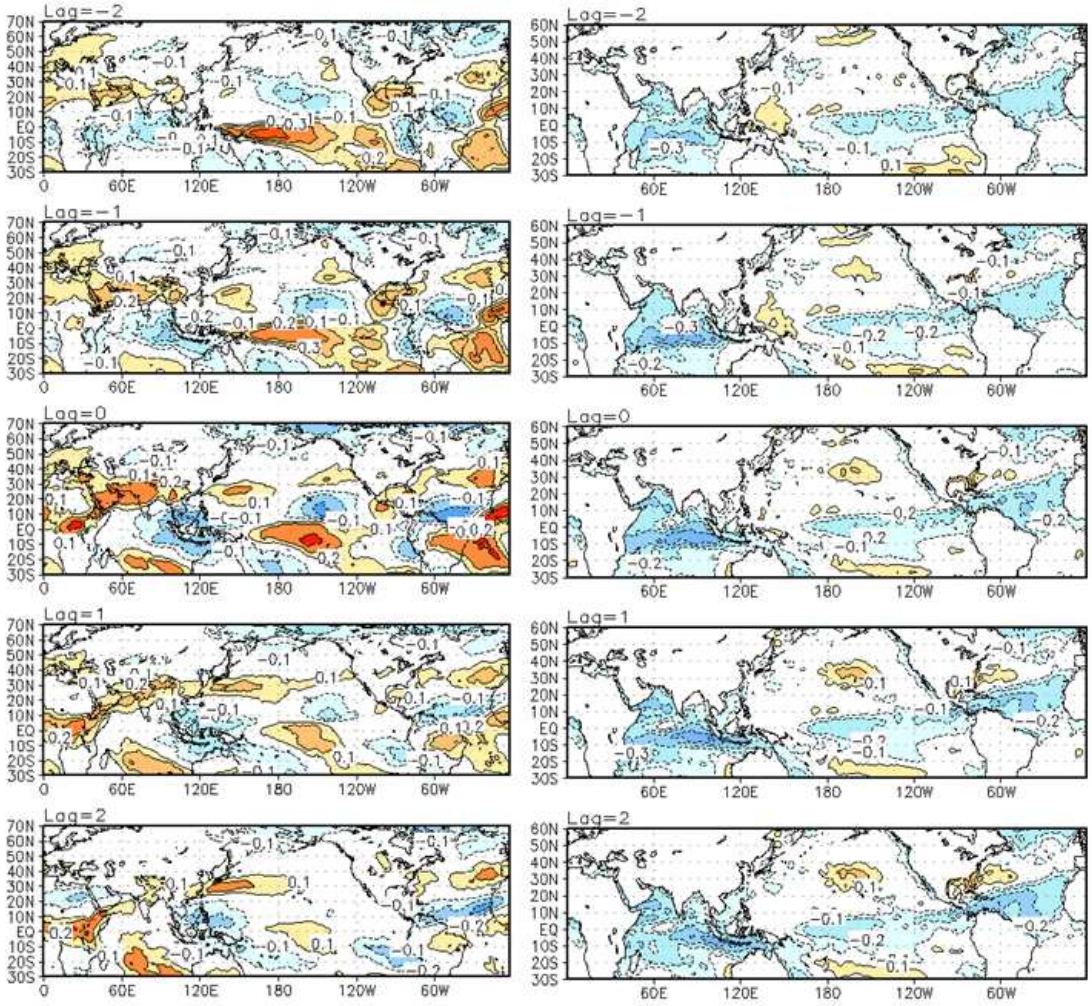

Figure 4.3: Left: lead/lag correlation (-2 to +2 pentads) of PC1 (MJO response) with outgoing longwave radiation (OLR), a proxy for tropical convection. The contour/shading interval is 0.1 and the zero contours are suppressed. Right: Same as left but for SST.

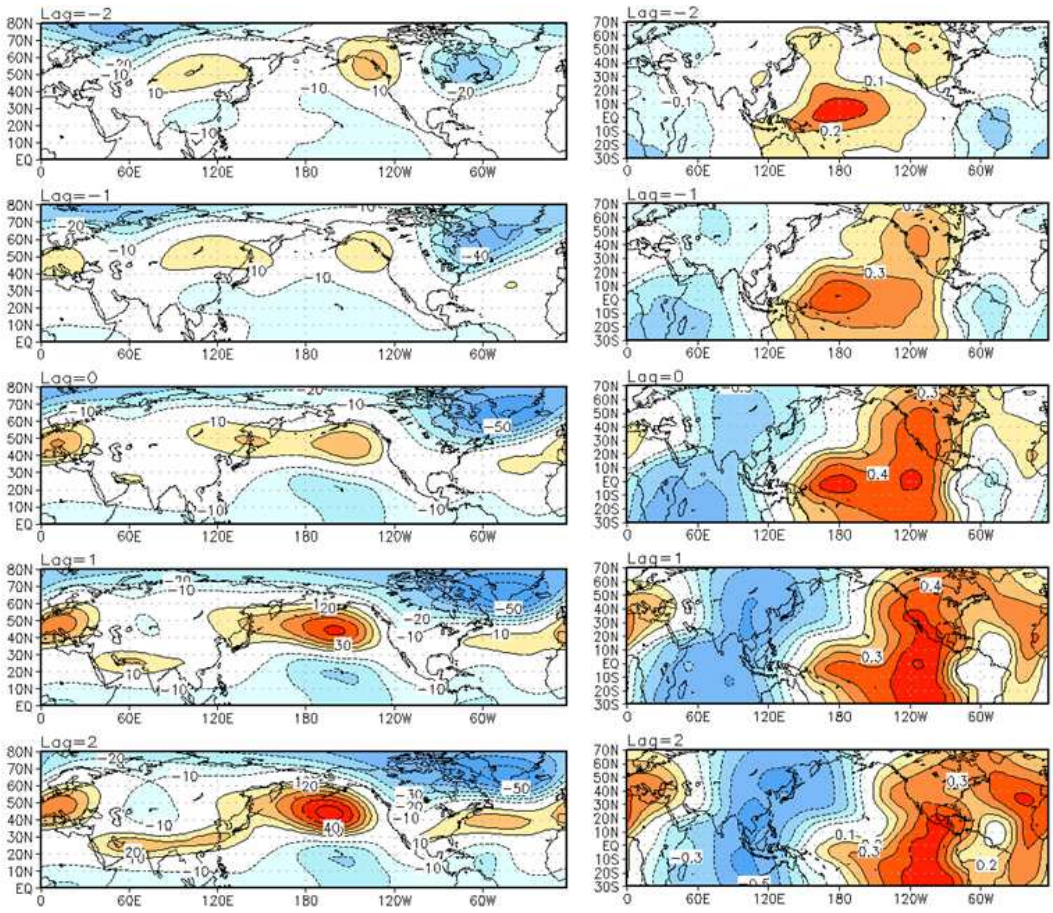

Figure 4.4: Same as Figure 4.2, except for the 2nd principal component (9.8% of explained variance). This pattern also constitutes the MJO extratropical response, leading the 1st PC by three pentads (r=0.9). Therefore this pattern is the development of the MJO extratropical teleconnection.

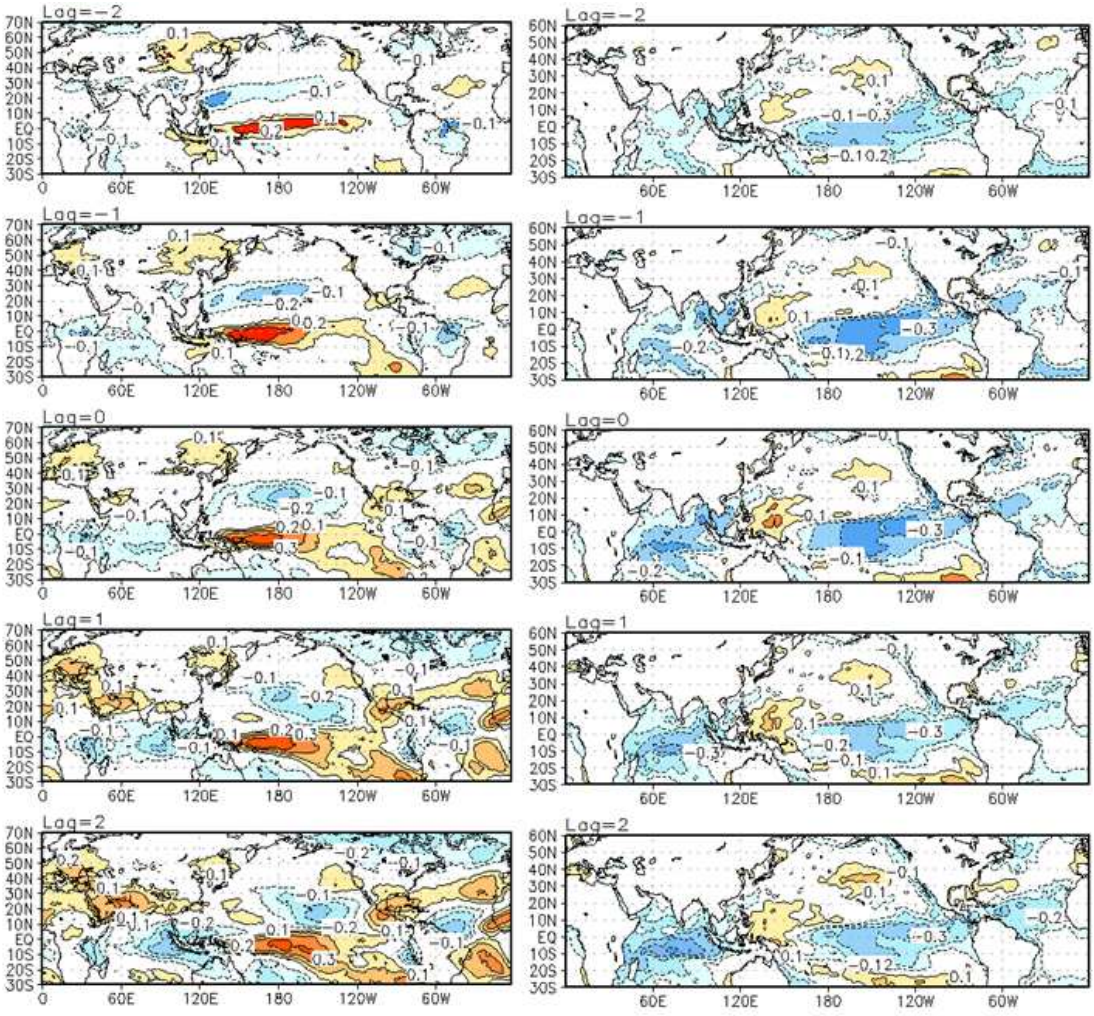

Figure 4.5: Same as Figure 4.3, except for PC2, which along with the leading pattern comprise the MJO response.

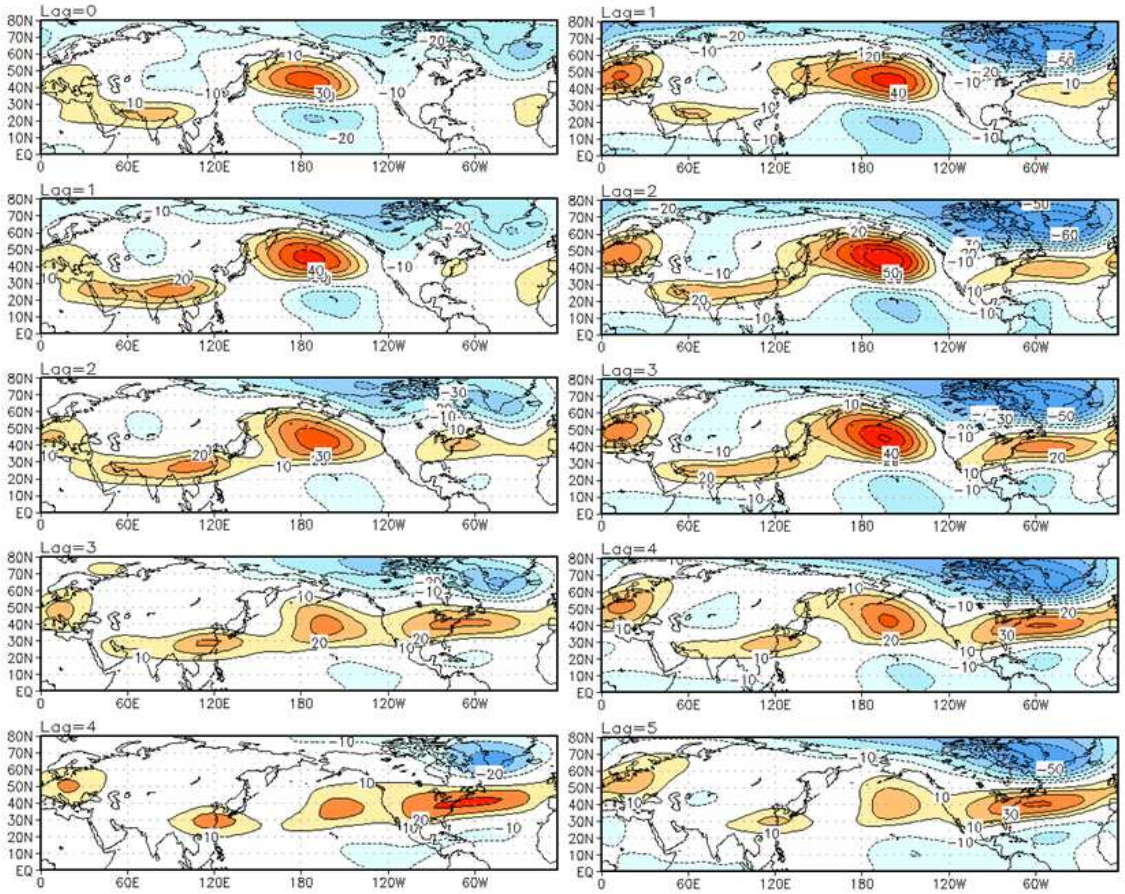

Figure 4.6: Left: Lag regression (lag=0 to lag=4) between CPC MJO Index 1 and the 200-hPa geopotential height. Contour interval is 10m, with the zero contours suppressed. Right: Same as left, but for PC2 (lag=1 to lag=5). Spatial correlations from top to bottom are 0.82, 0.82, 0.84, 0.88, and 0.92.

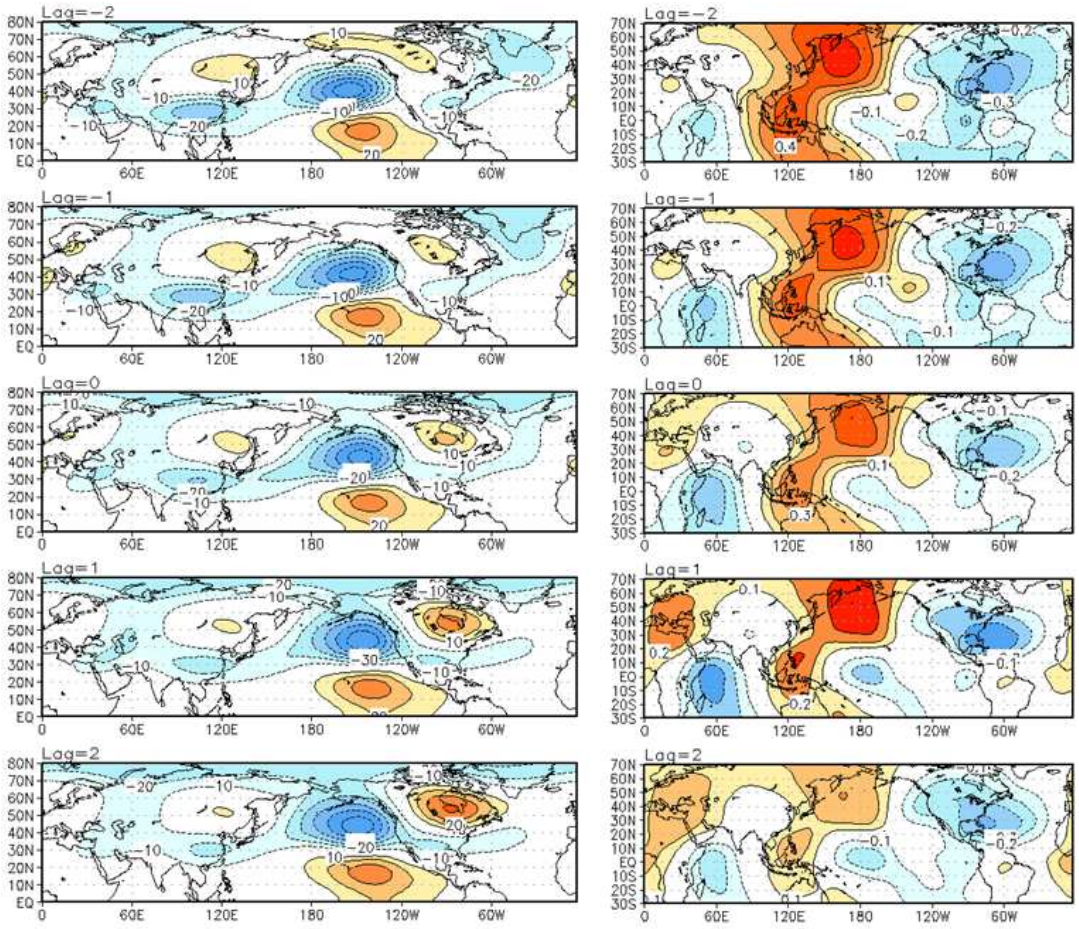

Figure 4.7: Same as Figure 4.2, except for the 3rd principal component (4.0% of explained variance). This pattern is recognizable as the ENSO response, with the polarity shown here being consistent with El Niño. The pattern is highlighted by its stationary footprint, consistent with a pattern of primarily interannual variability.

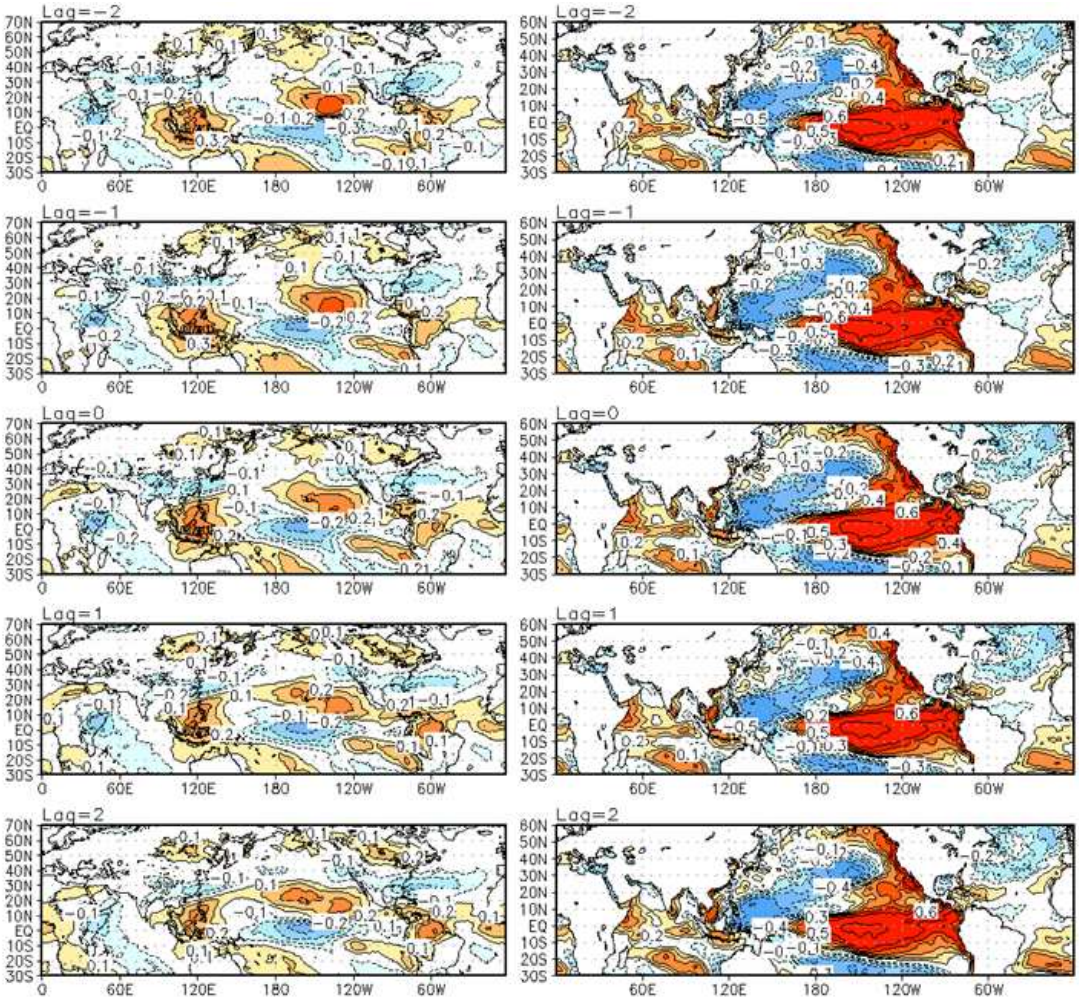

Figure 4.8: Same as Figure 4.3, except for PC3. This pattern is most clearly associated with ENSO as seen by its strong SST footprint over the tropical Pacific.

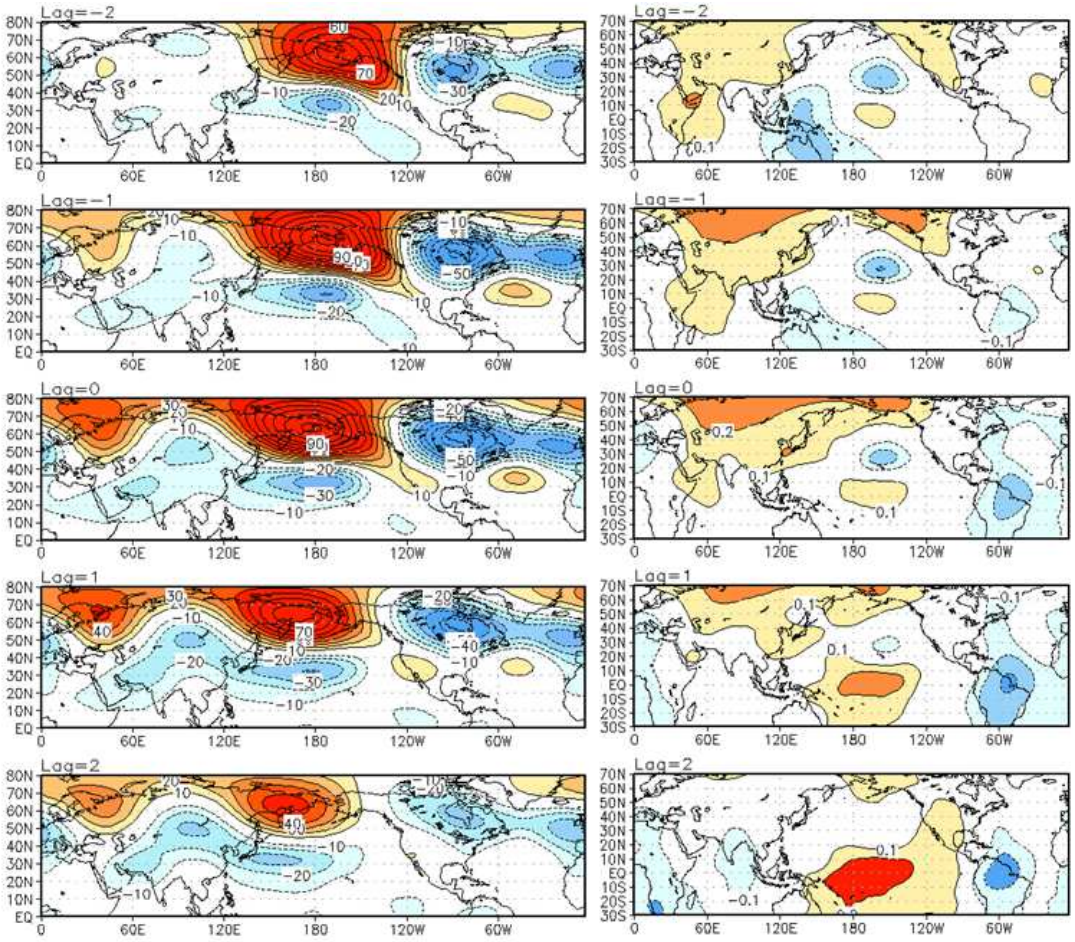

Figure 4.9: Same as Figure 4.2, except for the 4th principal component (3.4% of explained variance). This pattern is most clearly the North Pacific Oscillation/West Pacific (NPO/WP), identified by the strong north-south dipole just east of the Date Line and a downstream center of action over North America. The velocity potential pattern is notably weak, suggesting this pattern is primarily driven by extratropical dynamics.

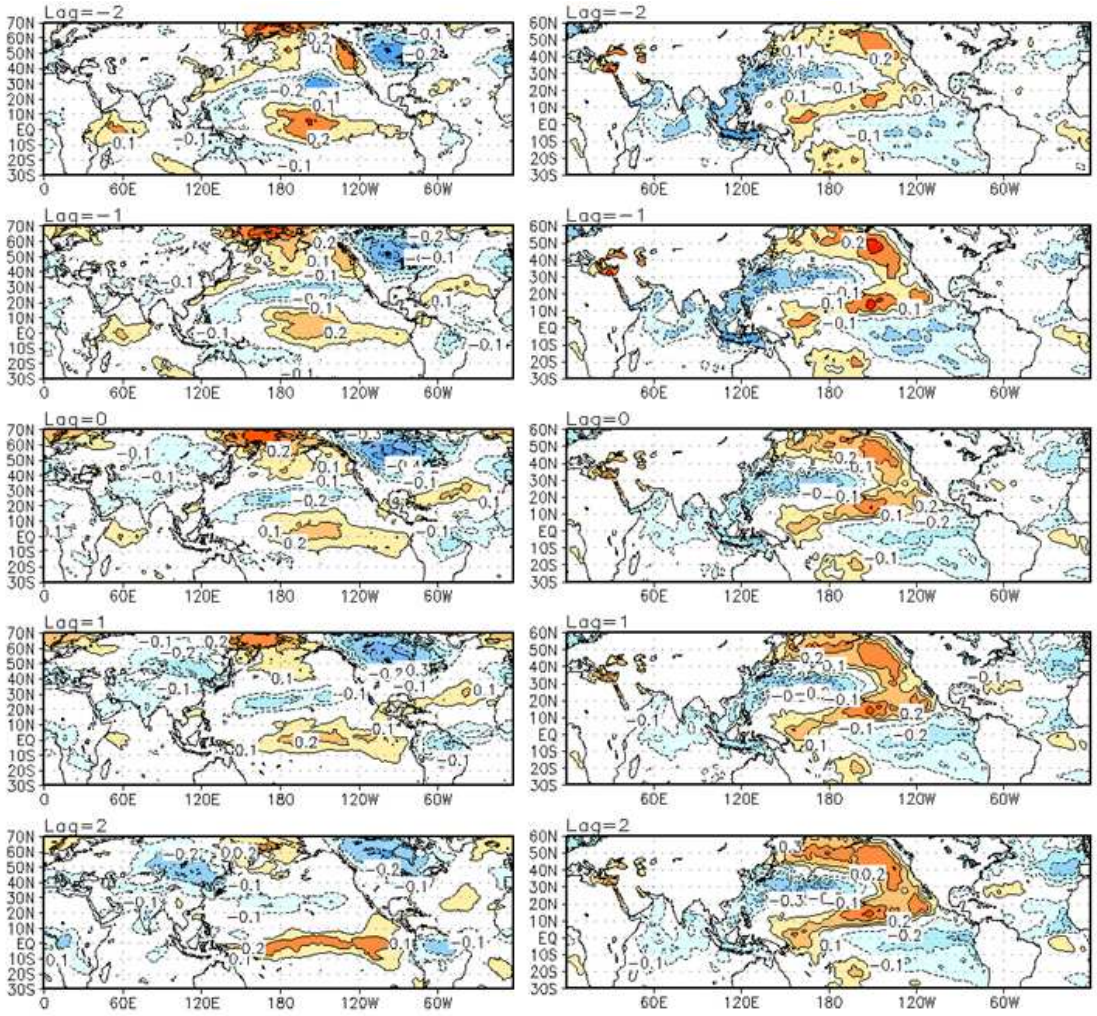

Figure 4.10: Same as Figure 4.3, except for PC4, which constitutes the NPO/WP. This pattern is highlighted by growing SST anomalies over the North Pacific.

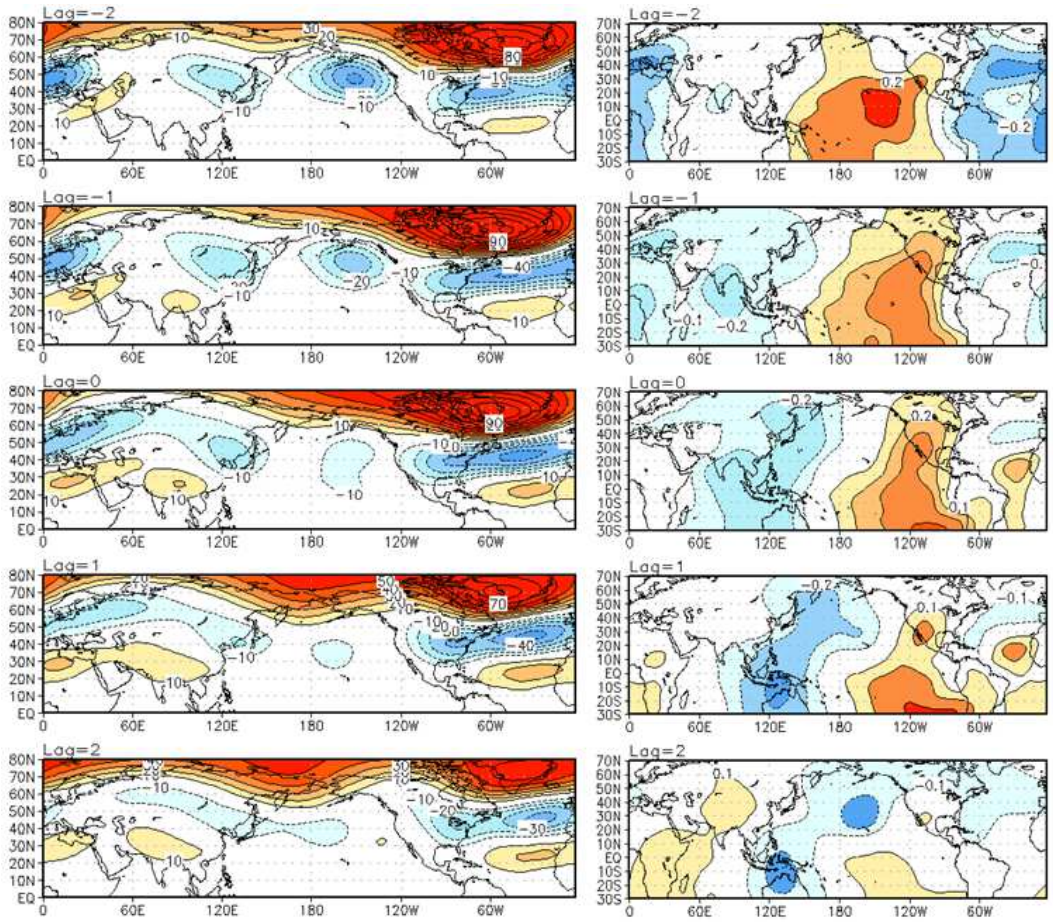

Figure 4.11: Same as Figure 4.2, except for the 5th principal component (3.3% of explained variance). This pattern is most clearly associated with the North Atlantic Oscillation (NAO) and its well-known dipole over the North Atlantic. This pattern also takes on a more annular structure, consistent with the oft-studied relationship between the NAO and Northern Annular Mode (NAM).

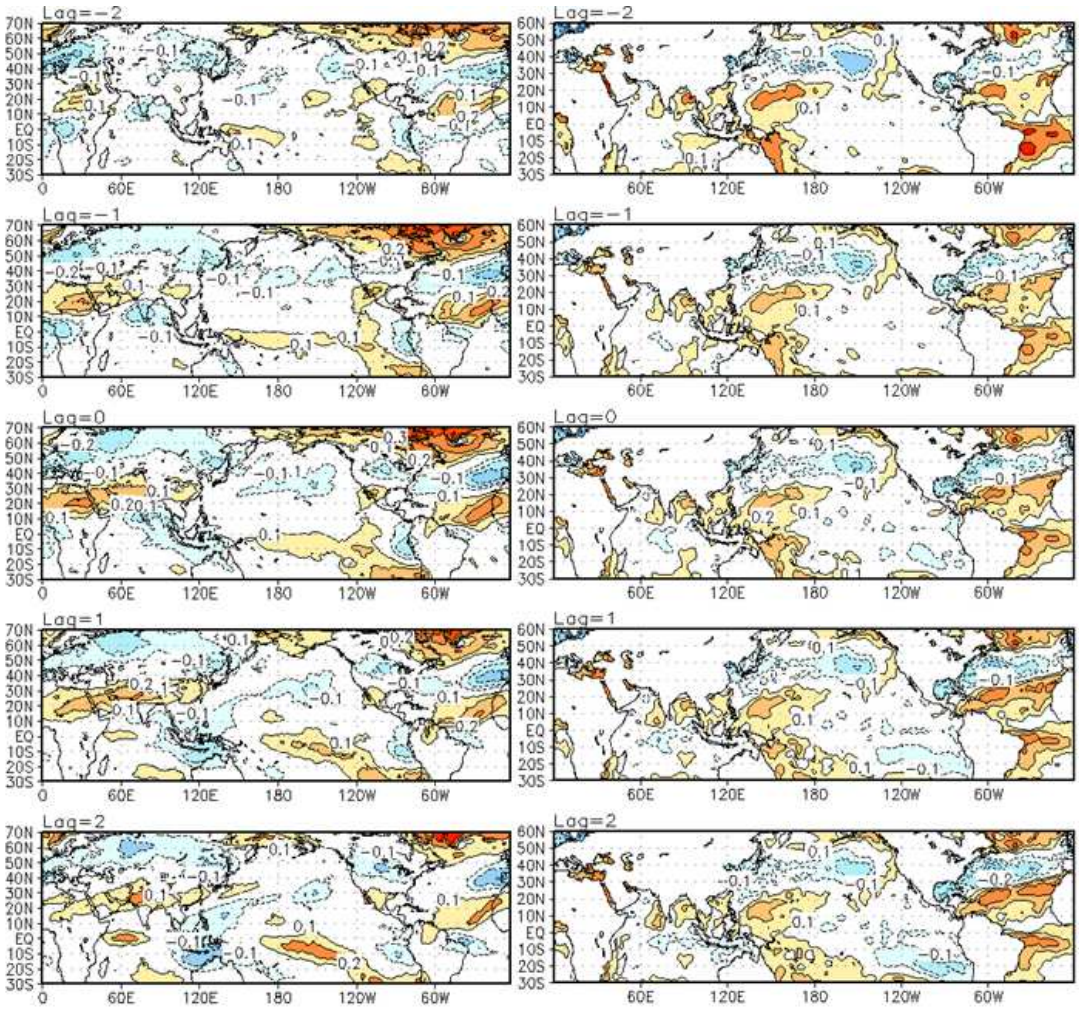

Figure 4.12: Same as Figure 4.3, except for PC5. This pattern represents the NAO, and shows the strengthening of the well-known SST tripole over the North Atlantic.

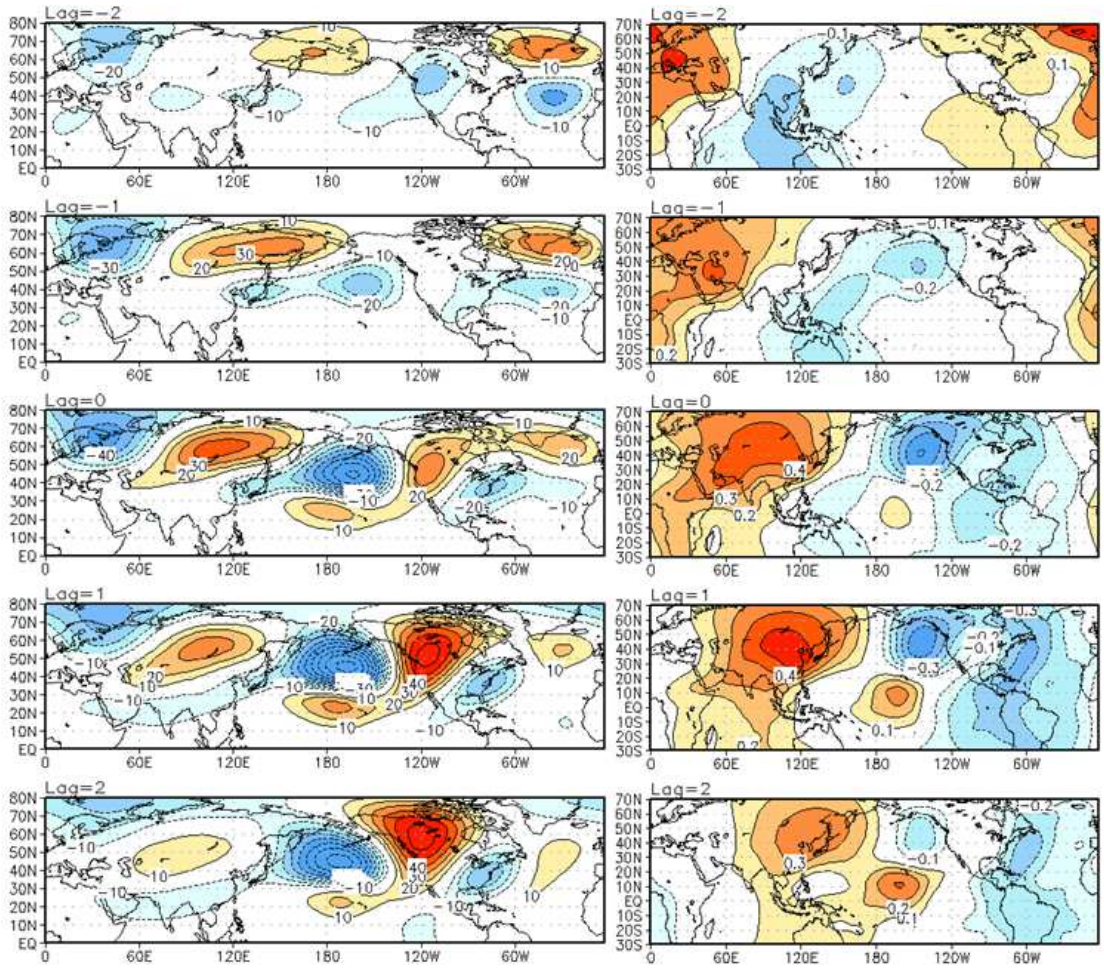

Figure 4.13: Same as Figure 4.2, except for the 6th principal component (3.3% of explained variance). This pattern is most closely related to the development of the Pacific-North America (PNA) pattern, which consists of four centers of action arcing from west of Hawaii to southeastern North America. The velocity potential evolution reveals divergent anomalies centered largely in the midlatitudes.

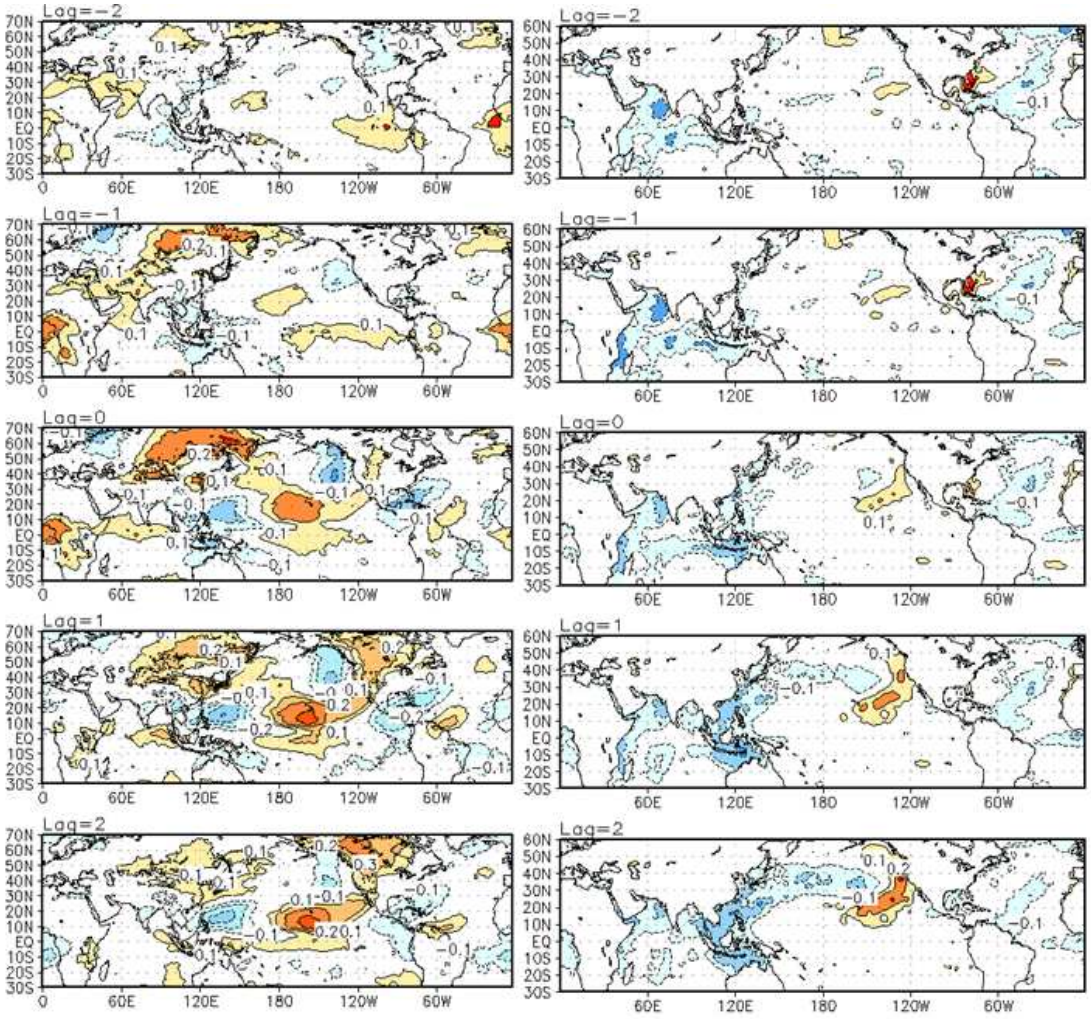

Figure 4.14: Same as Figure 4.3, except for PC6. Associated with the development of the PNA pattern, the OLR footprint lacks a pronounced near-equatorial footprint. The west-east dipole centered near 15°N is consistent with the secondary circulation associated with that pattern's subtropical center of action.

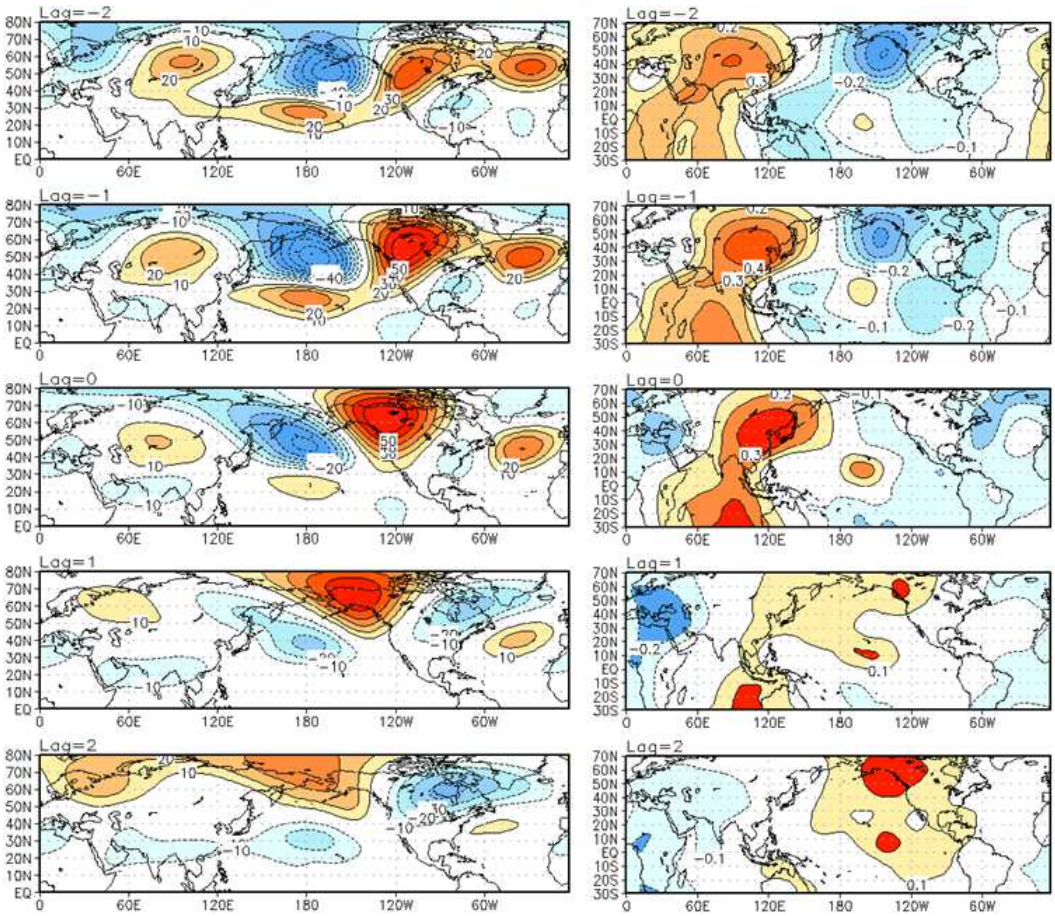

Figure 4.15: Same as Figure 4.2, except for the 7th principal component (3.2% of explained variance). This pattern is most closely related to the decay of the Pacific-North America (PNA) pattern, exhibiting a strong correlation with PC 6 at a two pentad lag (r=0.75). There is some evidence of a transition from a PNA to an NPO/WP pattern.

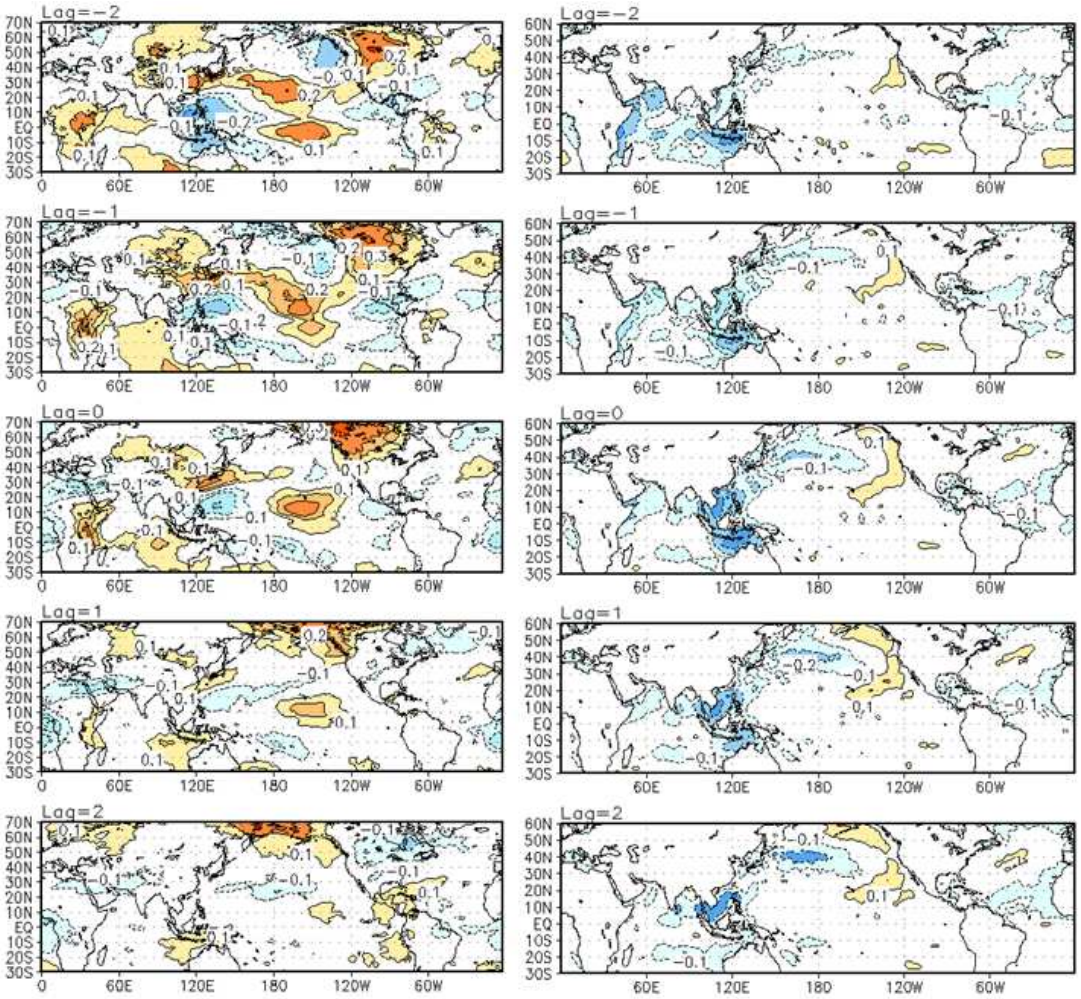

Figure 4.16: Same as Figure 4.3, except for PC7.

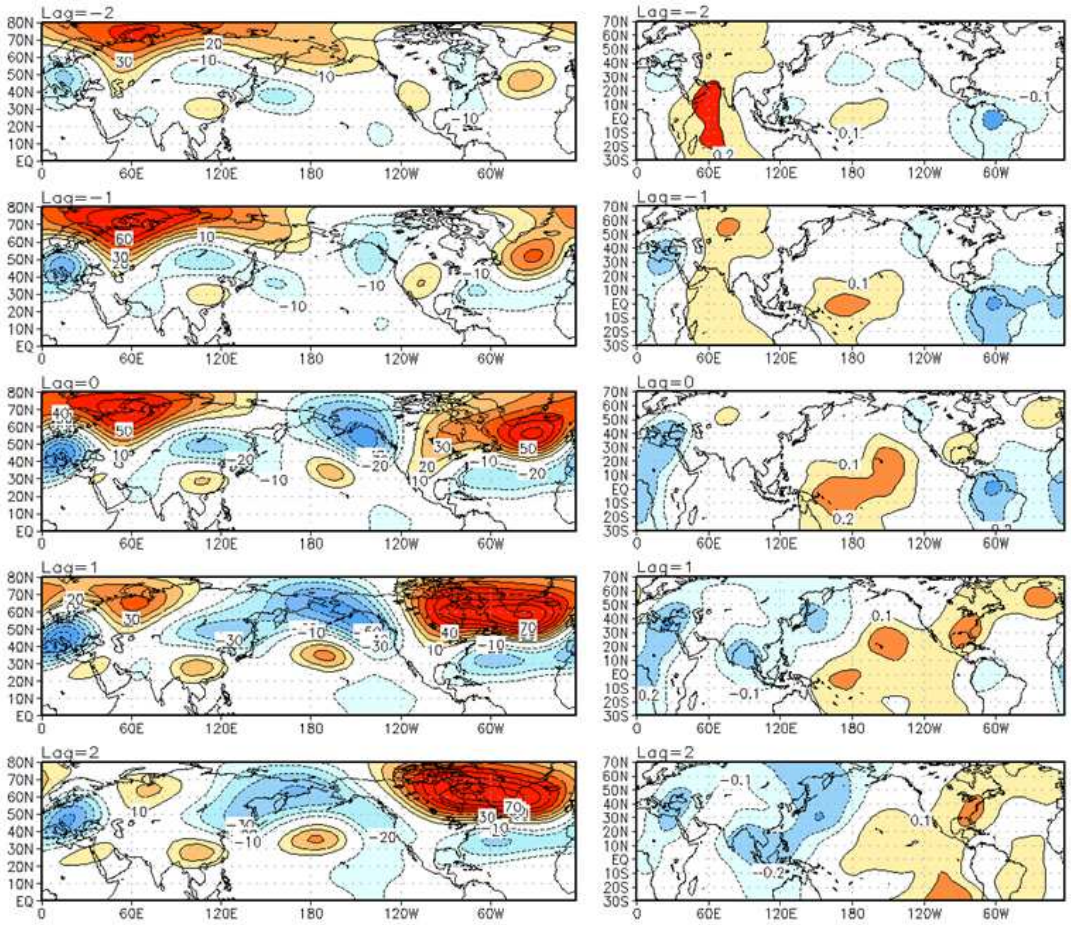

Figure 4.17: Same as Figure 4.2, except for the 8th principal component (3.0% of explained variance). This pattern shows westward propagation of high-latitude height anomalies, with a weak connection to anomalous tropical divergence.

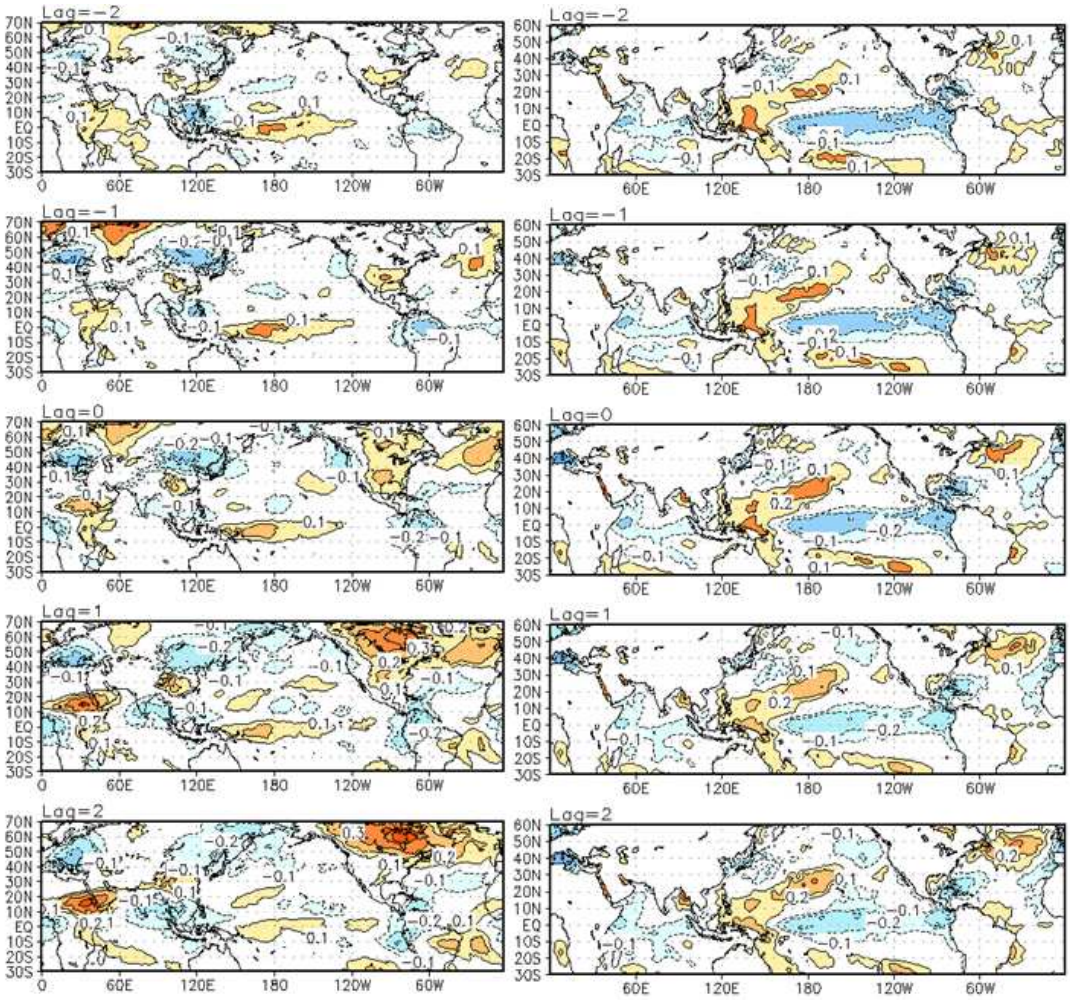

Figure 4.18: Same as Figure 4.3, except for PC8.

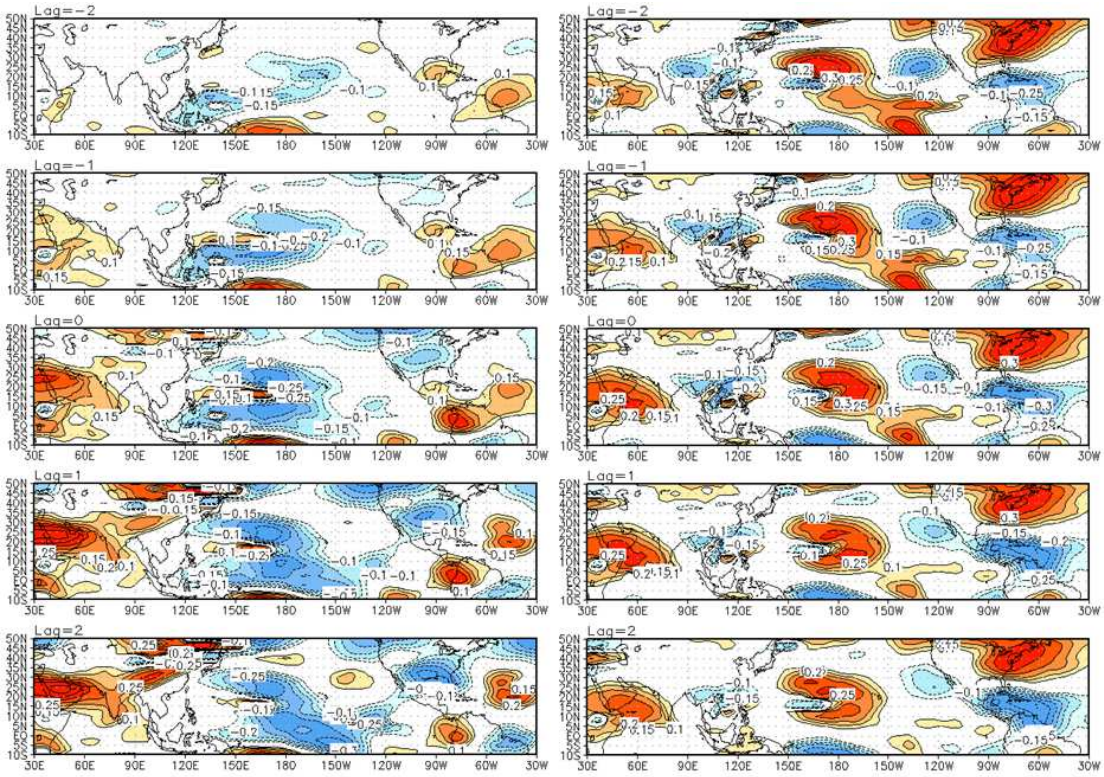

Figure 4.19: Left: Correlation of PC2 (MJO response) with the RWS term, $-\boldsymbol{v}_{\chi}' \cdot \nabla \eta_c$, that corresponds to advection of the climatological absolute vorticity by the anomalous meridional divergent wind. Contour interval is 0.05 starting with the 0.1 contour. Values are plotted to be proportional to height tendency in the Northern Hemisphere. Right: Same as left except for PC3 (ENSO response).

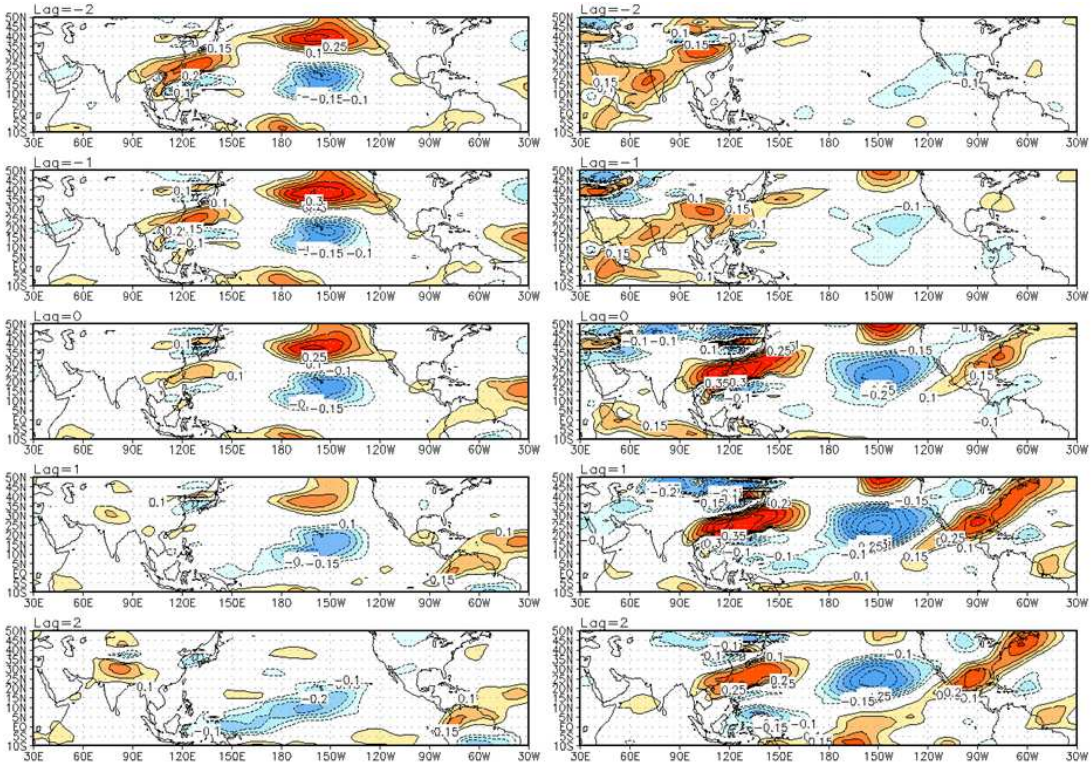

Figure 4.20: Left: Same as Figure 4.19, except for PC4 (NPO/WP). Right: Same as Figure 4.19, except for PC6 (PNA).

Chapter 5: Attribution of the Extreme Winter of 2013-2014

Part I. The Key Role of the NPO/WP

a. Background

The 2013-2014 winter (December 2013 – February 2014) was anomalously cold across large swaths of central-eastern North America. Multiple, intense cold snaps prompted prolonged media attention, sent energy prices skyward, and led to scientific hypotheses on the cause of an extreme regional winter season in an otherwise warming global climate (Palmer 2014, for example). A careful analysis of the established winter patterns of monthly atmospheric circulation variability and their near-surface temperature footprints attributes the 2013-2014 extreme winter across North America, largely, to the NPO/WP.

The NPO/WP acronym is used for North Pacific Oscillation (NPO) and the West Pacific (WP) teleconnection pattern, as discussed in the introductory chapter. The NPO, a north-south seesaw in winter sea-level pressure over the North Pacific on monthly (and shorter) time scales, was identified by Sir Gilbert Walker in 1924. The NPO was known to synoptic forecasters of the United States Weather Bureau as early as 1916 because of its significant influence on US winter weather. They noted that the oscillation phase with higher pressure over Alaska and lower pressure over Hawaii was linked with colder conditions over eastern North America, much as during the 2013-2014 winter. The WP pattern was defined by Wallace and Gutzler (1981) from teleconnection analysis of the mid-tropospheric geopotential height field in boreal winter. It consists of a north-south dipole over the western Pacific basin in the

Northern Hemisphere. Later analysis showed the WP and NPO to be essentially the same variability, with the NPO being the sea-level pressure reflection of the WP geopotential height pattern (Wallace and Gutzler 1981; Nigam 2003; Linkin and Nigam 2008).

The NPO/WP variability pattern is the Pacific basin analog of the NAO (Nigam 2003; Nigam and Baxter, 2014). Both consist of a north-south dipole in sea level pressure and tropospheric height anomalies across their basins as well as latitudinal displacement of the climatological jet streams. Not surprisingly, each alters the storm tracks near and downstream of their centers of action, with the NAO impacts pronounced over far eastern North America and Europe, and the NPO/WP ones influential over northeastern Asia and North America. Large amplitude monthly and seasonal geopotential height anomalies resembling the WP pattern would thus be well-positioned to significantly impact the surface climate over North America – the case in 2013-2014 winter.

There is some recent literature that has related NPO variability to changes in central Pacific SSTs, namely, central Pacific El Niño events (DiLorenzo et al, 2013; Furtado et al. 2012), mostly on decadal time scales. Our analysis suggests that links on monthly and seasonal time scales are tenuous at best, as the SST and outgoing longwave radiation (OLR, used as a proxy for tropical convection) footprints of the NPO/WP as revealed here are weak (correlations of ~0.2 or less, not shown). In a subsequent section, an SST-centric analysis is discussed that further suggests that anomalous tropical convection/SSTs cannot be readily indicted as a causal mechanism of the NPO/WP. To some extent, this was also discussed in Chapter 4,

wherein the NPO/WP was not found to be a pattern of climate variability closely linked to the tropics.

Another variability pattern of some significance during the 2013-14 winter is the Tropical-Northern Hemisphere (TNH) pattern. The TNH was identified by Mo and Livezy (1986), and was believed to be related to El Niño Southern Oscillation (ENSO) variability. Nigam and Baxter (2014) however showed ENSO's extratropical winter response to be distinct from the TNH pattern. Rotated empirical orthogonal function (EOF) analysis of 200-hPa heights (as in this study, and Nigam and Baxter 2014) yields two patterns related to SST variability in the tropical Pacific: *a)* a height response in the western hemisphere extratropics and global tropics with little subseasonal variability (ENSO's classic winter season response), and *b)* a more extratropically confined response exhibiting greater month-to-month variability (TNH-like pattern).

The objective of this analysis is quantitative attribution of the 2013-2014 winter circulation and temperature anomalies over North America. The identification of the key building blocks and related reconstruction provide mechanistic insight on the development of phenomenally cold winter temperatures. Our implication of NPO/WP variability – currently viewed as a mode of internal variability – for the highly abnormal 2013-2014 winter has potentially wide-reaching implications for subseasonal-to-seasonal climate predictability. The data sets and analysis methods are briefly discussed next while the obtained findings and its implications follow in later sections.

b. Data and Methods

The analysis draws on the Climate Forecast System Reanalysis (CFSR; Saha et al. 2010) for 200-hPa geopotential height (Z_{200}), 850-hPa temperature (T_{850}) and winds, and 700-hPa vertical velocity (ω_{700}), all at monthly resolution and on a 2.5° global grid. The pentad (i.e., 5-day averaged) T_{850} and 200-hPa streamfunction from the CFSR are used to assess subseasonal variability. The precipitation data (on a 0.5° continental grid) is obtained from NOAA-Climate Prediction Center's unified gauge-based dataset (Chen et al., 2002). The January 1979 – February 2014 period is analyzed, with anomalies defined with respect to the 1981-2010 climatology, as in NOAA's Climate Diagnostic Bulletin (hereafter, CDB; monthly archive is online).

The NPO/WP pattern is obtained alongside other variability patterns in a rotated EOF analysis of monthly, winter (December, January, February) Z_{200} anomalies in the Northern Hemisphere (30°S-90°N). The leading eight patterns are rotated using the varimax technique, as in Nigam and Baxter (2014). In this analysis, the NPO/WP emerges as the third-leading pattern, explaining ~11% of the monthly winter variance, after the NAO (~17%) and ENSO response (~13%) patterns. The THN is the fifth-leading mode in this analysis, explaining ~6% of the variance.

To assess the contribution of the NPO/WP, TNH, and other variability patterns to the extreme 2013-2014 winter, the T_{850}, Z_{200}, and precipitation (and ω_{700}) anomalies are reconstructed. Multiplication of each rotated EOF pattern (spatial) with its principal component (time-varying) value for the target month, and summing the various EOF contributions yields the reconstructed signal; the principal components (PCs) are orthogonal, facilitating reconstruction. The December 2013, and January

and February 2014 reconstructions were averaged to produce the 2013-2014 winter season anomalies, discussed in the next section.

To assess subseasonal variability, a similar analysis is performed on the pentad 200-hPa streamfunction (ψ_{200}) anomalies; streamfunction is a preferred variable for analysis of tropical-extratropical interaction. Following Baxter and Nigam (2013) and the approach used in Chapter 4, an extended, rotated EOF analysis is conducted to extract the subseasonal modes of spatiotemporal variability. Analysis of ψ_{200} yields a clearer identification of the Madden-Julian Oscillation's (MJO) extratropical response, precluding its aliasing onto the extratropical variability patterns. The 120-day running mean anomaly is removed from data prior to analysis, to filter out interannual variability. The data are 'extended' using a five-pentad sampling window. In this analysis, NPO/WP emerges as the fourth-leading mode, behind two modes that capture the time-lagged MJO response, and the Pacific–North American (PNA) pattern.

While the reconstructions themselves are informative, mechanistic links between the NPO/WP circulation and temperature anomalies over North America are also investigated. To this end, the various terms constituting thermal advection are evaluated for the 2013-2014 winter season:

$$(A)\ -\boldsymbol{V}_{850}^{NPO/WP}\cdot\nabla T_{850}^{C}$$

$$(B)\ -\boldsymbol{V}_{850}^{NPO/WP}\cdot\nabla T_{850}^{NPO/WP*}$$

$$(C)\ -\boldsymbol{V}_{850}^{C}\cdot\nabla T_{850}^{NPO/WP*}$$

Term (A) constitutes the advection of climatological T_{850} by the NPO/WP contribution to the 850-hPa wind. Term (B) represents a quasi-nonlinear advection –

of the *first-order* NPO/WP temperature signal ($T^{NPO/WP*}$) by the NPO/WP related winds. As the *observed* NPO/WP T_{850} anomaly is the reconstruction target, it cannot be used here. The first-order temperature signal is estimated, indirectly, from Term A using the thermal damping from synoptic transient eddies (Lau 1979).[2] Finally, term (C) constitutes the advection of the first-order NPO/WP temperature signal by the climatological 850-hPa wind.

c. Results

The 2013-2014 winter was characterized by significantly below-normal temperatures across much of North America. The NPO/WP principal component was strongly negative, consistent with higher pressure/heights over Alaska and colder-than-normal temperatures over central-eastern North America. The NPO/WP PC averaged over the three winter months exhibited the most negative seasonal value over the entire analysis period (cf. Fig. 5.4b). Figure 1a shows the observed T_{850} anomalies, with temperatures as cold as −7°C centered southwest of Hudson Bay. The anomalously cold temperatures extend from northwestern Canada southeastward to well-populated parts of the central-eastern United States. Above-normal T_{850} was observed over much of Alaska, US west coast, and southwestern U.S. The structure and magnitude of the observed anomalies are closely reconstructed (Fig. 5.1b) using PCs of the NPO/WP, NAO, TNH, and East Atlantic (EA, Wallace and Gutzler 1981) patterns; panels *c-f* show the individual contributions. The NPO/WP contribution clearly resembles the observed anomaly most closely, followed distantly by the TNH.

[2] The first-order NPO/WP temperature signal $T_{850}^{NPO/WP*}$ is estimated as $-V_{850}^{NPO/WP} \cdot \nabla T_{850}^{C} \approx -\gamma T_{850}^{NPO/WP*}$ where the right hand side represents thermal (Newtonian) damping of lower tropospheric temperature by synoptic transients. γ is taken as (3 days)$^{-1}$ following Lau (1979, Table-I).

The red outlined box in the panels marks a region of the Northern Plains (40-55N, 100-80W) whose area-averaged T_{850} anomalies are used in time series analyses. The region was selected due to its proximity to the core of the cold anomaly and the populated areas in the north central-eastern quadrant of the continent.

Figure 2 displays the 200-hPa geopotential height anomaly for this winter. As in Figure 5.1, the reconstructed Z_{200} anomaly is displayed alongside the observed (CFSR) one, along with the individual contributions. As with T_{850}, the NPO/WP's Z_{200} contribution is dominant over North America and closely similar to the observed anomaly there. Figure 5.2e indicates that TNH was also a contributor over North America but with significantly smaller amplitudes than NPO/WP. It is worth noting that both NAO and EA patterns were also active, with strong projections on the observed T_{850} and Z_{200} anomalies but in the downstream Atlantic and European sectors.

While bitterly cold temperatures in the central-eastern United States defined the 2013-2014 winter, the precipitation anomaly was also notable. Most significant, perhaps, was the anomalously dry winter over the West Coast, especially California (Fig. 5.3a). The TNH and NPO/WP contributions can explain most of the observed precipitation deficits extending from the Alaskan panhandle to southern California (Figs. 5.3*a*, *c*, and *e*). In fact, from central California to most of the Alaskan panhandle, those two patterns account for over 75% of the observed precipitation deficit (in some cases the reconstruction yields a deficit higher than observed). Over southern California and the Desert Southwest, the reconstruction from the TNH and NPO/WP generally explains 50-75% of the observed precipitation anomalies. Of the

two patterns, the TNH explains more variability over California, a region of intense study given the multiyear drought that has impacted that region.

The precipitation signals are consistent with the observed and reconstructed 700-hPa vertical velocity anomalies across western North America (Fig. 5.3, right panels). The NPO/WP explains some of the wet signal also along the eastern seaboard, though other variability is clearly more important in that region.

In order to place the 2013-2014 winter in historical context, the time series of the area-averaged T_{850} anomalies over the Northern Plains (red box, Fig. 5.1) is examined in Figure 5.4b, which also shows the standardized NPO/WP principal component; the two are correlated at 0.69, a high value. The winter exhibiting the most negative seasonal T_{850} anomaly (i.e., most persistently cold) is this past one (2013-2014), when the NPO/WP PCs are also most negative. The TNH pattern also contributed to the recent record cold winter (cf. Fig. 5.1e) but its contribution is secondary to NPO/WP's. The relative contribution of the two patterns in other extreme winters (when regional T_{850} exceeded ± 1 standard deviation) is examined via a scatter plot of the two PCs in Figure 5.4c. It is noteworthy that every winter month satisfying the threshold for cold (warm) extremeness had a negative (positive) PC value but only in case of the NPO/WP. The TNH PC was not found as tightly correlated as it exhibits positive values in both cold and warm winters, albeit more often in the cold ones.

The subseasonal variability in the extreme 2013-2014 winter over the Northern Plains is briefly examined in Figure 5.4a. The pentad T_{850} anomaly index (standardized) co-varies with the pentad NPO/WP principal component, with the

exception of the last few pentads. Over this extreme winter, the two pentad indices are correlated at 0.56;[3] the correlation is 0.45 over all analyzed winters (1979-2014). The pentad correlation for this winter and across all winters is impressive (exceeding the 99.9% confidence limit according to a student's t-test), highlighting the preeminence of the NPO/WP pattern in influencing the winter surface climate over Northern Plains, even on subseasonal time scales. Correlations in the 0.4-0.6 range indicate that the NPO/WP influence is far from complete: Subseasonally, this is reflected in the near-zero principal component values of NPO/WP during mid-January of 2014 (cf. Fig. 5.4a). The significant contribution of TNH variability on monthly time scales was noted earlier.

The observationally rooted analysis presented above attributes the extreme 2013-2014 winter temperatures over North America to NPO/WP variability. The statistical attribution is provided a mechanistic underpinning in this section which elaborates on the temperature advection processes, in particular the phenomenal cold advection experienced by the Northern Plains and the central-eastern United States. The advection of climatological T_{850} can account for the spatial structure of NPO/WP-related anomalies east of the Rocky Mountains, but not its magnitude (Fig. 5.5b). Using this field (Fig. 5.5b) and a 3-day Newtonian damping (to represent thermal damping by synoptic transient eddies), NPO/WP's first-order T_{850} signal is constructed (see Footnote 2; not shown). The advection of this first-order T_{850} signal by the climatological 850-hPa wind field (Fig. 5.5d) contributes significantly to the

[3] A higher pentad correlation is obtained with T_{850} leading by 1-pentad. This results from the retrogression of the NPO/WP pattern whose North American center attains peak amplitude in advance of other regions. The NPO/WP PC is, of course, keyed to the overall mature structure. The T_{850} lead over the Northern Plains is, by no means, indicative of causality; see Figure 5.5.

total NPO/WP temperature advection (the sum of panels *b-d*, shown in panel *a*). In fact, the temperature anomaly resulting from the total NPO/WP advection (with 3-day thermal damping) is larger than the NPO/WP T_{850} reconstruction itself. Clearly other terms in the thermodynamic energy equation, such as the adiabatic and latent heating, are important. The quasi-nonlinear advection term (Fig. 5.5c), however, is mostly unimportant relative to the other two advection terms.

d. Discussion

A key element of the scientific method is seeking support for the proposed hypothesis by expanding the inquiry domain. After attributing the anomalously cold 2013-2014 North American winter (and drought over the Pacific-Northwest) to the heightened negative phase of the NPO/WP pattern, we inquire if NPO/WP variability can be implicated in the generation of unusually warm North American winters as well. In March 2012, large swaths of central-eastern North America were warmer than normal by as much as 5°C and the Pacific Northwest wetter by 25-50% (CDB, Fig. E6). Support for a prominent role of the NPO/WP (positive phase) in this warming episode follows from the large spatial anomaly correlation (-0.66) of this month's T_{850} anomalies with the NPO/WP T_{850} regression pattern (Fig. 5.1c), footprint of the precipitation anomaly, and the striking similarity of the March 2012 Z_{300} anomalies (CDB, Fig. S1) with the NPO/WP's (Fig. 5.2c but for the sign). The projection of the March 2012 Z_{200} anomalies onto the wintertime NPO/WP loading pattern was 1.24, a significantly positive value.

A pertinent question in context of this attribution is the longevity of the NPO/WP pattern. A monthly analysis is likely to be too coarse for this estimation but a pentad-

resolution spatiotemporal analysis (e.g., Baxter and Nigam 2013) should suffice. This analysis yields 25 days as the duration time scale of a NPO/WP episode, based on the autocorrelation fall-off to e^{-1}.

The origin of the NPO/WP remains enigmatic: Concurrent links to the tropical SSTs are tenuous but linkage with extratropical SSTs (especially in the Gulf of Alaska) is strong in the monthly analysis (Figure 1.8; Figure 4.10); additional analysis, including SST-leading links, is warranted given the prominent role of NPO/WP in influencing North America's winter hydroclimate. Interestingly, the Gulf of Alaska SSTs were notably positive this past winter (CDB, Fig. T18; Washington Post 2014), when the NPO/WP was strongly negative (cf. Fig. 5.4a) and Pacific storm tracks southward of their normal location (CDB, Fig. E13).

Finally, this analysis cautions against succumbing to the post-1980/90s temptation of ascribing various extratropical anomalies in the Pacific/North American sector to ENSO – a favorite go-to mechanism because a causal inference is drawable, unlike the extratropical rooted teleconnections whose origin/mechanisms remain to be elucidated. For example, a recent NOAA report on the causes and predictability of the California drought (Seager et al. 2014) utilizes climate modeling to suggest that the persistent, amplified circulation pattern over North America (the immediate synoptic-climate cause of the drought over California) may have been forced in part by the anomalously warm SSTs in the tropical West Pacific and related tropical convection. An influential role of these SSTs on North American winter climate is also highlighted in another recent study (Hartmann 2015). Neither of these studies, however, provides process-level observational support (e.g., through OLR or diabatic

heating analysis) for the posited causal link. The present study, with its emphasis on internal midlatitude variability, suggests that any tropical forcing is substantially weaker than the role of the NPO/WP, whose origin and evolution remain largely unknown, especially on seasonal time scales. This lack of mechanistic underpinning however does not make these teleconnections any less relevant in attribution analysis. Instead, a concerted research focus on their excitation, evolution, and longevity is warranted.

The following section will provide some analysis with respect to the Hartmann (2015) hypothesis. Namely, it will show that the SST pattern implicated in that analysis is more likely a response to anomalous extratropical atmospheric forcing and less a causal mechanism.

Part II. The North Pacific Mode and the role of West Equatorial Pacific SSTs

Hartmann (2015) put forth a hypothesis linking the extreme 2013-2014 winter over North America to a Pacific SST pattern identified as the North Pacific Mode (NPM; Deser and Blackmon, 1995). It is argued that anomalous SSTs in the western equatorial Pacific and associated tropical convection are the causal mechanism for the anomalous circulation over the North Pacific and resulting extratropical SST anomalies. While no observational evidence is given for this hypothesis, it is suggested that modeling experiments give support. The analysis is reproduced here and it is shown that a more careful consideration of the observational data refutes the hypothesis that West Pacific SSTs/convection are the causal mechanism behind the extreme 2013-2014 winter.

a. Data and Methods

The Hartmann (2015) analysis is repeated here using detrended OI SST data at monthly resolution (Reynolds et al., 2002). The time period for the EOF analysis is all months during 1982-2013, and the spatial domain is the same as in Hartmann (2015), 30ºS-65ºN and 120ºE-105ºW. 200-hPa geopotential height and OLR data are also utilized at 2.5º spatial resolution. The analysis shown here consists of monthly correlations using the PCs from only November through March, paralleling the paper in question and emphasizing the cold season.

b. Results

The leading EOFs emerging from the analysis are an ENSO pattern and the NPM pattern, explaining 27.0% and 7.8% of the total variance, respectively. The SST footprints are shown as one month lead/lag monthly correlations during the November through March season in Figures 5.6 and 5.7. PC1 clearly corresponds to ENSO and is similar to the SST footprint revealed in Figure 1.8b, which was obtained using an atmosphere-only analysis. Throughout the three-month lead/lag period the pattern is constant in Figure 5.6. Some strengthening through the period is observed near the West Coast of North America, consistent with the extratropical atmospheric forcing one might expect as a nearly steady-state response to ENSO. The equatorial Pacific footprint is notably constant and the strongest signal is near the classic Niño 3.4 region ($r>0.9$).

Figure 5.7 shows the SST footprint of PC2, which constitutes the NPM and is consistent with the analysis in Hartmann (2015), meaning we are successfully able to reproduce those results. In contrast with the ENSO pattern, this pattern is highlighted

by the strongest SST signals being off the equator and more evenly distributed throughout the North Pacific basin (similar to Figure 1.8c). Throughout the three-month lead/lag period, the positive SST correlations increase over the western equatorial Pacific and the central tropical Pacific near 10^{o}N. The argument suggesting that the pattern arises due to SSTs in the West Pacific already seems suspect given that the SST footprint is clearly stronger elsewhere. Note that this is not the case with ENSO, whose SST footprint is clearly strongest in the equatorial Pacific.

Figures 5.8 and 5.9 depict the lead/lag correlations between OLR and the ENSO and NPM PCs, respectively. The canonical OLR dipole over the Pacific and Maritime Continent is clear in Figure 5.8, and as with SST, remains constant. This is consistent with the understanding of ENSO as a low-frequency pattern of equatorial Pacific variability. The OLR pattern associated with the NPM also exhibits a marked stationarity, though there is some eastward shift in the negative OLR correlations over the western tropical Pacific and a subtle increase in magnitude.

The last variable analyzed that will help everything fall into place is the 200-hPa height field, shown in Figures 5.10 and 5.11. The geopotential height response in Figure 5.10 is clearly identifiable as the ENSO teleconnection, expected given the discussion of the SST and OLR footprints. During the lead/lag sequence, the correlations over North America uniformly increase in magnitude, as well as over the tropical Pacific. This is consistent with the understanding of ENSO-related convection as a causal mechanism for anomalous upper-level circulation in the subtropics and extratropics. Figure 5.11 shows very important differences, wherein the geopotential height footprints tend to decrease with time over the North Pacific

and North America. The one month lead panel in Figure 5.11 reveals an NPO/WP-like pattern which decreases in magnitude in subsequent leads. This shows that the extratropical atmosphere *leads* the NPM SST pattern.

c. Discussion

The results discussed above strongly refute the hypothesis put forth in Hartmann (2015). It is shown that, using only observational methods, the SST pattern obtained in that paper does not lead but rather lags the anomalous extratropical circulation. The example of ENSO is included as a control against which to compare tropical-extratropical interactions in the case of the NPM. The extratropical response observed in Figure 5.10 is consistent with a hypothesis which states that ENSO leads to anomalous patterns of tropical convection which, in turn, generate extratropical teleconnections. However, Figure 5.11 shows that, even with a constant pattern of anomalous tropical convection (Figure 5.9), the anomalous extratropical circulation weakens with time. This result is more consistent with the understanding of the NPO/WP and ensuing NPM SST pattern as a footprinting mechanism for eventual ENSO development (Vimont et al., 2001, 2003). In fact, there exists a significant lag correlation between PC1 and PC2 in this framework, with PC2 (NPM) leading PC1 (ENSO) by several months (r~0.55). Therefore it is more likely that the tropical SST and OLR footprints observed in association with the NPM are a result of extratropical influence on the tropics, rather than the other way around. This result is also consistent with the work presented in Chapter 4, which did not find a robust connection between the NPO/WP and tropical forcing on subseasonal time scales.

Chapter 5 Figures

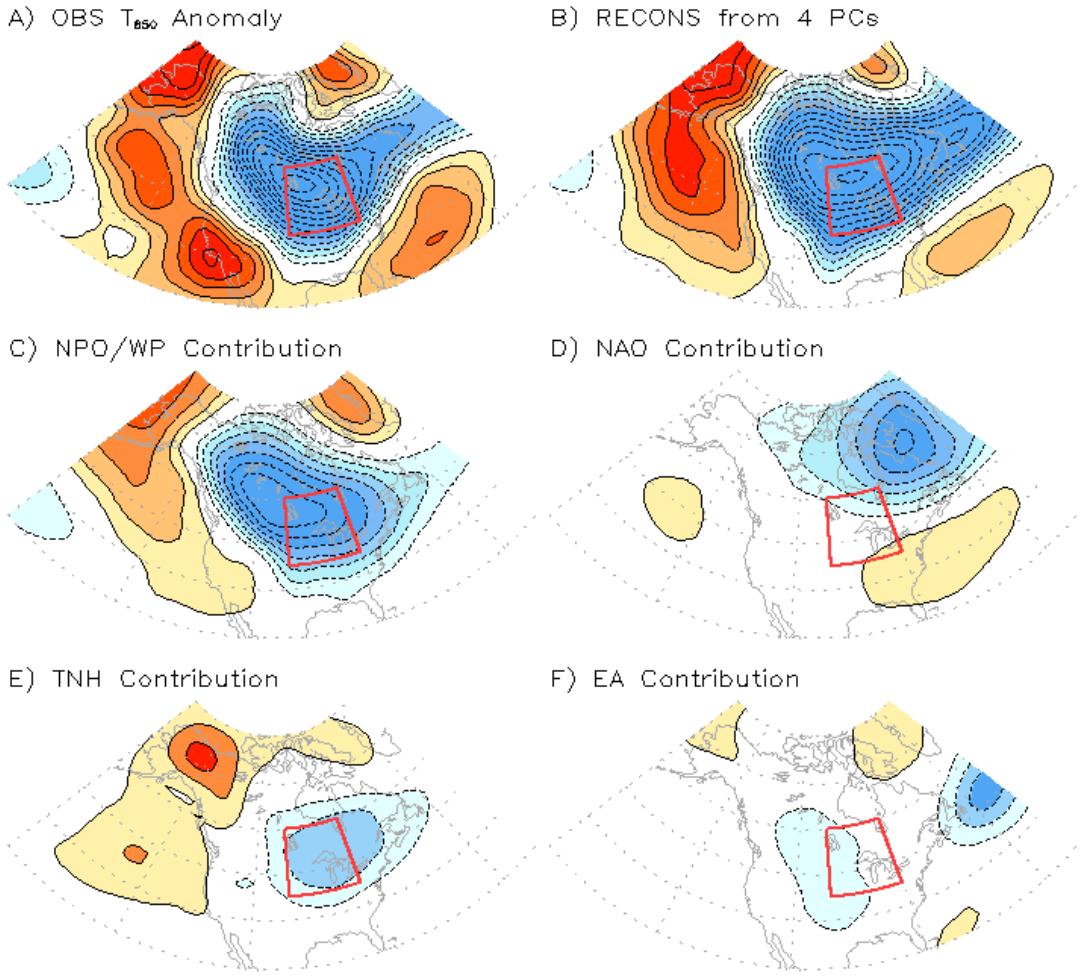

Figure 5.1: 850-hPa temperature anomalies for December 2013--February 2014, i.e., DJF 2013-14 winter: A) Observed. Panels *b-f* show T_{850} anomalies from a reconstruction based on principal components (PC) of the 200-hPa geopotential height (Z_{200}) variability; see text for analysis details: B) From four pertinent modes; C) from NPO/WP; D) from NAO; E) from TNH; and F) from East Atlantic (EA) pattern. T_{850} anomalies are reconstructions by multiplying the Z_{200} PC of each month by its regression pattern. The reconstructed winter month anomalies were then averaged to obtain the winter season (DJF) reconstruction. The contour interval and shading threshold is 0.5K. The red box (40-55N, 100-80W) marks the Great Plains averaging region for the T_{850} anomaly index discussed in subsequent analysis.

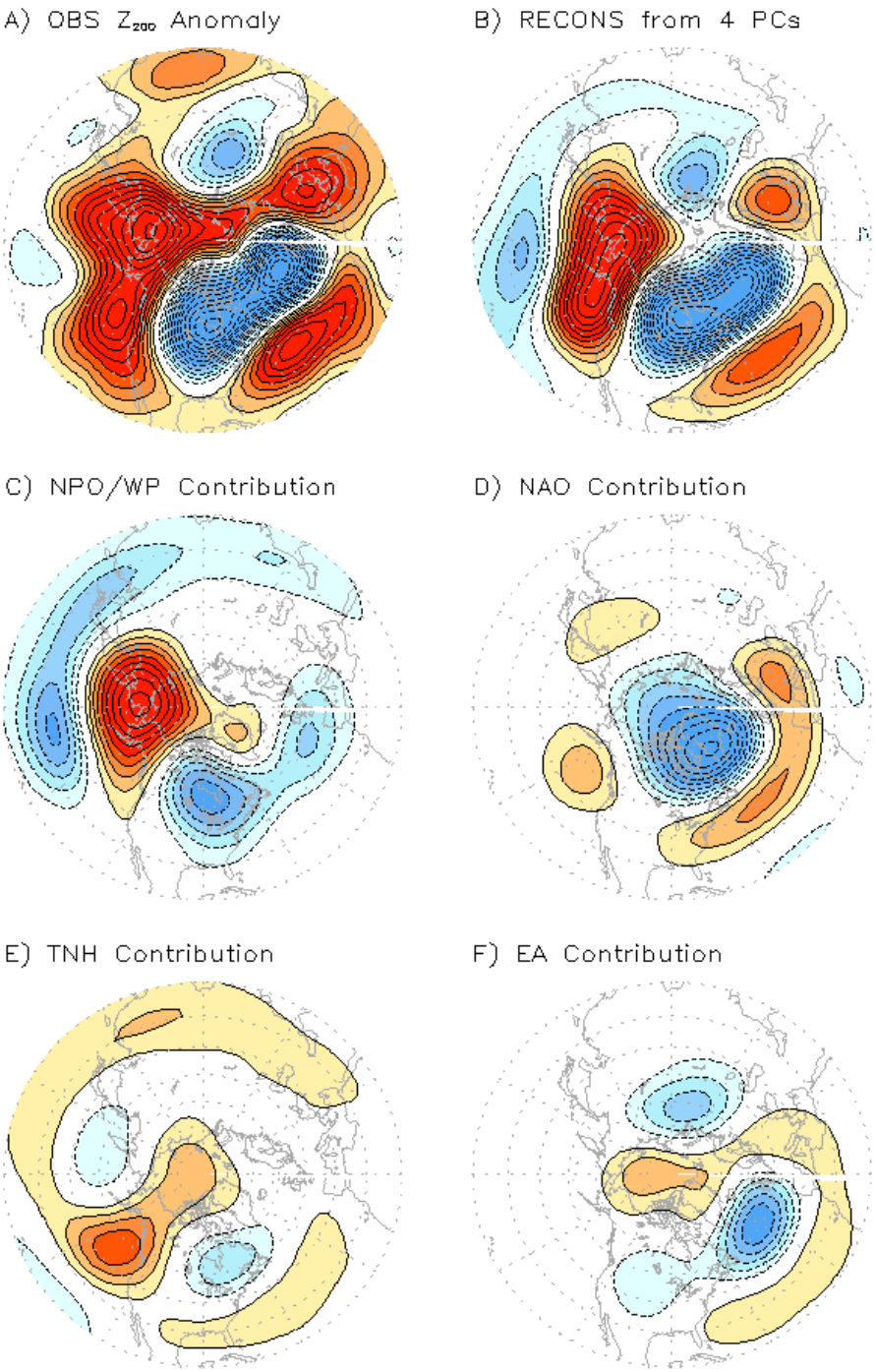

Figure 5.2: As in Figure 1, but for the 200-hPa geopotential height anomalies; contour interval and shading threshold is 15m. Principal components obtained from the variability analysis of this field are the basis for all reported reconstructions.

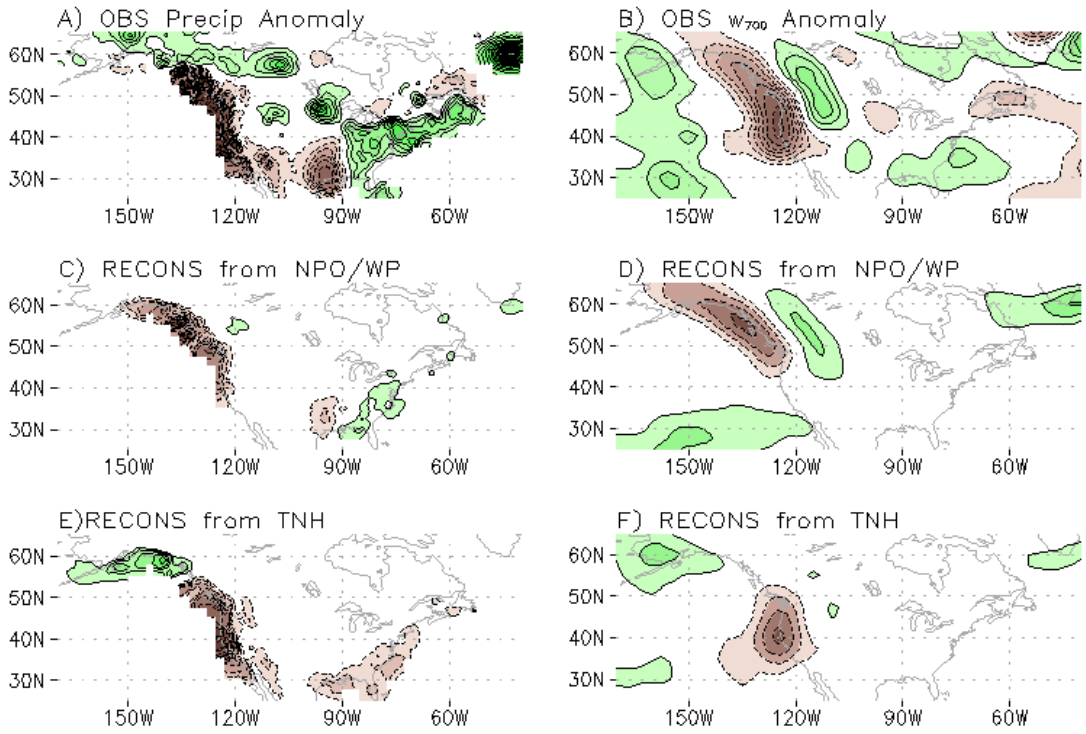

Figure 5.3: Precipitation and 700-hPa vertical velocity (w_{700}) anomalies during DJF2013-14: A) Observed precipitation anomaly, and its reconstruction from NPO/WP (C) and TNH (E) principal components. B) Observed w_{700} anomaly, and its reconstruction from the same principal components in D) and F), respectively. Contour interval and shading threshold is 0.25 mm/day for precipitation, and 1 cm/s for w_{700} (zero contour omitted).

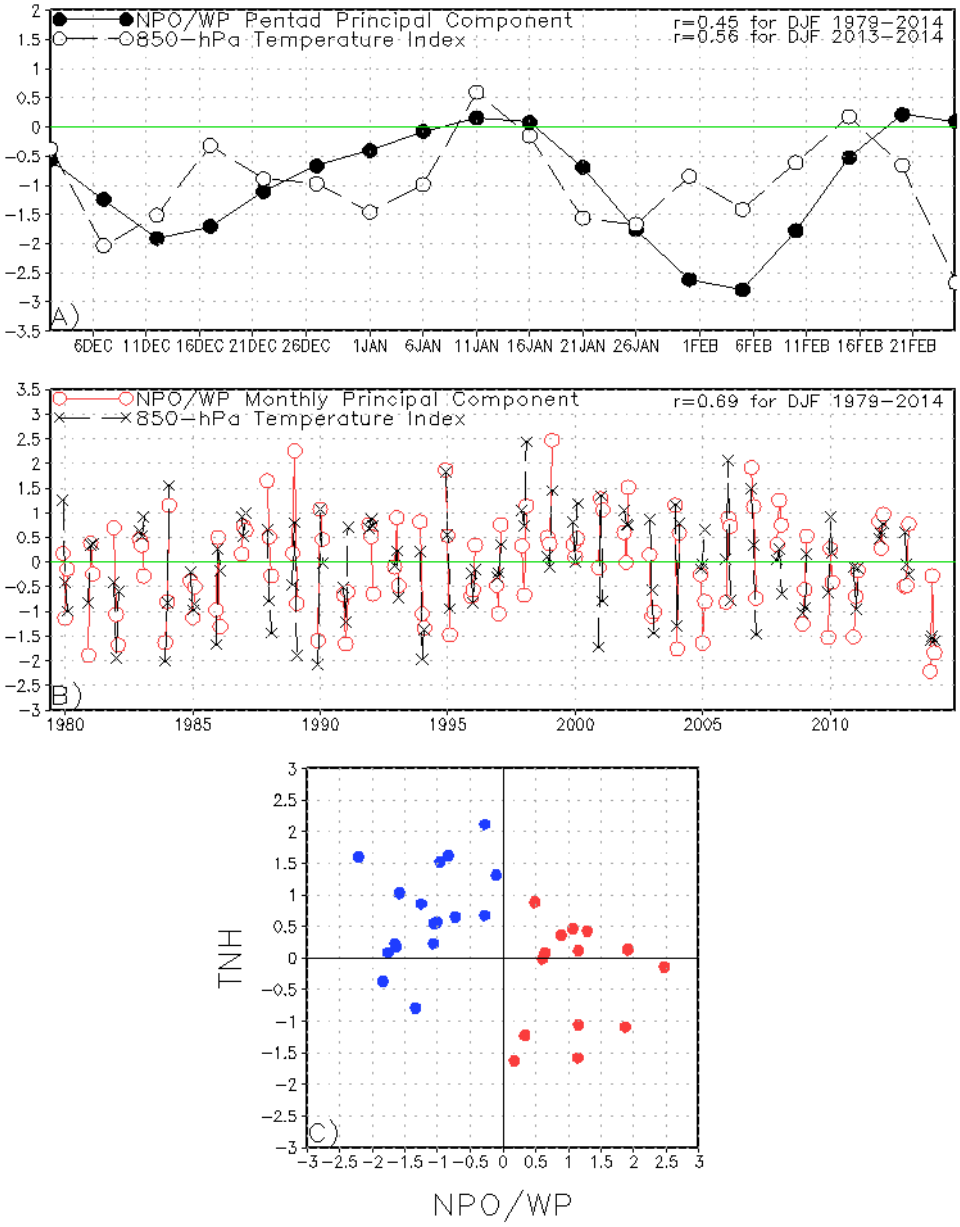

Figure 5.4: Pentad (A) and monthly (B) distribution of the NPO/WP principal component and T_{850} over the Great Plains (marked box in Fig. 1); the upper panel focuses on recent winter (DJF 2013-14) while the middle panel covers the entire analysis period winters (1979-2014). The 200-hPa winter geopotential height (streamfunction) variability during 1979-2014 utilized for the seasonal (pentad) analysis, with correlation coefficients noted in the legend. (C) Scatter plot of the NPO/WP and TNH principal components from the 1979-2014 monthly analysis, when the T_{850} anomaly over the Great Plains exceed ±1 standard deviation. Blue (red) dots denote cold (warm) winter months.

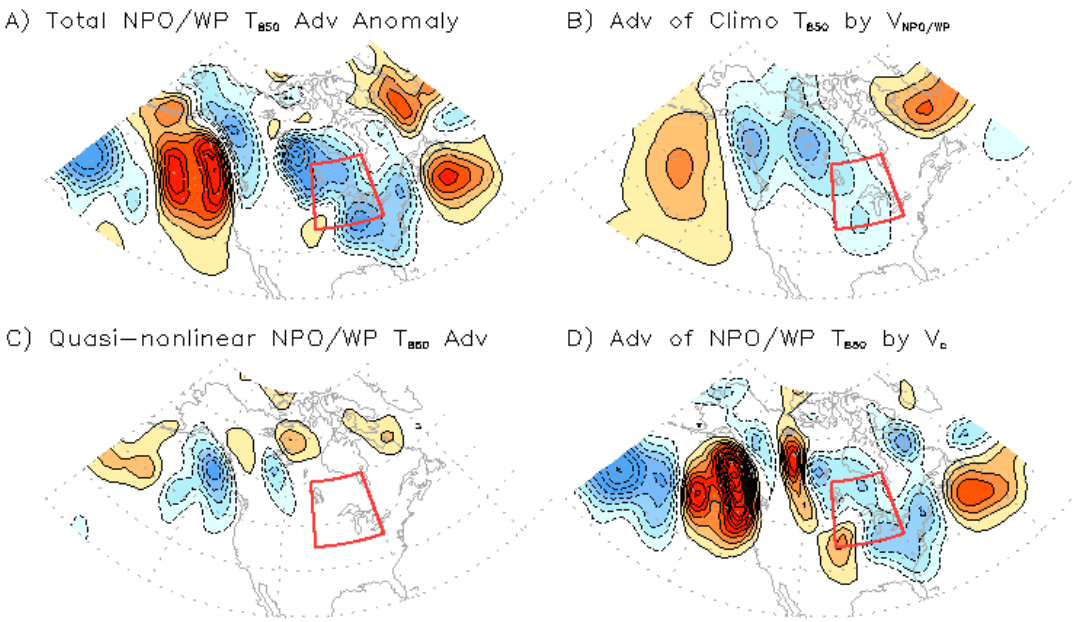

Figure 5.5: Reconstructed 850-hPa thermal advection related to NPO/WP. (A) Total thermal advection constituting the sum of panels *b-d*. (B) Advection of climatological 850-hPa temperature by the NPO/WP related wind anomaly, i.e., $\{-\vec{V}_a \bullet \vec{\nabla} T_c\}_{850\ \mathrm{hPa}}$, where $\vec{V}_a$ is the anomaly attributed to the NPO/WP and T_c is the climatological temperature. (C) Quasi-nonlinear term, $\{-\vec{V}_a \bullet \vec{\nabla} T_{NPO/WP}\}_{850\ \mathrm{hPa}}$, where $\vec{\nabla} T_{NPO/WP}$ is derived from panel (B) using a 3-day thermal dissipation time scale (cf. Lau 1979, Table 1). (D) The advection of $T_{NPO/WP}$ by the climatological 850-hPa wind, $\{-\vec{V}_c \bullet \vec{\nabla} T_{NPO/WP}\}_{850\ \mathrm{hPa}}$. Contour interval and shading threshold is 3.86E-6 K/s, a value that yields ΔT=1.0K for a 3-day thermal dissipation time scale. Data are also subject to a nine-point smoother to improve figure clarity.

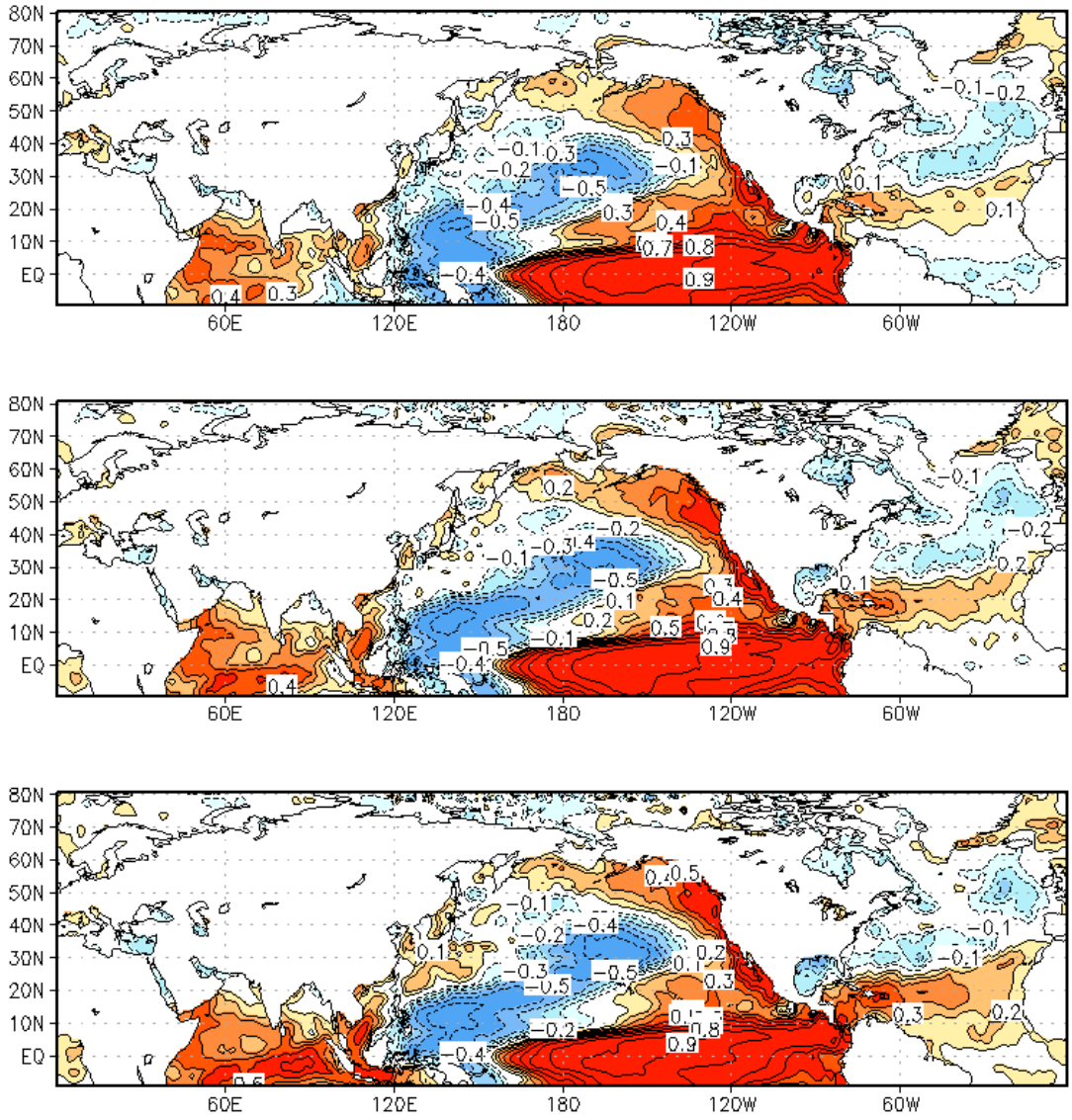

Figure 5.6: From top to bottom: one-month lead/lag correlation between PC1 (ENSO) and SST for November-March, 1982-2013. This PC explains 27.0% of the total variance (all months). Contour interval is 0.1, and the zero contours are suppressed.

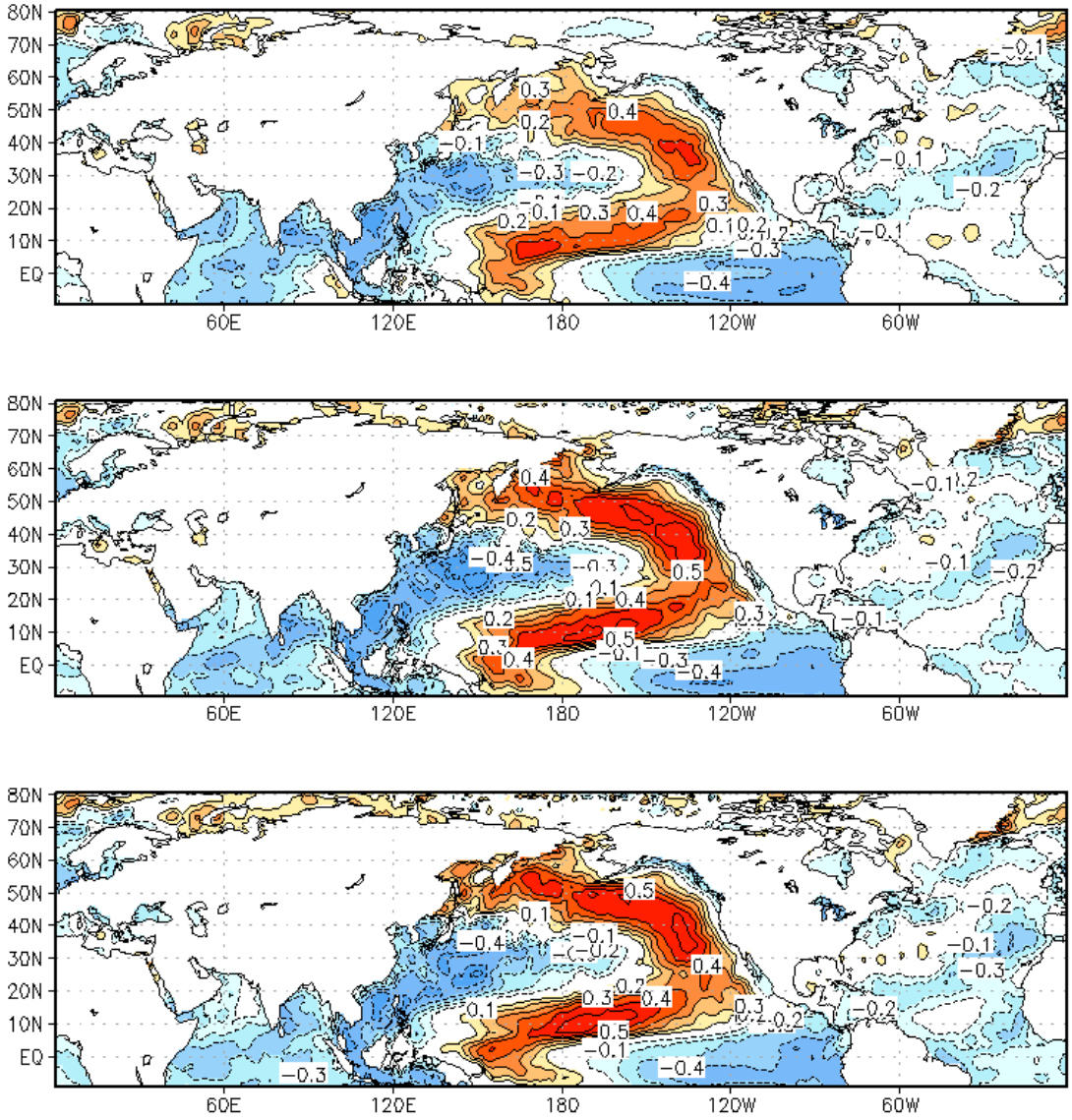

Figure 5.7: From top to bottom: one-month lead/lag correlation between PC2 (NPM) and SST for November-March, 1982-2013. This PC explains 7.8% of the total variance (all months). Contour interval is 0.1, and the zero contours are suppressed.

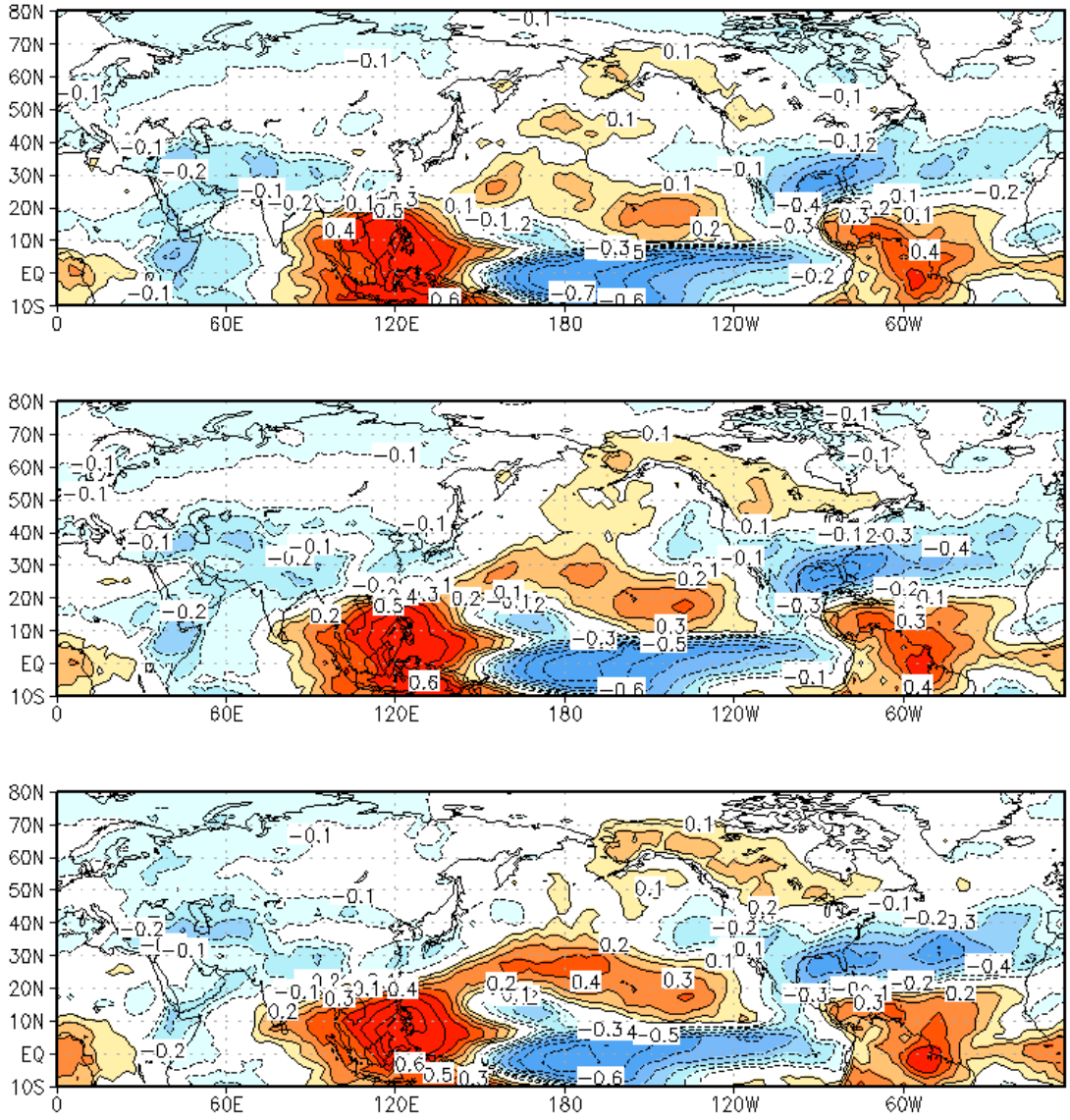

Figure 5.8: From top to bottom: one-month lead/lag correlation between PC1 (ENSO) and OLR for November-March, 1982-2013.

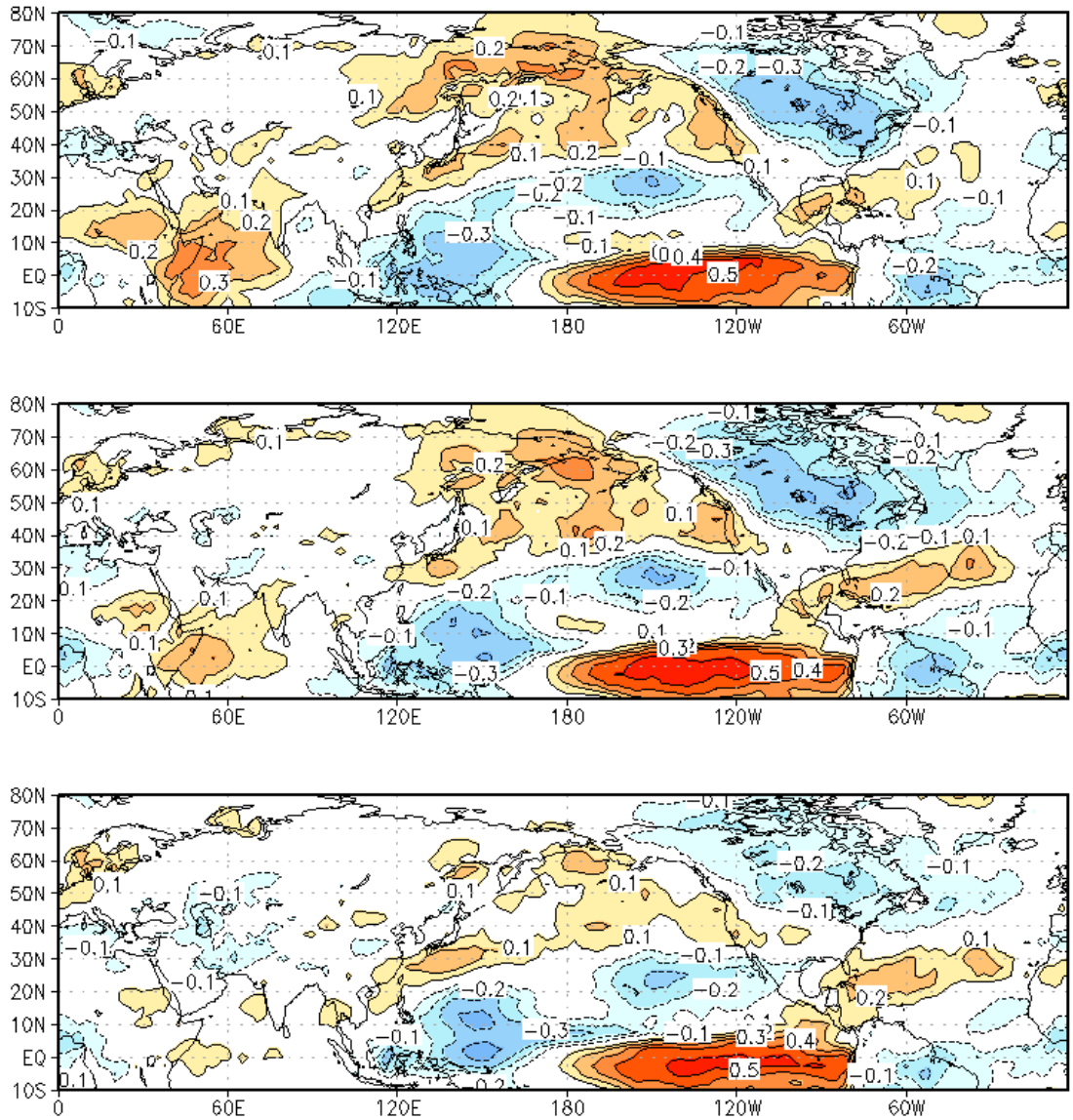

Figure 5.9: From top to bottom: one-month lead/lag correlation between PC2 (NPM) and OLR for November-March, 1982-2013.

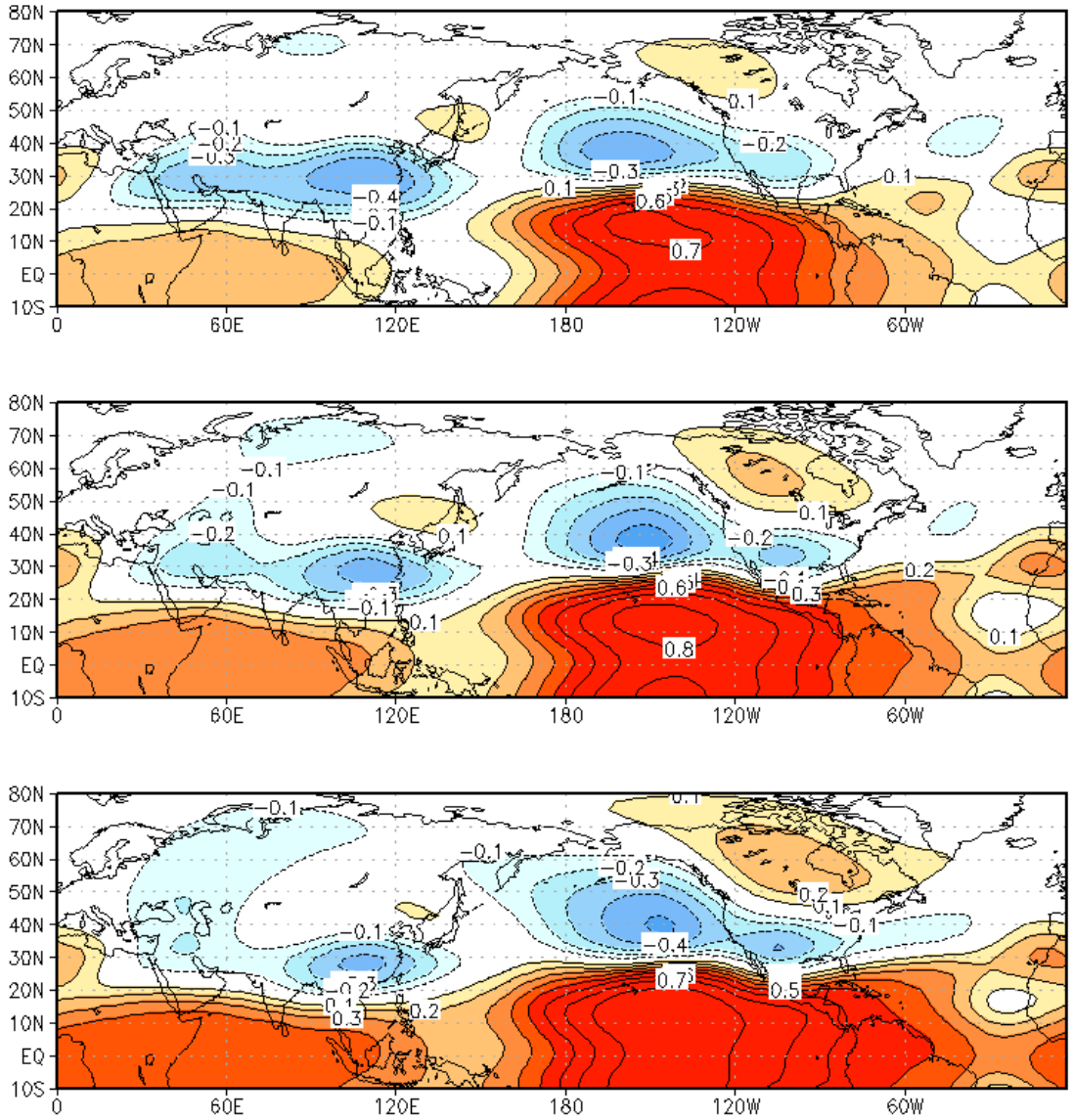

Figure 5.10: From top to bottom: one-month lead/lag correlation between PC1 (ENSO) and 200-hPa geopotential height for November-March, 1982-2013.

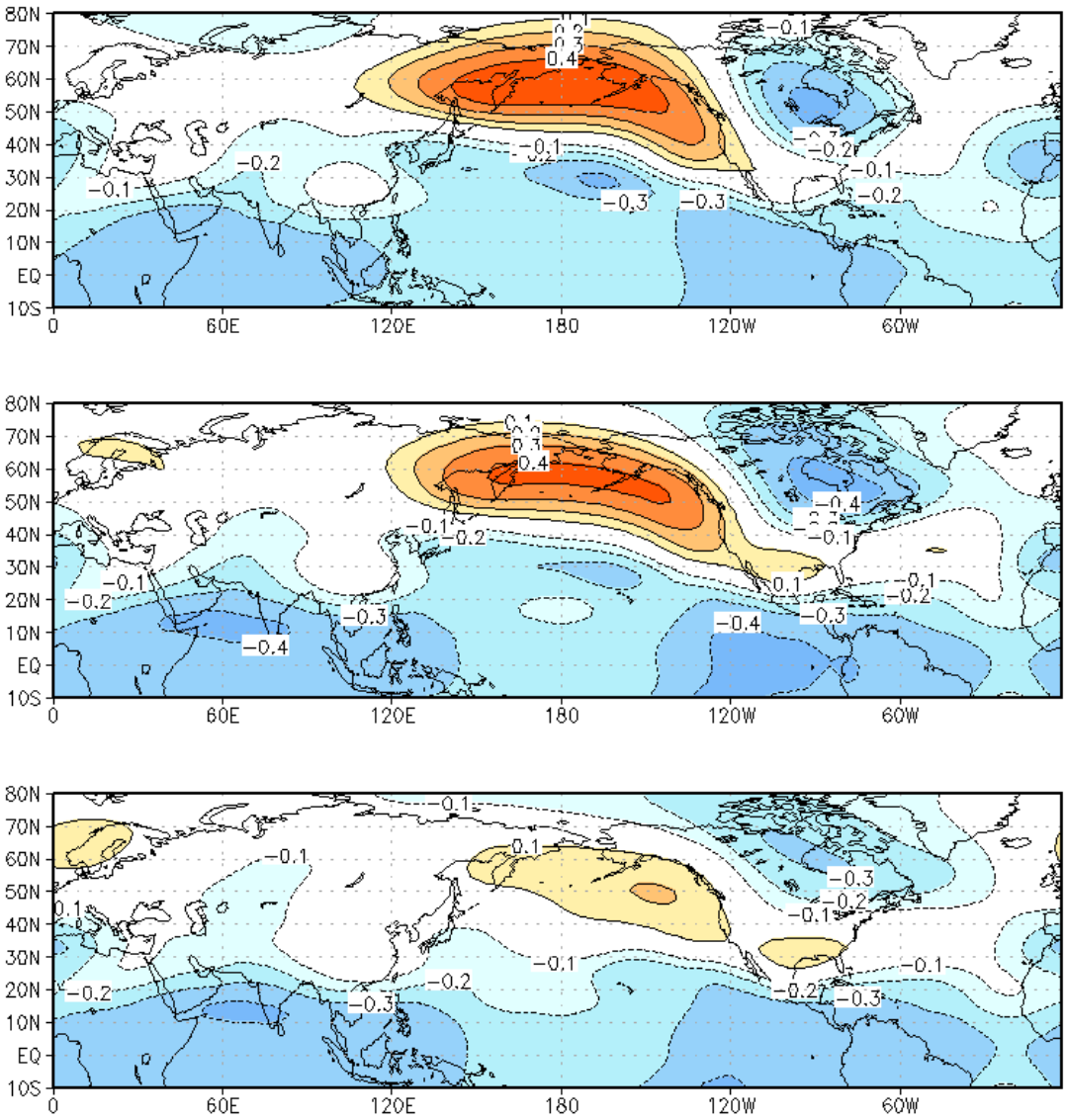

Figure 5.11: From top to bottom: one-month lead/lag correlation between PC2 (NPM) and 200-hPa geopotential height for November-March, 1982-2013.

Chapter 6: Conclusion

This concluding chapter will be presented in two sections. The first section will discuss detailed results of the thesis along with their implications. It will identify the key areas of active research that are advanced by this work, as well as speculate on some outstanding questions. The second section will leave the reader will some concluding remarks and outline some prospects for advancing this work in the future.

6.1 Summary of Results and Discussion

The various research results presented throughout this thesis work together to advance understanding of subseasonal climate variability and tropical-extratropical teleconnections. The various subsections will expand on the contributions made in a few key areas, including PNA-NAO interaction, MJO-PNA and MJO-NAO relationships, the relationship between tropical convection and the PNA, the MJO extratropical teleconnection, and the key role of the NPO/WP. Additionally, some discussion of the potential impacts of climate change on teleconnections will be presented.

a. PNA-NAO Interaction

The NAO and PNA are major patterns of variability that command attention from the climate community at large. Typically, these patterns are treated as independent, largely due to their derivation from monthly data using techniques that ensure temporal independence. In Chapter 3, however, it is shown that using extended EOF analysis of the pentad resolution 200-hPa geopotential height field reveals an

intriguing interaction between the Atlantic and Pacific Basins. The NAO is found to lead a PNA pattern of opposite sign. This result further motivates research into the spatiotemporal variability of teleconnection patterns and the physical mechanisms that link them. In this case, it is hypothesized that the NAO excites a wave train near the Arabian Peninsula that propagates to the extratropical Pacific domain via the Asian waveguide.

b. MJO-PNA and MJO-NAO Relationships

The MJO, as the leading pattern of subseasonal tropical climate variability, influences the extratropics by exciting a Rossby wave source in the subtropics via anomalous tropical divergent circulations. This extratropical response has historically been studied, in part, by assessing the response of the PNA and NAO teleconnection patterns to MJO-related convection (e.g. Lin et al. 2009 and Mori and Watanabe 2008). This approach, however, has some shortcomings. The PNA and NAO are historically derived, as in Barnston and Livezey (1987) and Wallace and Gutzler (1981), from the low-level or mid-level geopotential height field. Such an analysis is incapable of capturing the interaction between the baroclinic structure of the anomalous tropical circulation and the equivalent barotropic nature of the extratropical response. It might be preferable to conduct analysis of a more appropriate variable, either 200-hPa height or streamfunction, that varies substantially in both the tropics and extratropics. In this way tropical-extratropical interactions are more explicitly identified.

Chapter 3, which details the interaction between the PNA and NAO, also conducts analysis on data from which the contemporaneous MJO footprints have

been linearly removed. In this framework, the NAO and PNA still emerge as the leading patterns of wintertime variability, but with subtle displacements in their centers of action. The mature PNA and NAO patterns that emerge in historical analyses are therefore some combination of tropically-forced variability and internal extratropical variability.

This result is strongly supported by the findings presented in Chapter 4. In that streamfunction analysis, the NAO and PNA patterns are identified within the rich spectrum of spatiotemporal teleconnection patterns, including tropical-extratropical patterns identified as being the MJO and ENSO extratropical responses. In this context, the link between MJO and PNA is neatly severed, as there is little lag correlation between the two principal components. However, the link between NAO and MJO variability does remain in some modified form. There exists a statistically significant lag correlation between the MJO-related principal component and the NAO principal component. Given the lower-frequency nature of the NAO principal component, it is reasonable to suggest that the MJO is capable of exciting a low-frequency NAO response in the extratropics. Perhaps this response is state-dependent or phase-dependent and relies on some extratropical mechanism not explored here, such as tropospheric-stratospheric interaction.

c. Relationship between Tropical Convection and the PNA

While the PNA and MJO emerge as distinct spatiotemporal patterns of variability from the 200-hPa streamfunction analysis, some thought is given to the link between tropical convection and the PNA in a broader sense, even beyond possible MJO interactions. In the introductory chapter, monthly teleconnection analysis reveals that

the PNA pattern, while distinct from the extratropical ENSO response, retains a statistically significant SST footprint in the tropical Pacific. Chapter 4, which emphasizes subseasonal evolution of circulation anomalies, reveals a PNA pattern that has virtually zero connection to tropical Pacific SSTs. Additionally, the RWS analysis suggests that there is little in the way of a causal mechanism relating anomalous tropical divergence and the PNA pattern as it evolves on subseasonal time scales. The results suggest that the pattern that most closely corresponds to the canonical PNA pattern evolves mostly in response to extratropical mechanisms. It also suggests that the apparent link between the PNA and tropical Pacific SSTs on monthly time scales may result from aliasing of seasonal MJO preferences.

d. MJO Extratropical Teleconnection

Among the most important contributions of this thesis is the explicit identification of the wintertime MJO extratropical response alongside the various extratropical teleconnection patterns. This analysis allows for distinction between tropically forced teleconnections and those that are internal to the extratropics, especially in the case of the MJO, ENSO, and the PNA.

Chapter 2 details the MJO extratropical response from composite analysis, assessing the response in the circulation field as well as U.S. surface temperature and precipitation. Importantly, it is shown that it is preferable to monitor MJO activity in a velocity potential framework, due to its close physical relationship to the generation of remote geopotential height anomalies. The streamfunction analysis shown in Chapter 4 expands on that result to show how the MJO response can be derived from using only the rotational circulation. Analysis of the RWS confirms that the

anomalies in the rotational circulation are consistent with forcing from anomalous tropical divergent circulations.

The SST footprint of the MJO-related principal component reveals a modest but statistically significant low-frequency footprint in the equatorial central Pacific. This pattern could be important for two primary reasons: 1) it suggests that the MJO varies on interannual time scales, and 2) this interannual variability could help explain the difference in the extratropical response between canonical and non-canonical ENSO events (e.g. Yu et al. 2012). A new hypothesis generated from this result is that the different circulation patterns observed during El Niño Modoki (or central Pacific) events, when compared to canonical ENSO, are a result of subseasonal MJO activity that is biased toward the convective Pacific phase.

e. Key Role of the NPO/WP

The NPO/WP is a leading pattern of climate variability in northern winter. As seen in Chapter 1, its surface temperature footprint is most impressive over North America, rivaled only by the PNA footprint. As a basin analog to the NAO, it is instructive to compare the two in terms of their surface climate responses. The NAO is strongly correlated with temperatures over Eurasia, and to lesser extent, eastern North America. By contrast, the NPO/WP is strongly correlated with North American temperatures. In fact, over the most populated regions of eastern North America, the NPO/WP explains substantially more temperature variance across time scales than the NAO. Chapter 5 details how the NPO/WP was the greatest single pattern of variability that contributed to a recent cold North American winter. This is reasonable since the NPO/WP strongly modulates patterns of thermal advection over North

America, also shown in Chapter 5. The implication of this work is that more study is needed to understand the physical mechanisms that excite and maintain the NPO/WP, as historically little attention has been paid to that pattern compared to the NAO/AO.

Some recent efforts have attempted to link NPO/WP-like variability to low-frequency SST variability in the tropical West Pacific (Hartmann 2015). While it is tempting to search for a tropical forcing mechanism in light of the ENSO and MJO paradigms, it is not necessary to find the origins of prominent modes of extratropical variability in the tropics. In Chapter 5, a brief rebuttal of the Hartmann hypothesis is presented, suggesting that the NPO/WP is more likely to precede tropical SST anomalies, thus being more consistent with the understanding of the seasonal footprinting mechanism. Furthermore, results of the streamfunction analysis in Chapter 4 show that the NPO/WP is not readily attributable to tropical forcing on subseasonal time scales.

f. Potential Impacts of Climate Change on Teleconnections

In climate science an outstanding question is how known patterns of variability, like ENSO, might change in a warming climate. Likewise, one might ask whether the results presented here are in any way sensitive to climate change. While this question is largely beyond the scope of this thesis, some speculation on the topic is warranted.

The major teleconnection patterns, as stated in the introduction, can be thought of as resulting from the spatiotemporal variability of the climate's semi-permanent features. For example, both the NAO and NPO/WP each modulate the meridional position of the storm track in their respective basins. In a warming climate, a weakening and northward displacement of the jet stream and storm tracks is observed

and expected (Archer and Caldeira, 2008). The variability of the storm tracks, therefore, is also likely to change in space, even if the nature of the variability (meridional displacement, for example) is similar.

Sensitivity studies have been conducted on the monthly teleconnection analysis presented in Chapter 1 to assess whether the time period in question changes the loading patterns or their principal components (not shown). Analyzing periods of 1958-present and 1979-present results in very similar teleconnection patterns over the common period. The time series of patterns identified here as largely extratropical, such as the NAO and NPO/WP, are correlated above 0.95 in the common 1979-present period. This suggests that month-to-month extratropical variability is very stable over these time periods, and that secular warming trends are less important. However, the teleconnection pattern constituting the ENSO response is much more sensitive to the time period. The trend tends to dominate more in the tropics, from a signal-to-noise perspective, influencing the ENSO teleconnection loading pattern. Because ENSO is associated with a uniform warming of the tropics, trends are easily aliased. Therefore, in future analysis, it is preferable to detrend the 200-hPa data, to more clearly capture the interannual variability associated with ENSO. Note that this carries the added risk of removing potentially interesting decadal variability unrelated to secular warming.

6.2 Concluding Remarks and Prospects for Future Work

Teleconnection analysis provides useful insights into climate variability by assessing the relationships between remote geographic regions. In some cases, such

patterns are potentially predictable based on the known mechanistic underpinnings of their development. The most prominent example of this in the subseasonal domain is the MJO. It was shown in Chapter 2 and again in Chapter 4 that subseasonally varying tropical convection is related to far-field circulation changes and associated surface climate anomalies. In this light, efforts continue which seek to optimize the surface climate predictability that can be afforded from the MJO out to Weeks 3 and 4. The use of velocity potential as a preferred variable (based on the work presented in Chapter 2) in a statistical-dynamical hybrid is an avenue of work currently being undertaken at CPC to improve the empirical toolbox for the new, experimental Weeks 3 and 4 surface climate outlooks.

On longer time scales, monthly and seasonal climate prediction and discussions of potential predictability are often dominated by ENSO, largely due to its high predictability at short seasonal leads and its intuitive causality. However, some temptation towards implicating tropical convection for all extratropical climate anomalies results from the usefulness of MJO and ENSO on subseasonal and seasonal time scales, respectively. It is precisely for this reason that much of the work presented here seeks to rigorously assess any tropical underpinnings of the various teleconnection patterns. By using upper-level streamfunction at pentad resolution, MJO-related climate variability and the standing ENSO response can be nicely separated from the PNA, NAO, and NPO/WP. The latter are shown to be largely unrelated to antecedent anomalous tropical convection.

Chapter 3 demonstrates that there is a connection between the Atlantic and Pacific domains via wave propagation through the Eurasian waveguide. It is later

hypothesized that previously discovered relationships between the MJO and PNA are largely due to aliasing of the MJO extratropical response pattern onto the PNA loading pattern. The subseasonal analyses presented in Chapters 3 and 4 confirm that a PNA-like pattern can exist absent MJO-related convection and is likely related to upstream atmospheric processes over Eurasia.

Teleconnection analysis is also useful in reconstructing observed climate anomalies, as demonstrated in Chapter 5. There it is shown that the NPO/WP explains the most lower-tropospheric temperature variance over much of east-central North America relative to the other teleconnection patterns, and was the leading contributor to the observed temperature anomalies during the 2013-2014 winter. Additionally, the Hartmann (2015) hypothesis is refuted by showing that the NPO/WP precedes the anomalous SST pattern presented in Hartmann (2015) as a causal mechanism.

Based on the above discussion, an avenue for future research involves investigation of the various teleconnection patterns in the current suite of state-of-the-art dynamical models. The recurrence of extreme cold over parts of central and eastern North America over the past two winters has highlighted a weakness in the current paradigm of seasonal climate attribution and predictability. As mentioned above, prediction of winter (DJF) climate variability has historically relied largely on ENSO, which explains relatively little temperature variance over the most populated regions of North America. A concerted research effort to assess the predictability of the NPO/WP on seasonal time scales is necessary, and analysis of the North American Multi-Model Ensemble (NMME; Kirtman et al., 2014) hindcast in this regard represents low-hanging fruit. Potential physical sources of predictability to

explore include SST, troposphere-stratosphere interactions, and land-atmosphere interactions (such as snow cover and the interaction of zonal wind and topography).

Likewise, Chapter 4 establishes a new observational baseline for various subseasonal teleconnections, but their occurrence, structure, dynamics, and predictability in models is an outstanding question. The new subseasonal to seasonal (S2S) dynamical model hindcast database could serve as an appropriate starting point for this type of analysis.

Finally, the interannual variability of MJO-related convection and its potential association with tropical Pacific SSTs is an area that warrants further study. That this might be related to contemporary research on flavors of ENSO adds to the intrigue.

References

Archer, C., and K. Caldeira, 2008: Historical trends in the jet streams. Geophys. Res. Lett., 35, L08803.

Ashok, K., S. K. Behera, S. A. Rao, H. Weng, and T. Yamagata, 2007 : El Niño Modoki and its possible teleconnection. J. Geophys. Res., 112, C11007.

Bader, J., and M. Latif, 2005: North Atlantic Oscillation response to anomalous Indian Ocean SST in a coupled GCM. J. Climate, 18, 5382–5389.

Bao, M., and D. L. Hartmann, 2014: The response to MJO-like forcing in a nonlinear shallow-water model, Geophys. Res. Lett., 41.

Baxter, S., and S. Nigam, 2013: A subseasonal teleconnection analysis: PNA development and its relationship to the NAO. J. Climate, 26, 6733–6741.

Baxter, S. and S. Nigam, 2015: Key Role of the North Pacific Oscillation–West Pacific Pattern in Generating the Extreme 2013/14 North American Winter. J. Climate, 28, 8109–8117.

Baxter, S., S. Weaver, J. Gottschalck, and Y. Xue, 2014: Pentad Evolution of Wintertime Impacts of the Madden–Julian Oscillation over the Contiguous United States. J. Climate, 27, 7356–7367.

Barnston, A., and R. Livezy, 1987: Classification, seasonality, and persistence of low-frequency atmospheric circulation patterns. Mon. Wea. Rev., 115, 1083–1126.

Becker, E. J., E. H. Berbery, and R. W. Higgins, 2011: Modulation of cold-season U.S. daily precipitation by the Madden–Julian oscillation. J. Climate, 24, 5157–5166.

Chen, M., P. Xie, J. E. Janowiak, and P. A. Arkin, 2002: Global land precipitation: A 50-yr monthly analysis based on gauge observations. J. Hydrometeor., 3, 249–266.

Climate Prediction Center, 2012: Climate Diagnostics Bulletin. March 2012, 90 pp. [Available online at http://www.cpc.ncep.noaa.gov/products/CDB/CDB_Archive_pdf/PDF/CDB.mar2012_color.pdf.]

Climate Prediction Center, 2014: Climate Diagnostics Bulletin. February 2014, 90 pp. [Available online at http://www.cpc.ncep.noaa.gov/products/CDB/CDB_Archive_pdf/PDF/CDB.feb2014_color.pdf.]

Di Lorenzo, E., and Coauthors, 2013: Synthesis of Pacific Ocean climate and ecosystem dynamics. Oceanography, 26, 68–81.

Folland, C., Jeff Knight, Hans W. Linderholm, David Fereday, Sarah Ineson, and James W. Hurrell, 2009: The Summer North Atlantic Oscillation: Past, Present, and Future. J. Climate, 22, 1082–1103.

Franzke, C., S. Feldstein, and S. Lee, 2011: Synoptic analysis of the Pacific–North American teleconnection pattern. Quart. J. Roy. Meteor. Soc., 137, 329–436.

Furtado, J. C., E. Di Lorenzo, B. T. Anderson, and N. Schneider, 2012: Linkages between the North Pacific Oscillation and central tropical Pacific SSTs at low frequencies. Climate Dyn., 39, 2833–2846.

Hartmann, D. L., 2015: Pacific sea surface temperature and the winter of 2014. Geophys. Res. Lett., 42, 1894–1902.

Higgins, R., and K. Mo, 1997: Persistent North Pacific circulation anomalies and the tropical intraseasonal circulation. J. Climate, 10, 223–244.

Higgins, R. W., E. Schemm, W. Shi, and A. Leetmaa, 2000: Extreme precipitation events in the western United States related to tropical forcing. J. Climate, 13, 793–820.

Hoerling, M., A. Kumar, and M. Zhong, 1997: El Niño, La Niña, and the nonlinearity of their teleconnections. J. Climate, 10, 1769–1786.

Horel, J.D. and John M. Wallace, 1981: Planetary-Scale Atmospheric Phenomena Associated with the Southern Oscillation. Mon. Wea. Rev., 109, 813–829.

Hoskins, B. J., and T. Ambrizzi, 1993: Rossby wave propagation on a realistic longitudinally varying flow. J. Atmos. Sci., 50, 1661–1671.

Izadi, E., 2014: The Gulf of Alaska is unusually warm, and weird fish are showing up. Washington Post, 15 September 2014. [Available online at http://www.washingtonpost.com/news/speaking-of-science/wp/2014/09/15/the-gulf-of-alaska-is-unusually-warm-and-weird-fish-are-showing-up/.]

Janowiak, J. E., G. D. Bell, and M. Chelliah, 1999: A Gridded Data Base of Daily Temperature Maxima and Minima for the Conterminous United States: 1948–1993. NCEP/Climate Prediction Center Atlas 6, 50 pp.

Johnson, N.C., Dan C. Collins, Steven B. Feldstein, Michelle L. L'Heureux, and Emily E. Riddle, 2014: Skillful Wintertime North American Temperature

Forecasts out to 4 Weeks Based on the State of ENSO and the MJO. Wea. Forecasting, 29, 23–38.

Johnson, N.C. and Steven B. Feldstein, 2010: The Continuum of North Pacific Sea Level Pressure Patterns: Intraseasonal, Interannual, and Interdecadal Variability. J. Climate, 23, 851–867.

Kiladis, G. N., and K. M. Weickmann, 1992: Circulation anomalies associated with tropical convection during northern winter. Mon. Wea. Rev., 120, 1900–1923.

Ben P. Kirtman, Dughong Min, Johnna M. Infanti, James L. Kinter, III, Daniel A. Paolino, Qin Zhang, Huug van den Dool, Suranjana Saha, Malaquias Pena Mendez, Emily Becker, Peitao Peng, Patrick Tripp, Jin Huang, David G. DeWitt, Michael K. Tippett, Anthony G. Barnston, Shuhua Li, Anthony Rosati, Siegfried D. Schubert, Michele Rienecker, Max Suarez, Zhao E. Li, Jelena Marshak, Young-Kwon Lim, Joseph Tribbia, Kathleen Pegion, William J. Merryfield, Bertrand Denis, and Eric F. Wood, 2014: The North American Multimodel Ensemble: Phase-1 Seasonal-to-Interannual Prediction; Phase-2 toward Developing Intraseasonal Prediction. Bull. Amer. Meteor. Soc., 95, 585–601.

Lau, N.-C., 1979: The observed structure of tropospheric stationary waves and the local balances of vorticity and heat. J. Atmos. Sci., 36, 996–1016.

L'Heureux, M., and R. W. Higgins, 2008: Boreal winter links between the Madden–Julian oscillation and the Arctic Oscillation. J. Climate, 21, 3040–3050.

Liebmann, B., and C. A. Smith, 1996: Description of a complete (interpolated) outgoing longwave radiation dataset. Bull. Amer. Meteor. Soc., 77, 1275–1277.

Lin, H., and J. Derome, 2004: Nonlinearity of extratropical response to tropical forcing. J. Climate, 17, 2597–2608.

Lin, H., J. Derome, and G. Brunet, 2007: The nonlinear transient atmospheric response to tropical forcing. J. Climate, 20, 5642–5665.

Lin, H., and G. Brunet, 2009: The influence of the Madden–Julian oscillation on Canadian wintertime surface air temperature. Mon. Wea. Rev., 137, 2250–2262.

Lin, H., G. Brunet, and J. Derome, 2009: An observed connection between the North Atlantic Oscillation and the Madden–Julian oscillation. J. Climate, 22, 364–380.

Lin, H., G. Brunet, and R. Mo, 2010: Impact of the Madden–Julian oscillation on wintertime precipitation in Canada. Mon. Wea. Rev., 138, 3822–3839.

Lin, H., G. Brunet, and B. Yu, 2015: Interannual variability of the Madden-Julian Oscillation and its impact on the North Atlantic Oscillation in boreal winter, Geophys. Res. Lett., 42.

Linkin, M. E., and S. Nigam, 2008: The North Pacific Oscillation–West Pacific teleconnection pattern: Mature-phase structure and winter impacts. J. Climate, 21, 1979–1997.

Madden, R., and P. Julian, 1971: Detection of a 40–50 day oscillation in the zonal wind in the tropical Pacific. J. Atmos. Sci., 28, 702–708.

Madden, R., and P. Julian, 1972: Description of global-scale circulation cells in the tropics with a 40–50 day period. J. Atmos. Sci., 29, 1109–1123.

Madden, R. A., and P. R. Julian, 1994: Observations of the 40–50 day tropical oscillation—A review. Mon. Wea. Rev., 122, 814–837.

Matthews, A. J., B. J. Hoskins, and M. Masutani, 2004: The global response to tropical heating in the Madden–Julian oscillation during northern winter. Quart. J. Roy. Meteor. Soc., 130, 1991–2011.

Mo, K. C., and R. W. Higgins, 1998: Tropical convection and precipitation regimes in the western United States. J. Climate, 11, 2404–2423.

Mo, K., and R. Livezey, 1986: Tropical-extratropical geopotential height teleconnections during the Northern Hemisphere winter. Mon. Wea. Rev., 114, 2488–2515.

Mo, K. C. and Glenn H. White, 1985: Teleconnections in the Southern Hemisphere. Mon. Wea. Rev., 113, 22–37.

Mori, M., and M. Watanabe, 2008: The growth and triggering mechanisms of the PNA: A MJO-PNA coherence, J. Meteorol. Soc. Jpn. Ser. II, 86, 213–236.

Nigam, S., 2003: Teleconnections. Encyclopedia of Atmospheric Sciences, J. R. Holton, J. A. Pyle, and J. A. Curry, Eds., Academic Press, 2243–2269.

Nigam, S., and S. Baxter, 2015: Teleconnections. Encyclopedia of Atmospheric Sciences, 2nd ed. G. North, Ed., Elsevier Science, 90–109.

North, G.R., Thomas L. Bell, Robert F. Cahalan, and Fanthune J. Moeng, 1982: Sampling Errors in the Estimation of Empirical Orthogonal Functions. Mon. Wea. Rev., 110, 699–706.

Palmer, T., 2014: Record-breaking winters and global climate change. Science, 344, 803–804.

Qin, J. and Walter A. Robinson, 1993: On the Rossby Wave Source and the Steady Linear Response to Tropical Forcing. J. Atmos. Sci., 50, 1819–1823.

Reynolds, R.W., Nick A. Rayner, Thomas M. Smith, Diane C. Stokes, and Wanqiu Wang, 2002: An Improved In Situ and Satellite SST Analysis for Climate. J. Climate, 15, 1609–1625.

Riddle, E. E., M. Stoner, N. Johnson, M. L'Heureux, D. Collins, and S. Feldstein, 2013: The impact of the MJO on clusters of wintertime circulation anomalies over the North American region. Climate Dyn., 40, 1749–1766.

Saha, S., and Coauthors, 2010: The NCEP Climate Forecast System Reanalysis. Bull. Amer. Meteor. Soc., 91, 1015–1057.

Sardeshmukh, P.D. and Brian J. Hoskins, 1988: The Generation of Global Rotational Flow by Steady Idealized Tropical Divergence. J. Atmos. Sci., 45, 1228–1251.

Schreck, C. J., J. M. Cordeira, and D. Margolin, 2013: Which MJO events affect North American temperatures? Mon. Wea. Rev., 141, 3840–3850.

Seager, R., M. Hoerling, S. Schubert, H. Wang, B. Lyon, A. Kumar, J. Nakamura, and N. Henderson, 2014: Causes and predictability of the 2011-14 California drought, Assessment Rep., NOAA, 40 pp. [Available online at http://cpo.noaa.gov/sites/cpo/MAPP/Task%20Forces/DTF/californiadrought/california_drought_report.pdf.]

Thompson, D. W. J., and J. M. Wallace, 1998: The Arctic oscillation signature in wintertime geopotential height and temperature fields. Geophys. Res. Lett., 25, 1297–1300.

van den Dool, H. M., S. Saha, and Å Johansson, 2000: Empirical Orthogonal Teleconnections. J. Climate, 13, 1421–1435.

Ventrice, M. J., M. C. Wheeler, H. H. Hendon, C. J. Schreck, C. D. Thorncroft, and G. N. Kiladis, 2013: A modified multivariate Madden–Julian oscillation index using velocity potential. Mon. Wea. Rev., 141, 4197–4210.

Vimont, D. J., D. S. Battisti, and A. C. Hirst (2001), Footprinting: A seasonal connection between the tropics and mid-latitudes, Geophys. Res. Lett., 28(20), 3923–3926.

Vimont, D. J., J. M. Wallace, and D. S. Battisti (2003), The seasonal footprinting mechanism in the Pacific: Implications for ENSO, J. Clim., 16(16), 2668–2675.

Walker, G. T., 1924: Correlation in seasonal variations in weather IX: A further study of world weather. Mem. Indian Meteor. Dept., 24, 275–332.

Wallace, J., and D. Gutzler, 1981: Teleconnections in the geopotential height field during the Northern Hemisphere winter. Mon. Wea. Rev., 109, 784–804.

Wang, W., M.-P. Hung, S. Weaver, A. Kumar, and X. Fu, 2014: MJO prediction in the NCEP Climate Forecast System version 2. Climate Dyn., 42, 2509–2520.

Wheeler, M. C., and H. H. Hendon, 2004: An all-season real-time multivariate MJO index: Development of an index for monitoring and prediction. Mon. Wea. Rev., 132, 1917–1932.

Xie, P., M. Chen, and W. Shi, 2010: CPC unified gauge-based analysis of global daily precipitation. Extended Abstracts, 24th Conf. on Hydrology, Atlanta, GA, Amer. Meteor. Soc, 2.3A. [Available online at https://ams.confex.com/ams/90annual/techprogram/paper_163676.htm.]

Yu, J., Y. Zou, S.T. Kim, and T. Lee, 2012: The changing impact of El Niño on US winter temperatures. Geophys. Res. Lett., 39, L15702.

Zhou, S., and A. J. Miller, 2005: The interaction of the Madden–Julian oscillation and the Arctic Oscillation. J. Climate, 18, 143–159.

Zhou, S., M. L'Heureux, S. Weaver, and A. Kumar, 2012: A composite study of the MJO influence on the surface air temperature and precipitation over the continental United States. Climate Dyn., 38, 1459–1471.